Short senolytic or senostatic interventions rescue progression of radiation-induced frailty and premature ageing in mice

Rescue of radiation-induced premature frailty

Edward Fielder*, Tengfei Wan*, Ghazaleh Alimohammadiha, Abbas Ishaq[1], Evon Low, B. Melanie Weigand[2], George Kelly, Craig Parker, Brigid Griffin, Diana Jurk[2], Viktor I. Korolchuk, Thomas von Zglinicki#, Satomi Miwa#

***shared first authors**

#shared last authors

Affiliations:

Newcastle University Biosciences Institute, Newcastle University, Newcastle upon Tyne, NE4 5PL, UK

[1]present address: Alcyomics Ltd, The Biosphere, Newcastle Helix, Drayman's Way. NE4 5BX.

[2]present address: Robert and Arlene Kogod Center on Aging, Department of Physiology and Biomedical Engineering, Mayo Clinic, 200 First Street SW, Rochester, MN 55905, USA

Abstract:

Cancer survivors suffer from progressive frailty, multimorbidity and premature morbidity. We hypothesize that therapy-induced senescence and senescence progression via bystander effects is a significant cause of this premature ageing phenotype. Accordingly, the study addresses the question whether a short anti-senescence intervention is able to block progression of radiation-induced frailty and disability in a pre-clinical setting. Male mice were sub-lethally irradiated at 5 months of age and treated (or not) with either a senolytic drug (Navitoclax or dasatinib + quercetin) for 10 days or with the senostatic metformin for 10 weeks. Follow up was for one year. Treatments commencing within a month after irradiation effectively reduced frailty progression ($p<0.05$) and improved muscle ($p<0.01$) and liver ($p<0.05$) function as well as short-term memory ($p<0.05$) until advanced age with no need for repeated interventions. Senolytic interventions that started late, after radiation-induced premature frailty was manifest, still had beneficial effects on frailty ($p<0.05$) and short-term memory ($p<0.05$). Metformin was similarly effective as senolytics. At therapeutically achievable concentrations metformin acted as a senostatic neither via inhibition of mitochondrial complex I, nor via improvement of mitophagy or mitochondrial function, but by reducing non-mitochondrial ROS production via NOX4 inhibition in senescent cells. Our study suggests that the progression of adverse long-term health and quality-of-life effects of radiation exposure, as experienced by cancer survivors, might be rescued by short-term adjuvant anti-senescence interventions.

Introduction

Cancer has become an increasingly survivable disease, with cancer-specific mortality in developed countries having dropped sharply in the last few decades. Many cancer types have now high cure rates (Bray et al., 2018), and in some fields the emphasis has started to shift towards efforts to improve the quality of survivorship after successful cancer treatment (Damlaj, El Fakih, & Hashmi, 2019).This is necessary as long-term survivors of childhood and adult cancers undergo a wide-range of negative health and quality of life changes that lead to increased frailty, multi-morbidity and mortality compared to the general population (Bluethmann, Mariotto, & Rowland, 2016; Cupit-Link et al., 2017; Robison & Hudson, 2014). These changes are indicative of accelerated or premature ageing in long-term cancer survivors, for which there is currently no validated therapy.

Premature ageing in cancer survivors appears to be largely caused by DNA-damaging cancer therapies. Numerous biological processes have been proposed as drivers of this (Cupit-Link et al., 2017; Ness et al., 2018), with therapy-induced cell senescence prominent amongst them (Short, Fielder, Miwa, & von Zglinicki, 2019).

Cell senescence is a complex cellular stress response program that can be induced by DNA damage (e.g. radio- or chemotherapy) and involves persistent cell cycle arrest, aberrant regulation of metabolism (specifically energy metabolism), epigenetic programming and secretory processes (Gorgoulis et al., 2019; von Zglinicki, 2021). Therapy-induced senescence may constitute a cytostatic clinical response contributing to stable disease (te Poele, Okorokov, Jardine, Cummings, & Joel, 2002), however, there is increasing evidence that therapy-induced senescent cells can promote both primary relapse and secondary cancers, often leading to less successful treatment outcomes of consequent disease (Jena, Das, Bharadwaj, & Mandal, 2020; Saleh, Tyutyunyk-Massey, & Gewirtz, 2019). Senescent cells release both pro-inflammatory and pro-oxidant signaling molecules (the Senescence-Associated Secretory Phenotype, SASP) which can damage and induce senescence in bystander cells (Nelson et al., 2012), and thus spread the phenotype from the point of origin throughout tissues and organisms (da Silva et al., 2019; Xu et al., 2018). As such, adjuvant tumour therapy not only induces transiently (and locally) high concentrations of senescent cells but may also result in faster accumulation of these cells both locally and systemically over the whole life course (Short et al., 2019).

Accumulation of senescent cells is causal for a wide range of ageing-associated diseases and disabilities as evidenced by the far-reaching successes of interventions that reduce the systemic load of senescence [for review see (Short et al., 2019)]. In fact, acute ablation of senescent cells by continuous pharmacogenetic or pharmacologic intervention has been able to reduce chemotherapy-induced multimorbidity (Demaria et al., 2017) and liver toxicity (Baar et al., 2017) as well as radiation-induced haematoxicity (Chang et al., 2016) and sarcopaenia (Zhu et al., 2015) in mice. However, if induction of secondary senescence by bystander effects is a major driver of post-therapeutic senescence, continuous anti-senescence interventions might not be necessary. Rather, we hypothesized that specific ablation of senescent cells (senolytic intervention) or specific inhibition of the SASP (senostatic intervention) shortly after adjuvant cancer therapy might be sufficient to rescue enhanced mortality, multimorbidity and frailty in cancer survivors over their life course (Short et al., 2019).

Senolytics are potent drugs with frequently serious side effects (Demaria, 2017) that would raise significant safety concerns in a preventive setting, even in a high-risk group like tumour survivors. In contrast, senostatics (sometimes also termed senomorphics) are chemicals that do not kill (senescent) cells but block SASP signals, thus inhibiting the spread of senescence via bystander

effects. In fact, senostatic interventions, including the dietary restriction mimetics rapamycin and metformin, or dietary restriction itself, caused lasting reductions of senescent cell burden in different tissues of mice with improved lifespan and healthspan (Blagosklonny, 2017; Fontana, Nehme, & Demaria, 2018; Lopez-Otin, Galluzzi, Freije, Madeo, & Kroemer, 2016; Selvarani, Mohammed, & Richardson, 2021). However, their efficiency to rescue premature ageing has not been pre-clinically tested in comparison to senolytic intervention.

The senostatic metformin has an extraordinarily good safety profile, which has been testified in its long clinical history as well as in a myriad of clinical trials. However, the drug acts through multiple pathways, and it is not at all clear how it reduces the SASP in a therapeutically achievable setting. It is often assumed that it blocks complex I of the electron transport chain, thus reducing production of reactive oxygen species in mitochondria, which in turn would reduce NF-κB activation and thus the SASP (Moiseeva et al., 2013). However, metformin efficiently blocks complex I only in millimolar concentrations, while tissue concentrations that can be achieved in mice or man are one to two orders of magnitude lower (Wilcock & Bailey, 1994). A mechanistic examination of the senostatic effect of metformin *in vivo* is therefore urgently warranted.

To address these questions in a pre-clinical setting, we used a simple mouse model of premature ageing induced by fractionated whole-body irradiation (Fielder et al., 2019). For proof of principle, we used first generation senolytics with well-documented efficacy (Navitoclax and Dasatinib+Quercetin) in a wide range of age-associated deficiencies and tissues. We focussed on frailty as a primary outcome because premature frailty is a well-documented, clinically important problem of long-term cancer survivors (Ness et al., 2013) as well as a strong predictor of multimorbidity and mortality in humans (Kojima, Iliffe, & Walters, 2018) and mice (Whitehead et al., 2014). Sarcopenia, metabolic disease and, especially, cognitive decline (Orszaghova, Mego, & Chovanec, 2021) are major complications in long-term tumour survivors, therefore we included phenotype assays in these domains combined with tissue-specific ex-vivo analyses primarily in hippocampus, muscle and liver. We show here that i) irradiation-induced lifelong premature ageing can be rescued by a one-off post-irradiation senolytic intervention, ii) senolytics are still partially efficient in reducing progression after establishment of a premature ageing phenotype, iii) a relatively short metformin intervention is similarly effective in rescuing premature ageing and iv) metformin at therapeutic concentrations acts as a senostatic neither via inhibition of complex I, nor via improvement of mitophagy or mitochondrial function, but by reducing non-mitochondrial ROS production in senescent cells.

Results

1. Short-term post-irradiation senolytic interventions rescue premature ageing

Male C57Bl/6J mice received fractionated sub-lethal whole-body irradiation (IR, 3 x 3Gy) at an age of 5 to 6 months and were treated with a short course (10 days) of senolytics by oral gavage at one month after irradiation, i.e. when acute radiation sickness had abated (Fig. 1A). Doses were 5mg/kg/day Dasatinib and 50mg/kg/day Quercetin (D+Q) as typically applied in senolytics mouse studies (Palmer et al., 2019; Schafer et al., 2017; Zhu et al., 2015). As a senolytic, Navitoclax has been used at widely different doses in mice, ranging from 1.5mg/kg/day (Tarantini et al., 2021; Yabluchanskiy et al., 2020) to 50mg/kg/day (Bussian et al., 2018; Chang et al., 2016). Because Navitoclax causes thrombocytopenia at higher concentrations (Wilson et al., 2010), we decided to use Navitoclax in the lower concentration range, e.g. at 5 mg/kg/day. Irradiated mice experienced premature ageing as documented by a doubling of the rate of frailty progression, decreased neuromuscular coordination, decreased short-term memory and increased general and cancer-associated mortality ((Fielder et al., 2019) and Fig. 1). When mice were treated with either senolytic drug at 1 month after IR indicators of premature ageing were rescued over almost one year of follow-up (Figs. 1B – G). Although frailty was not reversed, rates of frailty progression decreased after senolytic treatment to values comparable to non-irradiated mice (Fig. 1B). The frailty index is composed of 30 different assessments. Early intervention with each of the senolytics improved 6 of them, namely mouse grimace scale, body condition, breathing rate, eye discharge/swelling, whisker loss and body weight loss. In addition, Navitoclax treatment also reduced loss of fur colour and tumour incidence (Figure 1-figure supplement 2). Irradiated mice progressively lost neuromuscular coordination as indicated by increasingly poorer performance in the wire hanging (Fig. 1C) and rotarod (Fig. 1D) tests. Improvements for both interventions became greater with increasing age, with Navitoclax being more effective than D+Q (Figs 1C, D). Short-term memory was assessed using spontaneous alternation frequency in a Y-maze test at 16 months of age (Fielder et al., 2019). It was improved substantially following Navitoclax treatment, with a modest improvement following D+Q (Fig. 1E). Liver damage was assessed by the activity of alanine transaminase (ALT) and aspartate aminotransferase (AST) in serum, which indicates leakage from hepatocytes, at 16 months of age. ALT activity in serum was reduced under both interventions (Fig. 1F), suggesting that they enabled better liver maintenance. However, intervention-dependent changes were not significant for AST although ALT and AST activities were positively correlated amongst all mice (Correlation coefficient = 0.533, P=0.0000234). Picrosirius Red staining did not show a significant effect of senolytics on liver fibrosis. Although cohort sizes were not powered to assess long-term survival effects, both treatments tended to result in improved survival and lower tumour prevalence at death in comparison to irradiated control mice (Fig. 1G). While normal skin ageing is characterized by epidermal thinning, irradiation-induced premature ageing is accompanied by hypertrophy of the epidermis in the skin (Figure 1 – Figure supplement 3A,B). Neither D+Q nor Navitoclax treatment reduced epidermal hypertrophy at late age (Figure 1 – figure supplement 3C).

Sublethal irradiation resulted in persistently enhanced levels of markers for cellular senescence in multiple tissues of mice for up to 12 months (Le et al., 2010; Seol et al., 2012). Senescence marker levels in one year old irradiated mice were similar to those found in normally ageing mice older than 24 months (Hudgins et al., 2018; Jurk et al., 2014). We focused first on liver in which hepatocyte senescence contributes causally to age-associated functional decline (Jurk et al., 2014; Ogrodnik et al., 2017). As senescence markers, we measured nuclear size and karyomegaly (Aravinthan & Alexander, 2016; Ogrodnik et al., 2017), nuclear HMGB1 exclusion (Davalos et al., 2013), nuclear

accumulation of Telomere-Associated DNA Damage Foci (TAF) and frequencies of TAF-positive hepatocyte nuclei (Hewitt et al., 2012; Ogrodnik et al., 2017). Among TAF-positive cells, we assayed both cells with any TAF and those with at least 3 TAF, because of previous evidence suggesting that the latter might be more representative of cells in 'full' or 'late' senescence (Zou, Sfeir, Gryaznov, Shay, & Wright, 2004) (Jurk et al., 2014). The markers indicated higher frequencies of senescent hepatocytes at 7 months after irradiation (Figure 1 – figure supplement 4A-F). Marker changes were similar to those seen in normally ageing mice at ages above 30 months (Figure 1 – figure supplement 4G-K). Navitoclax intervention at 6 months of age resulted in reduced senescent hepatocyte frequencies in liver 10 months later as indicated by all markers tested (Figure 1 – figure supplement 5A-F). However, D+Q intervention led to reduced nuclear size and hepatocyte karyomegaly but did not maintain a significant long-term reduction of HMGB1-negative or TAF-positive hepatocytes (Figure 1 – figure supplement 5A-F).

Senescent cell burden, specifically in the hippocampus, is associated with memory deficits in ageing mice (Fielder et al., 2020; Musi et al., 2018; Ogrodnik et al., 2021). To assess the mechanistic basis for the observed improvements of short-term memory (Fig. 1E), we measured markers for a senescence-like phenotype (nuclear size, loss of nuclear Lamin B1 expression and TAF frequencies) and for neuroinflammation (ionized calcium-binding adapter molecule 1 (Iba1)-positive cell density and soma size) in the CA1 and CA3 hippocampal regions (Figure 1 – figure supplement 6). Both D+Q and Navitoclax reduced nuclear size (Figure 1 – figure supplement 6A,B) and TAF frequencies (Figure 1 – figure supplement 6E-I) as markers for a senescent phenotype in CA1 and CA3 pyramidal layer neurons, but Navitoclax had no effect on laminB1 expression (Figure 1 – figure supplement 6C,D). Similarly, Navitoclax had no effect on frequencies of Iba1-positive microglia Figure 1 – figure supplement 6J,K), although microglia soma size was reduced in CA1 and CA3 after both treatments (Figure 1 – figure supplement 6L,M).

We also examined the effects of D+Q or Navitoclax treatment on morphological and functional parameters of hind limb muscle (Figure 1 – figure supplement 7). Interestingly, improvements of neuromuscular coordination (Fig. 1C) and strength/endurance (Fig. 1D) were not associated with enhanced muscle fibre diameter (Figure 1 – figure supplement 7A,B), decreased frequency of p21-positive myonuclei (Figure 1 – figure supplement 7C,D) or decreased frequency of TAF-positive myonuclei (Figure 1 – figure supplement 7E) as senescence marker. Neither irradiation alone or combination with either of the senolytic interventions changed hind limb muscle fibrosis or fat accumulation as assessed by Picro-SiriusRed/FastGreen staining.

It is often assumed that the effect of senescent cells onto physiological characteristics is mediated via the SASP, especially the induction of a chronic inflammatory state (Ogrodnik et al., 2018). Concentrations of 18 cytokines/chemokines that are part of a typical SASP were measured in serum at the end of the experiment by cytokine array (Eve Technologies). Although short senolytic treatment at 6 months of age was sufficient to reduce senescence markers in liver and brain persistently (Figure 1 – supplements 5 and 6), none of the analysed cytokines was significantly different from controls at late age (Figure 1 – supplement 8).

2. Late senolytic interventions block further progression of irradiation-induced premature ageing

So far, our data showed that a short senolytic intervention at an early timepoint can rescue irradiation-induced premature accumulation of senescent cells as well as premature physiological

ageing. We next asked the question, whether senolytics could still be effective if mice were treated late after irradiation, when premature ageing was already manifest. Animals were again irradiated at 5 months of age, but senolytic interventions were delayed for 6 months and mice were treated with the senolytics D+Q or Navitoclax (using the same regimen as before) at 11 months of age (Fig. 2A). At this timepoint, the frailty index in irradiated mice was already significantly above that in sham-irradiated mice (Fig. 2B). However, similar to early intervention, late senolytic treatment did not reduce the frailty index score, but rescued its further accelerated progression (Fig. 2B). Late intervention with each of the senolytics improved largely the same components of the frailty index as early senolytic intervention, namely mouse grimace scale, body condition, breathing rate, and eye discharge/swelling (Figure 1 – figure supplement 2). Mice that had been treated with senolytics at 11 months of age still showed a tendency for improved results of the hanging wire test at 14 months (Fig. 2C), however, rotarod performance was not better than in irradiated animals (Fig. 2D). Late intervention with either senolytic improved short-term memory at late age (Fig. 2E). Neither liver damage (Fig. 2F) nor tumour incidence (Fig. 2G) following late senolytic treatment was significantly reduced. Epidermal thickness was unchanged (Figure 2 – figure supplement 2).

In agreement with a diminished effect of late treatments on liver damage, there was also less impact on persistent systemic cell senescence as assessed by nuclear size, nuclear HMGB1 expression and TAF frequencies in liver (Figure 2 – figure supplement 3D-F), however, treatment with Navitoclax still reduced nuclear size (Figure 2 – figure supplement 3A), karyomegaly (Figure 2 – figure supplement 3B) and frequencies of HMGB1-negative hepatocytes (Figure 2 – figure supplement 3C) suggesting a reduced senescent burden. There was no improvement of hind limb myofibre cross sectional area but rather a tendency (significant for Navitoclax) to reduce it (Figure 2 – figure supplement 4A,B). There was no reduction of TAF frequencies in muscle (Figure 2 – figure supplement 4C). However, in agreement with improved memory maintenance (Fig 2E) we found a reduction of neuroinflammation markers in the CA1 (both markers) and CA3 (microglia soma size only) regions of the hippocampus following both late interventions (Figure 2 – figure supplement 5).

Together, these data show that a short-term senolytic intervention even if applied at an advanced age still has beneficial effect on irradiation-induced premature progression of frailty and cognitive decline.

3. A short-term intervention with the senostatic metformin rescues irradiation-induced premature ageing

Senolytics can have serious side effects, for instance Navitoclax-induced thrombocytopenia at higher doses (Demaria, 2017), that may be limiting for preventive applications. Senostatic or senomorphic caloric restriction mimetics, which block senescence-stabilizing signalling, can also reduce net accumulation of senescent cells in tissues (da Silva et al., 2019; C. Wang et al., 2010). One example is metformin, which has been shown to act as a senostatic (Moiseeva et al., 2013) and has an excellent safety profile as testified by about 70 years of clinical application. We therefore decided to treat our irradiated mice with metformin for a relatively short period (10 weeks), starting at one month after irradiation, and assessed the long-term effects of this treatment (Fig. 3A). The amount of 1mg/g food, as used here, had previously been found to extend lifespan and healthspan of mice (Martin-Montalvo et al., 2013). Similar to senolytic interventions, metformin treatment rescued the enhanced rate of frailty progression due to irradiation (Fig. 3B). Among the components of frailty, metformin improved mouse grimace scale, body condition, breathing rate, whisker loss and body weight loss at late age (Figure 1 – figure supplement 2). It also improved neuromuscular

coordination as tested by hanging wire test (Fig. 3C), but had only a minor effect on performance on the rotarod at late age (Fig. 3D), which might be due to the high body weights of mice fed soaked food. At 16 months of age, metformin-treated animals tended to perform better in the short term memory test (Fig. 3E), showed less liver damage (Fig. 3F) and tumour prevalence at death was reduced to the levels as in sham-irradiated mice (Fig. 3G). Metformin treatment also tended to reduce irradiation-induced epidermal hypertrophy assessed at 16 months of age (Figure 3 – figure supplement 2).

All tested senescence markers in livers of metformin-treated mice indicated the reduction of senescent cell frequencies at old age (16 months) (Figure 3 – figure supplement 3A-F). Similarly, senescence and neuroinflammation markers in the CA1 and CA3 regions of the hippocampus were deceased (Figure 3 – figure supplement 4A-F). Interestingly, metformin treatment improved skeletal muscle fibre maintenance as shown by larger cross-sectional area of both oxidative and non-oxidative muscle fibres (Figure 3 – figure supplement 5A,B) and reduced TAF frequencies in myocyte nuclei (Figure 3 – figure supplement 5C). Metformin treatment also led to a persistent reduction of the levels of the pro-inflammatory SASP components IL-17, CCL2 and TNFα in serum of mice at 16 months of age, e.g. more than half a year after cessation of treatment (Figure 3 – figure supplement 6).

In conclusion, these data indicate that a relatively short treatment with the senostatic metformin rescues multiple domains of irradiation-induced premature ageing in mice for at least 10 months after cessation of the intervention.

4. At therapeutic concentrations, metformin inhibits the SASP by reducing NOX4 activity in senescent cells

Metformin can block the SASP, and thus act as a senostatic, by inhibiting complex I of the electron transport chain, thus causing a reduction of mitochondrial ROS production, which in turn will reduce the activity of the NF-κB transcription factor, the major driver of the pro-inflammatory SASP. This pathway has been identified *in vitro*, using millimolar concentrations of metformin (Moiseeva et al., 2013). However, therapeutically achievable metformin concentrations in the vast majority of tissues in mice or man are typically well below 100 μM (Wilcock & Bailey, 1994). In permeabilised human fibroblasts *in vitro*, metformin inhibits complex I-dependent respiration with pyruvate and malate in concentrations around 1 mM or higher but has no detectable effect on oxygen consumption rates at 100 μM (Fig. 4A). Supplementation of the complex II substrate succinate completely restored respiration under metformin, confirming that metformin at high concentrations inhibits complex I specifically (Fig. 4A). Even when senescent human fibroblasts were treated with various concentrations of metformin for 10 days to mimic longer term *in vivo* interventions, low metformin concentrations (100 μM) did not decrease mitochondria dependent ATP production compared with senescent untreated controls. In contrast, 2 mM metformin shifted cellular ATP production almost entirely to glycolysis with little contribution from mitochondrial oxidative phosphorylation (Fig. 4B). Interestingly, the senescence-associated enhanced H_2O_2 production from whole cells (as measured by Amplex Red assay) was rescued only by low (up to 400 μM), but not by high metformin concentrations (Fig. 4C). Reduction of ROS production in senescent cells by long-term treatment with low metformin concentrations was confirmed by measuring cellular ROS levels using DHE fluorescence (Fig. 4D), with a stronger effect for metformin as compared to rapamycin. In accordance with the ROS data (Figs. 4C, D), low concentrations of Metformin were more effective than higher ones in reducing a wider range of cytokines in the secretome of senescent fibroblasts

(Fig. 4E). Together, these data indicate that low, therapeutically relevant concentrations of metformin reduce the release of ROS and SASP cytokines from senescent cells, which can explain the senostatic activity of metformin *in vivo*. Importantly, this effect was not mediated by complex I inhibition.

To identify potential alternative mechanisms of the senostatic activity of metformin, we subjected human fibroblasts treated with either low (100 μM) or high (2 mM) metformin concentrations to a stress response pathway identifier assay by cytometry by time of flight (CyTOF). Two or three antigens were chosen to represent each of seven cellular stress response pathways, namely heat shock, oxidative stress response, xenobiotics response, ER-UPR, Mito-UPR, nutrient signalling pathway/autophagy and DNA damage response (DDR)/senescence, resulting in a panel of 21 antibodies (Table 2). Cells were treated with test interventions for 2 days and analysed by CyTOF using the antibody panel. Starvation, heat shock and oxidative stress by H_2O_2 treatment were used as positive control interventions. In the positive control experiments, activation of heat shock and oxidative stress response pathways were evident following the respective control treatments together with induction of autophagy and a DDR/senescence, while starvation impacted primarily onto the mTOR pathway, together validating the assay (Fig. 5A). Treatment with high metformin reduced the levels of marker proteins in a wide range of pathways, including heat shock, oxidative stress response, ER-UPR, Mito-UPR, nutrient signalling pathway/autophagy and DDR/senescence. In contrast, low metformin only reduced indicators of oxidative stress response as expected (compare Figs. 4C, D) and nutrient signalling (Fig. 5A). This suggested that low metformin might activate autophagy and mitophagy via suppression of the mTOR pathway and thus contribute to a reduction of mitochondrial ROS production in senescence. Therefore, we next examined mitophagy activity in human fibroblasts transfected with the mitophagy reporter mt-mKeima (Katayama, Kogure, Mizushima, Yoshimori, & Miyawaki, 2011), which localises to mitochondria and displays a shift in fluorescence emission under low pH, when mitochondria are delivered into lysosomes (indicated in red, Fig. 5B). As shown before (Dalle Pezze et al., 2014; Korolchuk, Miwa, Carroll, & von Zglinicki, 2017), mitophagy activity was reduced in senescent cells. This reduction occurred within hours after irradiation and mitophagy remained low in irradiated cells for multiple days (Fig. 5C). Treatment with rapamycin improved mitophagy at all time points, but 100 μM metformin had no effect (Fig.5C). Mitochondrial dysfunction in senescence is characterized by high ROS production together with low respiratory coupling (Passos et al., 2007). In accordance with their effects on mitophagy, rapamycin, but not metformin, suppressed senescence-associated mitochondrial superoxide production as measured by MitoSOX fluorescence (Fig. 5D). Moreover, metformin did not rescue mitochondrial dysfunction in senescent cells as assessed by respiratory control ratio with the complex I-linked substrate, pyruvate+malate (Fig. 5E).

Together, these data suggested that low metformin has no effect on mitochondrial (dys)function in senescence. Therefore, we tested the alternative possibility that it might primarily reduce non-mitochondrial, rather than mitochondrial, ROS production in senescent cells. ROS production by the NADPH oxidase 4 (NOX4) has been shown to contribute to replicative (Lener et al., 2009), oncogene-induced (Weyemi et al., 2012) and stress-induced senescence (Goy et al., 2014) although its knock-out had no impact on lifespan in mice (Rezende et al., 2017). To test the hypothesis that low metformin might act as a senostatic via reduction of the major cytoplasmic ROS generator NOX4, we first measured the abundance of NOX4 in senescent fibroblasts, which was enhanced as expected (Fig. 6A, B). Moreover, NOX4 did not colocalise with mitochondria (Figure 6 – figure supplement 1). A low concentration of metformin (100 μM) reduced NOX4 protein levels in senescent human fibroblasts as shown by both immunofluorescence (Fig. 6A) and Western blotting (Fig. 6B). To test whether manipulation of NOX4 alone would be sufficient to explain the senostatic activity of

metformin, we over-expressed NOX4 in young fibroblasts and assessed its effects on markers of senescence, SASP and ROS. In comparison to EGFP-overexpressing controls, NOX4-overexpressing fibroblasts were more often positive for Sen-β-Gal (Fig. 6C) and produced higher levels of ROS (Fig. 6D). Importantly, cells overexpressing NOX4 produced significantly more of the SASP interleukin IL-6 (Fig. 6E), and there was a strong positive correlation between NOX4 and IL-6 levels (Fig. 6F), but not between EGFP and IL-6 (Fig. 6G). Finally, we treated fibroblasts in stress-induced senescence with the NADPH oxidase inhibitor Diphenyleneiodonium chloride (DPI), which reduced both Sen-β-Gal activity as a marker for the senescent phenotype (Fig 6H) and DHE fluorescence, indicative of decreased production of senescence-associated ROS (Fig 6I).

Together, our data indicate that metformin at low, therapeutically achievable concentrations reduces senescence-associated ROS production by diminishing NOX4 abundance in senescent cells, which in turn causes the reduction of other facets of the senescent phenotype, importantly including a reduction of SASP production.

Discussion

Irradiation is a mainstay of successful therapy for the vast majority of cancers. However, sublethal irradiation causes progressive, premature frailty in both humans (Ness et al., 2018; Robison & Hudson, 2014) and mice (Fielder et al., 2019). Frailty is a medical syndrome characterised by system-wide decreased physiological reserves and thus increased vulnerability (Rockwood, Mitnitski, & Howlett, 2015) predicting multimorbidity and mortality in humans (Kojima et al., 2018) and mice (Whitehead et al., 2014). In long-term tumour survivors, frailty prevalence reaches a level equal to the general population of 60 – 70 year olds about 30 years earlier (Ness et al., 2013), and in mice frailty progression after sublethal whole-body irradiation is about twice as fast as in non-irradiated animals (Fielder et al., 2019). Together with multimorbidity and increased mortality, greatly enhanced frailty is a major component of a serious premature ageing phenotype in long-term tumour survivors, for which no treatment is available so far.

Adjuvant senolytic intervention can relieve some of the consequences of experimental irradiation or chemotherapy in mice. For instance, pharmacogenetic or pharmacologic senolytic intervention up to 12 weeks after irradiation or treatment with the radiation mimetic doxorubicin (partially) corrected treatment-induced loss of immune function (Chang et al., 2016; Palacio et al., 2019), bone loss (Chandra et al., 2020), cardiac dysfunction and loss of physical activity (Demaria et al., 2017) and liver damage (Baar et al., 2017). However, whether an adjuvant senolytic intervention would be able to rescue organism-wide radiation-induced premature ageing as documented by frailty levels has not been shown before. Moreover, there is very little data addressing the possible persistence of beneficial effects of senolytic interventions; most published experiments test the outcomes of senolytic treatments only within days to weeks after the intervention. We are only aware of a single paper (Zhu et al., 2015) showing that a beneficial effect of a treatment with D+Q (improvement of muscle strength in an irradiated mouse leg) could last for up to 7 months.

Our core hypothesis was that therapy-induced senescence would greatly and persistently accelerate the accumulation of senescent cells by enhancing secondary senescence via bystander signalling, thus causing progressive worsening of ageing-associated symptoms with time following a single bout of DNA-damaging therapies (Short et al., 2019). If this hypothesis is correct, eliminating therapy-induced senescent cells by a one-off, short senolytic or senostatic intervention adjuvant to radiation-

or chemotherapy should be sufficient to prevent progressive premature ageing and to normalise the rate of frailty progression.

Our data support this hypothesis. A single, relatively short adjuvant intervention with either senolytic or the senostatic metformin rescued the radiation-induced accelerated progression of multi-system frailty for at least almost one year. We started the interventions at one month after completion of radiation, i.e. when signs of acute radiation sickness in the mice had abated but levels of radiation-induced senescence in many tissues were still not significantly above controls (Mylonas et al., 2021; Palacio et al., 2019; Palacio, Krishnan, Le, Sharpless, & Beausejour, 2017). That this was sufficient to cause a significant reduction of senescence markers in tissues like liver and brain 10 months later is again in agreement with a central role of bystander-mediated accelerated progression of senescence following irradiation.

When senolytic interventions were performed only after enhanced frailty was established, beneficial long-term effects were reduced. There was no longer an effect on muscular or liver function and little improvement on senescence markers in liver at old age. Similarly, Mylonas et al. (Mylonas et al., 2021) recently reported that a late intervention with Navitoclax reduced senescence markers in kidney but did not improve kidney fibrosis. However, late interventions were still efficient in rescuing further frailty progression and liver maintenance and tended to improve short-term memory at high age consistent with a significant reduction of markers for neuroinflammation. This confirms recent data (Yabluchanskiy et al., 2020) showing improvements of brain senescence markers, neurovascular coupling and memory after relatively late (3 months past whole brain irradiation) pharmacogenetic (ganciclovir in 3MR mice) or Navitoclax intervention. Our results might be interpreted to suggest that ongoing brain cell senescence, including neuron senescence, could be a physiologically relevant driver of neuroinflammation.

While senolytic drugs work in principle on a systemic level, their senolytic activity is cell type-specific. For instance, Navitoclax has senolytic activity against HUVECs and fibroblasts, but not adipocytes *in vitro* (Zhu et al., 2016), while D+Q in combination eliminated senescent HUVECs, fibroblasts and fat progenitor cells (Zhu et al., 2015). The specific activity of these senolytics against many other senescent cell types is not known. Our data show cell type-specific differences in the capacity of Navitoclax vs D+Q for long-term reduction of senescence markers *in vivo*: under an early intervention regime, Navitoclax and D+Q reduced hippocampal pyramidal neuron senescence at late age equally well but had no effect on senescence marker in muscle fibres, while senescence markers in liver hepatocytes were only efficiently reduced by Navitoclax but not by D+Q. This pattern was different from the physiological responses in the same tissues: Navitoclax and D+Q improved function in the liver (as measured by ALT release), brain (short-term memory) and muscle (rotarod and hanging wire performance) with only a slightly better performance of Navitoclax in terms of memory and muscle function. The senostatic metformin might be expected to have less cell type specificity, and in fact it did reduce late age senescent cell frequencies both in liver, brain and muscle. Together, these data suggest that cognitive improvement by senolytics could be tissue-autonomous, but that there must be significant contributions from systemic effects causing improvements in muscular and possibly liver function. However, measuring the serum abundance of 18 major interleukins at late age, we did not find evidence for obvious impacts of any of the interventions, suggesting that the mediation of systemic effects might be more complex than persistent suppression of some pro-inflammatory cytokines.

The capacity of the dietary restriction mimetic metformin to extend lifespan and healthspan in mice (Martin-Montalvo et al., 2013) and probably man (Campbell, Bellman, Stephenson, & Lisy, 2017; C. P. Wang, Lorenzo, Habib, Jo, & Espinoza, 2017) is well documented. Among other mechanisms,

metformin, like dietary restriction itself (da Silva et al., 2019), inhibits the pro-inflammatory SASP (Moiseeva et al., 2013) and thus limits the spread of senescence via bystander effects. We therefore expected it to be similarly effective as senolytics in reducing persistent therapy-induced senescence and its physiological consequences, and our results confirmed this expectation.

It has been shown that metformin inhibits complex I of the mitochondrial electron transport chain, thus reducing ROS production (Moiseeva et al., 2013). ROS levels are high in senescent cells (Passos et al., 2010; Passos et al., 2007) and their ability to activate the SASP is well documented (Coppe, Desprez, Krtolica, & Campisi, 2010; Nelson, Kucheryavenko, Wordsworth, & von Zglinicki, 2018). Thus, it has been suggested that metformin diminishes the SASP via complex I inhibition (Moiseeva et al., 2013). However, metformin inhibits complex I only at supraphysiological concentrations. At therapeutically achievable and effective concentrations, it still reduces cellular ROS (Fig. 4C, D) and the SASP (Fig. 4E), but has no effect on mitochondrial complex I-linked oxygen consumption (Fig. 4A, B).

Complex I is a multiprotein enzyme consisting of more than 40 subunits. In ageing and cellular senescence, incompletely assembled subcomplexes of complex I accumulate and contribute to cellular ROS production (Miwa et al., 2014). Decreased efficacy of mitophagy in senescence and ageing is a possible cause of this accumulation (Dalle Pezze et al., 2014; Korolchuk et al., 2017). Therefore, we next tested whether metformin at therapeutic concentrations might be able to rescue the low mitophagy activity in senescence, using rapamycin as a positive control. Surprisingly, low metformin concentrations did not improve mitophagy (Fig. 5B, C). In agreement with this, they did not reduce mitochondrial ROS production as measured by MitoSOX fluorescence (Fig 5D) and did not rescue low mitochondrial coupling (Fig. 5E) in senescence, suggesting a non-mitochondrial pathway for reduction of ROS by therapeutic metformin concentrations. Suppression of NOX4 was identified as a mechanism by which low metformin reduces senescence-associated ROS production and SASP (Fig. 6). It had been shown that metformin suppresses NOX4 induction via activation of AMPK both at concentrations as high as 10 mM (Sato et al., 2016) and as low as 0.1 mM (Shi & Hou, 2021). However, protective effects of metformin against the radiation mimetic doxorubicin were only observed at low concentrations due to the suppression of platelet-derived growth factor receptor (PDGFR) expression by high metformin (Kobashigawa, Xu, Padbury, Tseng, & Yano, 2014). In vivo, high metformin doses shortened the lifespan of mice (Palliyaguru et al., 2020). Other receptor tyrosine kinases including FGFR1 have also been involved in the cellular responses to metformin (Shi et al., 2021). In low concentrations, metformin was able to suppress oxidative stress-associated senescence of adipose-derived stromal cells via activation of AMPK, but it is unclear whether this was NOX-dependent (Le Pelletier et al., 2021). A more detailed analysis of the network of signaling pathways mediating NOX4 suppression by low metformin is clearly warranted but remains outside the scope of the present study.

Our study has a number of limitations. Whole body irradiation is an over-simplified model for therapeutic irradiation of tumour patients. However, experiments with localised radiation to the brain have also shown improvements in cognition immediately after senolytic intervention (Yabluchanskiy et al., 2020). Moreover, senolytic intervention with D+Q after irradiation targeted to a single leg resulted in long-term improvements of muscle function (Zhu et al., 2015). These, together with our results, strongly suggest that senolytic or senostatic interventions could be effective against progressive frailty, multimorbidity and mortality even in realistic radiation therapy situations. We have now established a more realistic mouse model for targeted brain tumour radiation therapy. Pilot phenotyping results show progressive frailty development together with

cognitive decline not dissimilar to the effects of whole-body irradiation, and results of an intervention study will be published as soon as possible.

Ageing as a trait shows strong sexual dimorphism in many species including mice (Bronikowski et al., 2022) and man (Hagg & Jylhava, 2021). Unsurprisingly, both lifespan- (Nadon, Strong, Miller, & Harrison, 2017) and healthspan-extending interventions (Selman et al., 2009) frequently have sx-dependent efficacies. It is therefore important to test the impact of senolytic/senostatic interventions post-irradiation in both males and females. This could not be done in the present cohorts due to funding restrictions but will be done in the near future.

Furthermore, we studied mice that were irradiated as young adults, and our results would thus be most directly transferable to adolescent tumour survivors. However, frailty, cognitive decline and multimorbidity are specifically important problems in childhood tumour survivors. Moreover, relatively few comprehensive data are available about premature ageing phenotypes in the largest patient group, those who developed tumours at old age. Severity of radiation effects and efficacy of interventions might well be different in both the very young and the very old. Studies over a wide age range in mice should be performed in the future, using more realistic therapy models.

In conclusion, we have shown that short senolytic or senostatic interventions can effectively rescue premature progressive frailty and accelerated ageing induced by whole body irradiation over a significant part of the life history in male mice. We believe these results warrant further efforts to translate senolytic and senostatic interventions towards an adjuvant therapy for long-term tumour survivors.

502

503 **Materials and Methods**

504

Key Resources Table				
Reagent type (species) or resource	**Designation**	**Source or reference**	**Identifiers**	**Additional information**
strain, strain background (Mus musculus, male)	Wild-type	Charles River	C57BL/6	
cell line (Homo Sapiens)	Human foetal lung, male	ECACC	MRC5, Cat-Nr. 05072101	
antibody	Anti-HMGB1 (Rabbit monoclonal)	Abcam	Cat# ab79823, RRID:AB_1603373	(1:250)
antibody	Anti-TOMM20 (Mouse monoclonal)	Abcam	Cat# ab56783, RRID:AB_945896	(1:200)
antibody	Anti-Iba-1 (Rabbit monoclonal)	Abcam	Cat# ab178846, RRID:AB_2636859	(1:2000)
antibody	Anti-LMNB1 (Rabbit polyclonal)	Abcam	Cat# ab16048, RRID:AB_443298	(1:200)
antibody	Anti-NOX4 (Rabbit monoclonal)	Abcam	Cat# ab109225, RRID:AB_10861375	IF (1:200) WB (1:2000)
antibody	Anti-IL6 (Mouse monoclonal)	Abcam	Cat# ab9324, RRID:AB_307175	(1:500)

antibody	Anti-p21 (Rabbit monoclonal)	Abcam	Cat# ab109520, RRID:AB_10860537	(1:100)
antibody	Anti-Phosphor-Histone H2AX (Rabbit monoclonal)	Cell Signalling Technology	Cat# 9718, RRID:AB_2118009	(1:250)
antibody	Anti-Beta-Actin (Rabbit monoclonal)	Cell Signalling Technology	Cat# 5125, RRID:AB_1903890	WB (1:1000)
recombinant DNA reagent	pCHAC-mt-mKeima	Addgene	Cat-Nr. #72342	
recombinant DNA reagent	pcDNA3.1-hNOX4	Addgene	Cat-Nr. #69352	
recombinant DNA reagent	pcDNA3.1(+)eGFP	Addgene	Cat-Nr. #129020	
commercial assay or kit	Human Cytokine Array Proinflammatory focused 13-plex Assay	Eve Technologies	HDF13	
commercial assay or kit	Mouse High Sensitivity 18-Plex Discovery Assay	Eve Technologies	MDHSTC18	
commercial assay or kit	eBioscience™ Foxp3/Transcription Factor Staining Buffer Set	ThermoFisher	00-5523-00	
chemical compound, drug	Dasatinib	Merck	CDS023389	
chemical compound, drug	Quercetin	Merck	#1592409	

chemical compound, drug	Navitoclax	Stratech	#285063-USB	
chemical compound, drug	Metformin HCL API	Pharmahispania		
chemical compound, drug	Polyethylenglycol 400	Merck	#8074851000	

Study design

This study addressed the hypothesis that premature frailty and accelerated ageing after sublethal irradiation are caused by accelerated accumulation of senescent cells triggered by bystander signalling from radiation-induced senescence, and that thus a short treatment with either a senolytic or the senostatic metformin would be protective. A series of controlled laboratory experiments were performed to determine the progression of frailty and other markers of biological age following irradiation with and without intervention at prespecified time points. All studies were conducted at Newcastle University in agreement with ARRIVE guidelines (Kilkenny, Browne, Cuthill, Emerson, & Altman, 2010). On the basis of previous work, two-sided two-sample test were used to generate animal group sizes. Incorporating expected attrition rates during long-term follow-up, this resulted in group sizes of 12 animals at start of the experiments for physiological phenotyping. Data collection was performed at prespecified time points unless limited by animal distress as identified by facility staff and/or veterinary surgeons. Primary and secondary end points were prespecified. Each mouse represented one experimental unit. Mice were coded with randomized allocation to experimental groups and housing cages. Data collection, tissue collection and tissue analyses were done by staff members blinded to experimental group allocation with unblinding performed only after data acquisition was complete. For ex-vivo assessments, power calculations informed by previous experience indicated a minimum number of 5 animals per group. Tissues were either randomly selected or all available tissues were used for analysis.

To address the mechanism of senostatic activity of metformin in therapeutically achievable concentration, a stepwise series of controlled laboratory in vitro experiments was performed, where experimental outcomes guided alternative hypotheses. Individual cell culture dishes represented experimental replicates except in the case of mitophagy experiments, where each cell was treated as a biological unit. Again, *in vitro* treatments were coded and codes were broken only after data collection and analysis. *In vitro* experiments were independently reproduced at least three times.

Animals

Male C57Bl/6J mice were bought past weaning from Charles River and were maintained in groups of six littermates per cage as described (Cameron, Miwa, Walker, & von Zglinicki, 2012). The mice were fed standard pelleted food (CRM-P formulation rodent diet, SDS Diets), except those used for metformin treatment and their control, which received soaked food (same as above) with or without metformin from one-month post-IR. Mice were sacrificed at the end of the study by cervical

dislocation and tissues harvested, and stored in 4% paraformaldehyde for 24 hours for paraffin embedding, or frozen in liquid nitrogen. The work was licensed by the UK Home Office (PB048F3A0) and complied with the guiding principles for the care and use of laboratory animals.

Irradiation

At 5 months of age, mice were sub-lethally irradiated thrice (NDT320, 225kV) with 3 Gy of X-ray irradiation, with two days of recovery between each dose, as described (Fielder et al., 2019). Mice received 1% Baytril solution in drinking water for 2 days before, and for 14 days after, to the start and end of irradiation, respectively.

Senolytic and senostatic treatments

Mice were orally gavaged with either 5mg/kg/day dasatinib and 50mg/k/day quercetin or with 5mg/kg/day Navitoclax for 10 days total (5 days, 2 days recovery, and 5 days). Compounds were prepared for oral gavage in 10% Polyethylene Glycol (PEG400). Control mice were gavaged with PEG400 only. Interventions were started at 1 month post-irradiation for the early intervention group, and 7 months post-irradiation for the late intervention group. Dasatinib (CDS023389), quercetin (1592409), and PEG400 (8074851000) were purchased from Sigma-Aldrich (now Merck). Navitoclax (285063-USB) was purchased from Stratech.

Metformin hydrochloride was a kind gift from FARMHISPANIA, (Barcelona) and prepared at 1g/kg in dry food (0.1% (w/w) in food) and provided at 6mg/6ml water in 6g food per mouse in the cage as soaked food. The control group also received soaked food without metformin. Treatment was started at 1 month post-irradiation and was given daily for 10 weeks.

Mouse phenotyping

Frailty was assessed regularly using a 30-parameter index based on (Whitehead et al., 2014), with modifications as described in (Fielder et al., 2019). Rotarod, wire hanging and spontaneous alternation Y-Maze were performed as described in (Fielder et al., 2019). Tumour incidence at death was assessed by gross pathological examination.

Immuno-histochemistry (IHC) and immunofluorescence

Paraformaldehyde (PFA)-fixed paraffin embedded tissue samples were cut and stained with primary and secondary antibodies as detailed in Table 1, see also (Fielder et al., 2020) for a step-by-step protocol. Fixed cells were blocked with 2% normal goat serum + 0.1% BSA and stained overnight with the primary antibody at 4C (Tab 1).

Immuno-fluorescence in situ hybridisation (immuno-FISH)

The Immuno-FISH for telomere associated foci (TAF) were performed as previously described (Hewitt et al., 2012), (Fielder et al., 2020) with the following modifications for quadriceps: The blocking step used 1% BSA, 5% Normal Goat Serum in PBS, for 30 minutes at 30°C. Fluorescein Avidin DCS was substituted with Texas Red-labelled Avidin DCS (Vector Laboratories) in PBS for 30 minutes at 30°C. CCCTAA Cy-3 probe was substituted for TTAGGG probe (Pangene).

Microscopy and image analysis

IHC images were taken using a widefield light microscope ECLIPSE E800 (Nikon, Japan) at total magnification of 100x. Microscopy for IF and immuno-FISH was performed using a DMi8 fluorescence microscope (Leica, Germany) with total magnification of 400x for IF and 630x (with Z-stack/depth) for immuno-FISH.

Positive and negative nuclei were manually identified by observers blinded to the treatment groups, counted on 5 images per animal and the average was calculated as the individual value for the sample/animal. Nuclear size was manually measured with ImageJ software (NIH, USA).

Epidermal thickness was measured on 3 μm back skin sections stained with Picro-sirius red/fast green. 3 different regions were imaged per animal, and 25 measurements were taken in each region using the straight-line tool in ImageJ.

To identify TAF in brain, the colocalisation of DNA damage foci and telomeres were detected manually and confirmed in Icy software through 3D image setup as described (Hewitt et al., 2012), (Fielder et al., 2020). For liver and muscle, detection and 3D location of DNA damage foci and telomeres was automated using Icy software (Institut Pasteur & France Bioimaging, France). A Python programme was used to assess their colocalization. Results from this automated counting were validated against manual counts in individual liver and muscle sections.

Western blotting

Cells were collected using Accutase (StemCell Technologies #07922) and lysed using RIPA buffer supplemented with protease inhibitors. Western blotting was performed as described (Miwa et al., 2014) with antibodies against NOX4 and β-Actin as detailed in Table 1.

Liver function assessment

Liver function was assessed using the Alanine Transaminase Activity Assay Kit (Abcam, ab105134) and Aspartate Aminotransferase Activity Assay Kit (Abcam, ab105135) according to the manufacturer's instructions. Average of duplicates was used as individual data of a sample/animal, and then the data were grouped by treatment types and compared.

Cell culture

Human lung MRC5 fibroblasts were grown in Dulbecco's modified Eagle's medium (DMEM, Sigma, # D5671) supplemented with 10% heat-inactivated foetal Bovine Serum (FBS, Sigma), 100 units/ml penicillin, 100 μg/ml streptomycin and 2 mM L-glutamine at 37°C in a humidified atmosphere with 5% CO_2. Stress-induced senescence was induced by X-ray irradiation with 20 Gy or (for DPI experiments) with 200μM H_2O_2 in serum-free medium.

For metformin treatment, medium was replaced with fresh medium containing 100μM metformin or DMSO (vehicle control) immediately post irradiation. Treatment was maintained for 10 days, with medium changes every 3 days.

For NOX4 overexpression, pcDNA3.1-hNOX4 (Addgene #69352) was used, with pcDNA3.1(+)eGFP (Addgene #129020) as control. Plasmids were extracted using the EndoFree Plasmid Maxi Kit (Qiagen 12362). 80% confluence MRC5 cells (PD 15-25) were transfected using 500ng of plasmid per well with Lipofectamine 3000 (ThermoFisher L3000001). For selection, cells were grown for one week in G418 (400μg/ml) from the 3rd day post-transfection and fixed with 4% PFA for staining.

For NOX4 inhibition, senescent MRC5 cells treated with diphenyleneiodonium chloride (DPI, Bio-Techne 4673-26-1 at either 50nM, 10nM or DMSO control) for 3 days.

For Sen-β-Gal staining, cells were fixed for 5 min with 2% PFA in PBS-Mg before incubation with the staining solution (PBS-Mg containing 1mg/ml X-gal, 5mM potassium ferrocyanide and 5mM potassium ferricyanide, pH 5.5) overnight at 37C.

Mitophagy measurement

Neonatal human dermal fibroblasts (HDFns) were transduced with lentiviruses containing pCHAC-mt-mKeima (Addgene plasmid #72342) (Lazarou et al., 2015). Cells were irradiated with 20Gy X-ray radiation and the mt-mKeima signal was measured up to 3 days later. During this time cells were treated with metformin (100 µM) or rapamycin (10nM). The live-cell mt-mKeima signal was captured on a Leica DMi8 inverted microscope with a 63x oil objective. Numbers of red dots per cell, indicating lysosomal mt-mKeima signal were quantified using ImageJ.

ROS measurements

Cells were stained with dihydroethidium (DHE, ThermoFisher Scientific) to measure intracellular peroxides or with MitoSOX (ThermoFisher Scientific) to assess mitochondrial superoxide. Cells were incubated with either 10 µM DHE or 5 µM MitoSOX for 30 min at 37°C in the dark and analysed by flow cytometry or in a DMi8 fluorescence microscope (Leica).

Extracellular release of hydrogen peroxide was measured by Amplex Red assay (ThermoFisher Scientific) as described (Miwa et al., 2016) in a 96 well plate using a fluorescent plate reader (FLUOstar Omega, BMG Labtech) at excitation 544nm and emission 590 nm at 37°C.

Oxygen consumption rates

Cellular oxygen consumption rates (OCR) and media acidification rates (extracellular acidification rate, ECAR) in intact cells were measured in parallel using a Seahorse XF24 analyzer in unbuffered basic media (DMEM, Sigma, #D5030) supplemented with 5mM glucose, 2mM L-Glutamine and 3% FBS. Whilst the measurements were taken, the following compounds were injected to test mitochondrial activity and cellular bioenergetics: Oligomycin (0.5µM) to inhibit ATP synthase, carbonyl cyanide p-trifluoromethoxy-phenylhydrazone (FCCP) (2.5µM), a respiratory chain uncoupler, 2-deoxyglucose (2DG) (80mM), a glucose analogue competitively inhibiting glucose uptake and glycolytic flux, and Rotenone (0.5µM) and Antimycin (2.5µM), mitochondrial complex I and complex III inhibitors, respectively. Data analysis to calculate absolute ATP production rates was carried out using the methods described by Mookerjee and Brand (Mookerjee & Brand, 2015) taking into account the acidification rates due to mitochondrial CO_2 production (Birket et al., 2011; Brand, 2005).

Permeabilised cells were used to measure mitochondrial oxygen consumption rates using Pyruvate (10mM) and Malate (1mM) as complex I-linked substrate. Cells were permeabilised using Plasma membrane permeabiliser (PMP, Agilent Technologies) according to manufacturer's instructions, and oxygen consumption was measured in medium containing 220mM Mannitol, 70mM Sucrose, 10mM KH_2PO_4, 5mM $MgCl_2$, 2mM Hepes, 1mM EGTA and 0.2% (w/v) Fatty Acid Free BSA. To determine the effects of metformin on mitochondrial complex I activity, sequential additions of metformin (at concentrations as indicated in Figure 4A), Rotenone (0.5µM), Succinate (4mM), and FCCP (4µM) were made. For determination of Respiratory Control Ratio (RCR), permeabilised cells respiring with Pyruvate (10mM) and Malate (1mM) received 4mM ATP (State 3) followed by 0.5µM Oligomycin (State 4). RCR was calculated as state 3 divided by state 4 respiration rates.

Cytokine measurement

Cytokines secreted from MRC5 cells were analysed by Human Cytokine Array Proinflammatory focused 13-plex Assay (Eve Technologies, Calgary, Canada). The cells were grown in 75cm flasks, and the culture media was switched to serum free media for 24 hours and the media samples were collected for the analysis. Mouse serum was collected from the supernatant of whole blood after

centrifugation at 0.4g for 4 minutes and analysed using the Mouse High Sensitivity 18-Plex Discovery Assay (Eve Technologies, Calgary, Canada).

Mass Cytometry

Markers for multiple stress response pathways (Table 2) were analysed at single cell level simultaneously by mass cytometry (Helios, Fluidigm). MRC5 cells were treated with either 2mM or 0.1 mM metformin for 2 days. Positive controls were challenged with either 300 µM H_2O_2 in serum-free medium, heat shock (50°C for 45 min) or starvation (serum-free medium for 24 h). The cells were trypsinized, washed in PBS, and stained with metal-conjugated antibodies (Table 2). Antibodies were either pre-conjugated (Fluidigm), or purified antibodies were conjugated to lanthanide metals using the Maxpar antibody labeling kit (as per manufacturer's instructions; DVS Sciences) and were stabilised with an antibody stabilisation solution (Candor Bioscience) (Table 2). Cells were stained as described (Cytlak et al., 2020). Briefly, cells were first stained with 2.5µM Cisplatin (Fluidigm #201064) for 5 minutes in PBS for live/dead cell discrimination and washed promptly using Wash buffer (PBS containing 2% FBS). Then the cells were fixed using 1.6% formaldehyde in a working fixation buffer (eBioscience Foxp 3 fixation permeabilisation kit, ThermoFisher Scintific #00-5523) for 30 minutes, and washed twice with eBioscience perm buffer. Cells were stained in perm buffer for 1hr with the antibody cocktail containing each intracellular antibody (approximately 0.5µg in 100µl per sample) for 1 hour at room temperature and washed twice with PBS. Finally the cells were fixed with 1.6% formaldehyde in PBS with a nuclear marker, 125nM iridium (Cell-ID™ Intercalator-Ir, Fluidigm #201192B) for 1 hour, and washed using Wash buffer for overnight storage at 4°C. Prior to CyTOF acquisition, cells were washed twice in 200 µL MilliQ water (600xg for 5 minutes), counted, diluted to a maximum final concentration of $0.55x10^6$/ml in MilliQ water and filtered through a 40 µm filter (BD). EQ beads were added (10% by volume) and $0.1x10^6$ cells per sample were acquired on the Helios mass cytometer running CyTOF software v 6.7.1014. The data were analysed using FCS Express 7 (De Novo Software).

Statistics

Data were analysed with Microsoft Excel and Prism software (GraphPad). Values were expressed either as means with error bars representing SDs or as boxplots with median, upper and lower quartiles (boxes) and percentiles (whiskers). Graphs were overlaid with the values of all individual biological replicates. Linear regressions and survival curves show means and 95% confidence intervals. Depending on results of normality testing, groups were compared using unpaired t test, Mann-Whitney or One-Way Analysis of Variance with Tukey post-hoc test. Statistical significance is indicated as *p<0.05, **p<0.01, ***p<0.001, **** p<0.0001.

Acknowledgements

This study was supported by Cancer Research UK (www.cancerresearchuk.org) Pioneer Award C12161/A24009 and P&G/BBSRC (www.bbsrc.ukri.org) grant BB/S006710/1 to TvZ, an MRC – Arthritis Research UK, Centre for Integrated Research into Musculoskeletal Ageing (www.cimauk.org) Translation grant and UK SPINE Bridge (www.kespine.org.uk) grant B06 to SM and TvZ, a P&G/BBSRC DTP (www.bbsrc.ukri.org/skills/investing-doctoral-training/dtp) studentship (BH174490) to VIK and a BBSRC DTP (www.bbsrc.ukri.org/skills/investing-doctoral-training/dtp) studentship to DJ. The funders had no role in study design, data collection and analysis, decision to publish, or preparation of the manuscript. We thank the Comparative Biology Centre at Newcastle University, in particular Mr. Christopher Huggins, for their expert support with animal husbandry, Drs Andrew Filby and David McDonald at Flow Cytometry Core Facility, Newcastle University for their expert support with CyTOF experiments, and Dr I Karakesisoglou and Dr P Chazot, Durham University, for their support in early supervision of MW.

Figure legends:

Fig. 1: Short-term senolytic interventions rescue irradiation-induced accelerated ageing. A) Layout of the experiment. B) Frailty index vs mouse age for non-irradiated (Non-IR, black), irradiated (IR, red), and irradiated plus treated with either D+Q (green) or Navitoclax (blue) mice. Irradiation and treatment times are indicated by vertical lines. Dots indicate FI for individual mice, regression lines and 95% confidence intervals are indicated by bold and dotted lines, respectively. Individual frailty scores are enlarged for clarity in Figure 1- supplement 1. C) Wire Hanging Test results (% success) under the indicated treatments and ages. D) Maximum speed achieved on Rotarod under the indicated treatments and ages. E) Short-term memory assessed as spontaneous alternation in a Y maze under the indicated treatments. F) ALT activity in plasma at 16 months. G) Tumour prevalence at death. Data are from 12 mice per group at start with attrition to 8-10 mice over the course of the experiment.

Fig. 2: Late senolytic interventions partially block further progression of irradiation-induced accelerated ageing. A) Layout of the experiment. B) Frailty index vs mouse age for non-irradiated (Non-IR, black), irradiated (IR, red), and irradiated plus treated with either D+Q (green) or Navitoclax (blue) mice. Irradiation and treatment times are indicated by vertical lines. Dots indicate FI for individual mice, regression lines and 95% confidence intervals are indicated by bold and dotted lines, respectively. . Individual scores are enlarged for clarity in Figure 2- supplement 1. C) Wire Hanging Test results (% success) under the indicated treatments. D) Maximum speed achieved on Rotarod under the indicated treatments at 14 months of age. E) Short-term memory assessed as spontaneous alternation in a Y maze under the indicated treatments. F) ALT activity in serum, 16 months old. G) Tumour prevalence at death. Data are from 12 mice per group at start with attrition to 8-10 mice over the course of the experiment.

Fig. 3: A short-term intervention with the senostatic metformin rescues irradiation-induced accelerated ageing. A) Outline of the experiment. Animals were irradiated at 5 months of age and treated with either soaked food (controls) or metformin in soaked food (Met) from 6 months of age for 10 weeks. B) Frailty index vs mouse age for non-irradiated (no IR, black), irradiated (IR, red), and irradiated plus treated with metformin (blue) mice. Irradiation and treatment times are indicated by vertical lines. Dots indicate FI for individual mice, regression lines and 95% confidence intervals are indicated by bold and dotted lines, respectively. Individual scores are enlarged for clarity in Figure 3-supplement 1. C) Wire Hanging Test results (% success) under the indicated treatments and ages. D) Maximum speed achieved on Rotarod under the indicated treatments and ages. E) Short-term memory assessed as spontaneous alternation in a Y maze under the indicated treatments. F) ALT activity in plasma at 16 months of age. G) Tumour prevalence at death. Data are from 12 mice per group at start with attrition to 8-10 mice over the course of the experiment.

Fig. 4. At therapeutic concentrations, metformin reduces ROS and SASP but not by inhibition of complex I. A) Mitochondrial oxygen consumption rate of permeabilised MRC5 human fibroblasts treated sequentially (at timepoint indicated by arrow) with various concentrations of metformin (Met), 0.5µM rotenone (Rot), 4mM Succinate (Suc) and 2.5µM FCCP. M± SD, n=4. B) ATP production rate by Oxidative phosphorylation (OXPHOS) and glycolysis in young and senescent MRC5 human fibroblasts treated for 10 days with the indicated metformin concentrations. M± SD, n=4. C) Impact of metformin in the indicated concentrations on ROS production measured by AR in human fibroblasts. Cells were induced to senescence by IR and treated with metformin for 10 days. M± SD, N=3. D) Impact of rapamycin and metformin on ROS levels in human fibroblasts measured by DHE fluorescence in FACS. Left: representative FL3 histograms. Light blue: young, red: senescent (10d past IR), purple: senescent + 0.1mM metformin, black: senescent + 10nM rapamycin. Right: Average

DHE fluorescence intensities. M± SD, n=5. E) Cytokine concentrations in the supernatant of human fibroblasts. N= 2. Senescent fibroblasts were treated with the indicated metformin concentrations for 10 days. Source data are provided as Figure 4 -Source data 1.

Fig. 5. Low concentrations of metformin do not improve mitochondrial turnover and function. A) Impact of high (2mM) and low (100µM) concentrations of metformin on stress response pathways in human fibroblasts. CyTOF with the indicated antibodies was performed on human MRC5 fibroblasts treated for 2 days with the indicated interventions. Heat map colour codes indicate strong decrease (dark blue), mild decrease (light blue), no change (white), light increase (amber) or strong increase (red) as exemplified in Figure 5 – figure supplement 1. Data are pooled from two independent experiments. B) Dermal fibroblasts expressing mt-mKeima were irradiated with 20Gy and treated with either 100µM Metformin or 10nM Rapamycin for 3 days. Red fluorescence indicates mitochondria engulfed in lysosomes. C) Number of mitophagy events per cell. Dermal fibroblasts expressing mt-mKeima were irradiated with 20Gy and treated with either 100µM Metformin or 10nM Rapamycin for the indicated times. N= 196 – 271 cells per condition pooled from 3 biological repeats. D) Impact of rapamycin and metformin on mitochondrial superoxide levels in human fibroblasts either young or at 10d after IR measured (Sen) by MitoSOX fluorescence in FACS. N=5. E) Respiratory Control Ratio (RCR) of mitochondria in fibroblasts at 10d after IR treated with the indicated concentrations of metformin. N≥3.

Fig. 6. Low concentrations of metformin reduce ROS in senescence via suppression of NOX4. A) Human fibroblasts were irradiated with 20Gy and treated with 100µM Metformin for 10 days. Left: representative images of cells treated as indicated, red: NOX4 immunofluorescence, Blue: DAPI. Right: Quantification of NOX4 fluorescence intensity. B) Left: Representative NOX4 Western blot. Cells treated as above. A complete blot is provided as Figure 6 – Source data 1. Right: Average NOX4 signal intensity, normalised to total protein. C) Left: Sen-β-Gal staining in EGFP- and NOX4-overexpressing fibroblasts. Right: Average frequencies of Sen-β-Gal-positive cells. D) Left: DHE staining in EGFP- and NOX4-overexpressing fibroblasts. DHE fluorescence in red, cells visualised in phase contrast. Right: Average DHE fluorescence intensity per cell. E) Co-staining for NOX4 (red) and IL-6 (green) on EGFP- or NOX4-transfected fibroblasts. Right: Fluorescence intensity levels for EGFP (top), NOX4 (middle) and IL-6 in EGFP- and NOX4-transfected cells. F) Correlation between cellular NOX4 and IL6 fluorescence signals in NOX4-transfected cells. G) Correlation between cellular EGFP and IL6 fluorescence signals in EGFP-transfected cells. H) Left: Sen-β-Gal staining in senescent fibroblasts treated with the indicated concentrations of DPI. Right: Frequencies of Sen-β-Gal-positive cells. I) Left: DHE staining in senescent fibroblasts treated with the indicated concentrations of DPI. DHE fluorescence in red, cells visualised in phase contrast. Right: Average intensity of DHI fluorescence per cell. All experiments N≥3.

Supplementary Figures

Figure 1 – Figure supplement 1. Enlarged for Clarity A-D) Frailty index vs mouse age for A) non-irradiated (no IR, black), B) irradiated (IR, orange), and irradiated plus treated with an early intervention of either C) D+Q (green) or D) navitoclax (blue) mice. Dots at 50% opacity indicate FI for individual mice, regression lines and 95% confidence intervals are indicated by bold and narrow dotted lines, respectively. Darker dots indicate multiple animals with the same frailty index score.

Figure 1 – Figure supplement 2. Components of the frailty index (FI). Colours represent the mean FI of all animals alive at that given point (8 – 12 animals/group). Arrows indicate components that were improved under the interventions.

Figure 1 – Figure supplement 3. Impact of interventions on epidermal thickness. A) Epidermal thickness decreases in old (median age 32months) as compared to young adult (median age 10 months) mice. B) IR at 5 months of age results in increased epidermal thickness at 12 months. C) Treatment of irradiated mice with senolytics D+Q or Navitoclax at 7 months of age does not change epidermal thickness at 16 months of age. Data are from at least 7 animals/group.

Figure 1 – Figure supplement 4. Validation of senescence markers in liver. (A-F) Irradiated vs sham-irradiated mice at 12 months of age. A) nuclear area, B) Frequency of karyomegalic hepatocytes. C) HMGB1 immunohistochemistry. Left: representative HMGB1 micrographs (left: control, right: 7months past IR). Right: Frequencies of HMGB1-negative hepatocytes. D) TAF assay. Left: Representative TAF immunoFISH image (single focal plane, arrowhead indicates overlap of a telomere (red) with a γH2AX focus (green), e.g. TAF). Right: Average TAF frequency per hepatocyte nucleus. E) Frequency of TAF-positive hepatocytes. F) Frequency of hepatocytes with at least 3 TAF. (G-K) Young adult (8-14 months) vs old (32 months) mice. Nuclear area (G), frequencies of karyomegalic hepatocytes (H), frequencies of HMGB1-negative hepatocytes (I), TAF frequency per nucleus (J) and Frequency of hepatocytes with at least 1 TAF (K). Data are from at least 6 animals/group.

Figure 1-figure supplement 5. Impact of early senolytics treatment on hepatocyte senescence at late age (16 months). Nuclear size (A), percentage of karyomegalic hepatocytes (B), percentage of HMGB1-negative hepatocytes (C), TAF frequency per nucleus (D), frequency of TAF-positive cells and (E) frequency of cells with at least 3 TAF (F) in mice livers at 16 months of age, irradiated at 5 months and treated with either D+Q, Navitoclax or sham gavage at 6 months. Data are from at least 6 animals/group.

Figure 1 – Figure supplement 6. Senescence and neuroinflammation markers in hippocampus after early senolytic intervention. Neuron nuclear area in CA1 (A) and CA3 (B). C,D) Left: LaminB1 Immunostaining (green) in CA1 (C) and CA3 (D) regions of the hippocampus under the different treatments. Blue: DAPI. Arrowheads indicate Lmn1-positive (red) and –negative (white) nuclei. Right: Frequencies of laminB1-negative neurons in CA1 (top) and CA3 (bottom). E) TAF ImmunoFISH of neurons in the CA1 area. Left: Higher magnification of a single TAF (single plane image) and intensity scans for green (gH2AX) and red (telomere) fluorescence. Right: Maximum intensity projections. Frequencies of TAF-positive neurons in CA1 (F) and CA3 (H). Frequencies of neurons with at least 3 TAF in CA1 (G) and CA3 (I). Iba1+ cell density in CA1 (J) and CA3 (K). Iba1+ cell soma size in CA1 (L) and CA3 (M). Data are from at least 6 animals/group.

Figure 1 – Figure supplement 7. Functional and senescence markers in skeletal muscle after early intervention with D+Q or Navitoclax. Muscle fibre cross-sectional area in oxidative (A) and non-oxidative (B) fibres from irradiated mice at 16 months of age. Frequencies of p21-positive myonuclei in oxidative (C) and glycolytic (D) fibres. E) TAF frequencies in myonuclei. Data are from at least 5 animals/group.

Figure 1 – supplement 8. Cytokine/chemokine concentrations in serum of mice at 16 months of age as measured by cytokine array. Concentrations were measured by cytokine array (Eve Technologies) and z-scored. Four peptides in the array were not significant above background in any

mouse and were excluded. There are no significant differences for any peptide between treatment groups.

Figure 2 – Figure supplement 1. Enlarged for Clarity. Frailty indices vs mouse age for irradiated plus treated with a late intervention of either A) D+Q (green) or B) navitoclax (blue) mice. Dots at 50% opacity indicate FI for individual mice, regression lines and 95% confidence intervals are indicated by bold and narrow dotted lines, respectively. Darker dots indicate multiple animals with the same frailty index score.

Figure 2 – Figure supplement 2. Late intervention with either D+Q or Navitoclax (at 12 months of age) does not change epithelial thickness at 16 months. Data are from at least 7 animals/group.

Figure 2-figure supplement 3. Impact of late senolytics treatment on senescence markers in liver. Nuclear size (A), percentage of karyomegalic hepatocytes (B), percentage of HMGB1-negative hepatocytes (C), TAF frequency per nucleus (D), frequency of TAF-positive cells and (E) frequency of cells with at least 3 TAF (F) in mice livers at 16 months of age, irradiated at 5 months and treated with either D+Q, Navitoclax or sham gavage at 12 months. Data are from at least 6 animals/group.

Figure 2-figure supplement 4. Functional and senescence markers in skeletal muscle after late intervention with D+Q or Navitoclax. Muscle fibre cross-sectional area in oxidative (A) and non-oxidative (B) fibres from irradiated mice after late intervention at 16 months of age. C) TAF frequencies in myonuclei at 16 months of age after late senolytic intervention. Data are from at least 5 animals/group.

Figure 2 – Figure supplement 5. Impact of late intervention on neuroinflammation. Iba1+ cell density in CA1 (A) and CA3 (C). Iba1+ cell soma size in CA1 (B) and CA3 (D). Data are from at 5 -6 animals/group.

Figure 3 – Figure supplement 1. Enlarged for Clarity. Frailty index vs mouse age for mice that were irradiated and fed Metformin in soaked food. Dots at 50% opacity indicate FI for individual mice, regression lines and 95% confidence intervals are indicated by bold and narrow dotted lines, respectively. Darker dots indicate multiple animals with the same frailty index score.

Figure 3 – Figure supplement 2. Treatment of irradiated mice for 2.5 months with metformin (starting at 7 months of age) tends to reduce epidermal thickness at late age (16 months). Data are from at least 6 animals/group.

Figure 3 – Figure supplement 3. Impact of metformin on senescence markers in liver. Mice were irradiated at 5 months of age and treated with metformin for 10 weeks starting at 6 months of age. A) Nuclear size with representative images (left, blue DAPI, green autofluorescence) and quantification (right). B) Frequency of karyomegalic hepatocytes. C) Frequency of hepatocytes negative for nuclearHMGB1. D) TAF frequency per nucleus. E) Frequency of hepatocytes with at least one TAF. F) Frequency of hepatocytes with at least 3 TAF. Data are from at least 6 animals per group at 16 months of age.

Figure 3 – Figure supplement 4. Senescence and neuroinflammation markers in hippocampus after intervention with metformin. A) Neuron nuclear area in CA1 (top) and CA3 (bottom). B) Frequencies of laminB1-negative neurons in CA1 (top) and CA3 (bottom). C) Frequencies of TAF-positive neurons in CA1 (top) and CA3 (bottom). D) Frequencies of neurons with at least 3 TAF in CA1 (top) and CA3

(bottom). E) Iba1+ cell density in CA1 (top) and CA3 (bottom). F) Iba1+ cell soma size in CA1 (top) and CA3 (bottom). Data are from at 5 -6 animals/group.

Figure 3 -Figure supplement 5. Impact of metformin on hind limb muscle. Myofibre cross-sectional area of oxidative (A) and non-oxidative (B) fibres. C) Frequencies of TAF-positive myonuclei. Data are from at least 8 animals per group at 16 months of age.

Figure 3 – supplement 6. Cytokine/chemokine concentrations in serum of mice at 16 months of age as measured by cytokine array. Concentrations were measured by cytokine array (Eve Technologies) and z-scored. Four peptides in the array were not significant above background in any mouse and were excluded. Significant differences (t-test) are indicated as $p < 0.05$ (*) and $p=0.10$ (+).

Figure 5 – Figure supplement 1. Representative histogram overlay examples for use of CyTOF as stress pathway identifier. Treatments are indicated on the left. Colour codes at the bottom represent strong decrease (dark blue), mild decrease (light blue), no change (white), light increase (amber) or strong increase (red) and correspond to the heatmap in Fig. 5A.

Figure 6 – Figure supplement 1. NOX4 does not co-localise with mitochondria. Senescent MRC5 fibroblasts, representative double staining with Nox4 (green) and TOMM20 (red). Blue: DAPI.

References:

Aravinthan, A. D., & Alexander, G. J. M. (2016). Senescence in chronic liver disease: Is the future in aging? *J Hepatol, 65*(4), 825-834.

Baar, M. P., Brandt, R. M., Putavet, D. A., Klein, J. D., Derks, K. W., Bourgeois, B. R., et al. (2017). Targeted Apoptosis of Senescent Cells Restores Tissue Homeostasis in Response to Chemotoxicity and Aging. *Cell, 169*(1), 132-147 e116.

Birket, M. J., Orr, A. L., Gerencser, A. A., Madden, D. T., Vitelli, C., Swistowski, A., et al. (2011). A reduction in ATP demand and mitochondrial activity with neural differentiation of human embryonic stem cells. *J Cell Sci, 124*(Pt 3), 348-358.

Blagosklonny, M. V. (2017). From rapalogs to anti-aging formula. *Oncotarget, 8*(22), 35492-35507.

Bluethmann, S. M., Mariotto, A. B., & Rowland, J. H. (2016). Anticipating the "Silver Tsunami": Prevalence Trajectories and Comorbidity Burden among Older Cancer Survivors in the United States. *Cancer epidemiology, biomarkers & prevention : a publication of the American Association for Cancer Research, cosponsored by the American Society of Preventive Oncology, 25*(7), 1029-1036.

Brand, M. D. (2005). The efficiency and plasticity of mitochondrial energy transduction. *Biochem Soc Trans, 33*(Pt 5), 897-904.

Bray, F., Ferlay, J., Soerjomataram, I., Siegel, R. L., Torre, L. A., & Jemal, A. (2018). Global cancer statistics 2018: GLOBOCAN estimates of incidence and mortality worldwide for 36 cancers in 185 countries. *CA Cancer J Clin, 68*(6), 394-424.

Bronikowski, A. M., Meisel, R. P., Biga, P. R., Walters, J. R., Mank, J. E., Larschan, E., et al. (2022). Sex-specific aging in animals: Perspective and future directions. *Aging Cell, 21*(2), e13542.

Bussian, T. J., Aziz, A., Meyer, C. F., Swenson, B. L., van Deursen, J. M., & Baker, D. J. (2018). Clearance of senescent glial cells prevents tau-dependent pathology and cognitive decline. *Nature, 562*(7728), 578-582.

Cameron, K. M., Miwa, S., Walker, C., & von Zglinicki, T. (2012). Male mice retain a metabolic memory of improved glucose tolerance induced during adult onset, short-term dietary restriction. *Longev Healthspan, 1*, 3.

Campbell, J. M., Bellman, S. M., Stephenson, M. D., & Lisy, K. (2017). Metformin reduces all-cause mortality and diseases of ageing independent of its effect on diabetes control: A systematic review and meta-analysis. *Ageing Res Rev, 40*, 31-44.

Chandra, A., Lagnado, A. B., Farr, J. N., Monroe, D. G., Park, S., Hachfeld, C., et al. (2020). Targeted Reduction of Senescent Cell Burden Alleviates Focal Radiotherapy-Related Bone Loss. *J Bone Miner Res, 35*(6), 1119-1131.

Chang, J., Wang, Y., Shao, L., Laberge, R. M., Demaria, M., Campisi, J., et al. (2016). Clearance of senescent cells by ABT263 rejuvenates aged hematopoietic stem cells in mice. *Nat Med, 22*(1), 78-83.

Coppe, J. P., Desprez, P. Y., Krtolica, A., & Campisi, J. (2010). The senescence-associated secretory phenotype: the dark side of tumor suppression. *Annu Rev Pathol, 5*, 99-118.

Cupit-Link, M. C., Kirkland, J. L., Ness, K. K., Armstrong, G. T., Tchkonia, T., LeBrasseur, N. K., et al. (2017). Biology of premature ageing in survivors of cancer. *ESMO Open, 2*(5), e000250.

Cytlak, U., Resteu, A., Pagan, S., Green, K., Milne, P., Maisuria, S., et al. (2020). Differential IRF8 Transcription Factor Requirement Defines Two Pathways of Dendritic Cell Development in Humans. *Immunity, 53*(2), 353-370 e358.

da Silva, P. F. L., Ogrodnik, M., Kucheryavenko, O., Glibert, J., Miwa, S., Cameron, C., et al. (2019). The bystander effect contributes to the accumulation of senescent cells in vivo. *Aging Cell, 18*, e12848.

Dalle Pezze, P., Nelson, G., Otten, E. G., Korolchuk, V. I., Kirkwood, T. B., von Zglinicki, T., et al. (2014). Dynamic modelling of pathways to cellular senescence reveals strategies for targeted interventions. *PLoS Comput Biol, 10*(8), e1003728.

957 Damlaj, M., El Fakih, R., & Hashmi, S. K. (2019). Evolution of survivorship in lymphoma, myeloma and
958 leukemia: Metamorphosis of the field into long term follow-up care. *Blood Rev, 33*, 63-73.
959 Davalos, A. R., Kawahara, M., Malhotra, G. K., Schaum, N., Huang, J., Ved, U., et al. (2013). p53-
960 dependent release of Alarmin HMGB1 is a central mediator of senescent phenotypes. *J Cell*
961 *Biol, 201*(4), 613-629.
962 Demaria, M. (2017). Senescent cells: New target for an old treatment? *Mol Cell Oncol, 4*(3),
963 e1299666.
964 Demaria, M., O'Leary, M. N., Chang, J., Shao, L., Liu, S., Alimirah, F., et al. (2017). Cellular Senescence
965 Promotes Adverse Effects of Chemotherapy and Cancer Relapse. *Cancer Discov, 7*(2), 165-
966 176.
967 Fielder, E., Tweedy, C., Wilson, C., Oakley, F., LeBeau, F. E. N., Passos, J. F., et al. (2020). Anti-
968 inflammatory treatment rescues memory deficits during aging in nfkb1(-/-) mice. *Aging Cell,*
969 *19*(10), e13188.
970 Fielder, E., Weigand, M., Agneessens, J., Griffin, B., Parker, C., Miwa, S., et al. (2019). Sublethal
971 whole-body irradiation causes progressive premature frailty in mice. *Mech Ageing Dev, 180*,
972 63-69.
973 Fontana, L., Nehme, J., & Demaria, M. (2018). Caloric restriction and cellular senescence. *Mech*
974 *Ageing Dev, 176*, 19-23.
975 Gorgoulis, V. G., Adams, P. D., Alimonti, A., Bennett, D. C., Bischof, O., Bishop, C., et al.
976 (2019). Cellular Senescence: Defining a path forward. *Cell, 179*, 813-827.
977 Goy, C., Czypiorski, P., Altschmied, J., Jakob, S., Rabanter, L. L., Brewer, A. C., et al. (2014). The
978 imbalanced redox status in senescent endothelial cells is due to dysregulated Thioredoxin-1
979 and NADPH oxidase 4. *Exp Gerontol, 56*, 45-52.
980 Hagg, S., & Jylhava, J. (2021). Sex differences in biological aging with a focus on human studies. *Elife,*
981 *10*.
982 Hewitt, G., Jurk, D., Marques, F. D., Correia-Melo, C., Hardy, T., Gackowska, A., et al. (2012).
983 Telomeres are favoured targets of a persistent DNA damage response in ageing and stress-
984 induced senescence. *Nat Commun, 3*, 708.
985 Hudgins, A. D., Tazearslan, C., Tare, A., Zhu, Y., Huffman, D., & Suh, Y. (2018). Age- and Tissue-
986 Specific Expression of Senescence Biomarkers in Mice. *Front Genet, 9*, 59.
987 Jena, B. C., Das, C. K., Bharadwaj, D., & Mandal, M. (2020). Cancer associated fibroblast mediated
988 chemoresistance: A paradigm shift in understanding the mechanism of tumor progression.
989 *Biochim Biophys Acta Rev Cancer, 1874*(2), 188416.
990 Jurk, D., Wilson, C., Passos, J. F., Oakley, F., Correia-Melo, C., Greaves, L., et al. (2014). Chronic
991 inflammation induces telomere dysfunction and accelerates ageing in mice. *Nat Commun, 2*,
992 4172.
993 Katayama, H., Kogure, T., Mizushima, N., Yoshimori, T., & Miyawaki, A. (2011). A sensitive and
994 quantitative technique for detecting autophagic events based on lysosomal delivery. *Chem*
995 *Biol, 18*(8), 1042-1052.
996 Kilkenny, C., Browne, W. J., Cuthill, I. C., Emerson, M., & Altman, D. G. (2010). Improving bioscience
997 research reporting: the ARRIVE guidelines for reporting animal research. *PLoS Biol, 8*(6),
998 e1000412.
999 Kobashigawa, L. C., Xu, Y. C., Padbury, J. F., Tseng, Y. T., & Yano, N. (2014). Metformin protects
1000 cardiomyocyte from doxorubicin induced cytotoxicity through an AMP-activated protein
1001 kinase dependent signaling pathway: an in vitro study. *PLoS One, 9*(8), e104888.
1002 Kojima, G., Iliffe, S., & Walters, K. (2018). Frailty index as a predictor of mortality: a systematic
1003 review and meta-analysis. *Age Ageing, 47*(2), 193-200.
1004 Korolchuk, V. I., Miwa, S., Carroll, B., & von Zglinicki, T. (2017). Mitochondria in Cell Senescence: Is
1005 Mitophagy the Weakest Link? *EBioMedicine, 21*, 7-13.

Lazarou, M., Sliter, D. A., Kane, L. A., Sarraf, S. A., Wang, C., Burman, J. L., et al. (2015). The ubiquitin kinase PINK1 recruits autophagy receptors to induce mitophagy. *Nature, 524*(7565), 309-314.

Le, O. N., Rodier, F., Fontaine, F., Coppe, J. P., Campisi, J., DeGregori, J., et al. (2010). Ionizing radiation-induced long-term expression of senescence markers in mice is independent of p53 and immune status. *Aging Cell, 9*(3), 398-409.

Le Pelletier, L., Mantecon, M., Gorwood, J., Auclair, M., Foresti, R., Motterlini, R., et al. (2021). Metformin alleviates stress-induced cellular senescence of aging human adipose stromal cells and the ensuing adipocyte dysfunction. *Elife, 10*.

Lener, B., Koziel, R., Pircher, H., Hutter, E., Greussing, R., Herndler-Brandstetter, D., et al. (2009). The NADPH oxidase Nox4 restricts the replicative lifespan of human endothelial cells. *Biochem J, 423*(3), 363-374.

Lopez-Otin, C., Galluzzi, L., Freije, J. M. P., Madeo, F., & Kroemer, G. (2016). Metabolic Control of Longevity. *Cell, 166*(4), 802-821.

Martin-Montalvo, A., Mercken, E. M., Mitchell, S. J., Palacios, H. H., Mote, P. L., Scheibye-Knudsen, M., et al. (2013). Metformin improves healthspan and lifespan in mice. *Nat Commun, 4*, 2192.

Miwa, S., Jow, H., Baty, K., Johnson, A., Czapiewski, R., Saretzki, G., et al. (2014). Low abundance of the matrix arm of complex I in mitochondria predicts longevity in mice. *Nat Commun, 5*, 3837.

Miwa, S., Treumann, A., Bell, A., Vistoli, G., Nelson, G., Hay, S., et al. (2016). Carboxylesterase converts Amplex red to resorufin: Implications for mitochondrial H2O2 release assays. *Free Radic Biol Med, 90*, 173-183.

Moiseeva, O., Deschenes-Simard, X., St-Germain, E., Igelmann, S., Huot, G., Cadar, A. E., et al. (2013). Metformin inhibits the senescence-associated secretory phenotype by interfering with IKK/NF-kappaB activation. *Aging Cell, 12*(3), 489-498.

Mookerjee, S. A., & Brand, M. D. (2015). Measurement and Analysis of Extracellular Acid Production to Determine Glycolytic Rate. *J Vis Exp*(106), e53464.

Musi, N., Valentine, J. M., Sickora, K. R., Baeuerle, E., Thompson, C. S., Shen, Q., et al. (2018). Tau protein aggregation is associated with cellular senescence in the brain. *Aging Cell, 17*(6), e12840.

Mylonas, K. J., O'Sullivan, E. D., Humphries, D., Baird, D. P., Docherty, M. H., Neely, S. A., et al. (2021). Cellular senescence inhibits renal regeneration after injury in mice, with senolytic treatment promoting repair. *Sci Transl Med, 13*(594).

Nadon, N. L., Strong, R., Miller, R. A., & Harrison, D. E. (2017). NIA Interventions Testing Program: Investigating Putative Aging Intervention Agents in a Genetically Heterogeneous Mouse Model. *EBioMedicine, 21*, 3-4.

Nelson, G., Kucheryavenko, O., Wordsworth, J., & von Zglinicki, T. (2018). The senescent bystander effect is caused by ROS-activated NF-kappaB signalling. *Mech Ageing Dev, 170*, 30-36.

Nelson, G., Wordsworth, J., Wang, C., Jurk, D., Lawless, C., Martin-Ruiz, C., et al. (2012). A senescent cell bystander effect: senescence-induced senescence. *Aging Cell, 11*(2), 345-349.

Ness, K. K., Kirkland, J. L., Gramatges, M. M., Wang, Z., Kundu, M., McCastlain, K., et al. (2018). Premature Physiologic Aging as a Paradigm for Understanding Increased Risk of Adverse Health Across the Lifespan of Survivors of Childhood Cancer. *J Clin Oncol, 36*(21), 2206-2215.

Ness, K. K., Krull, K. R., Jones, K. E., Mulrooney, D. A., Armstrong, G. T., Green, D. M., et al. (2013). Physiologic frailty as a sign of accelerated aging among adult survivors of childhood cancer: a report from the St Jude Lifetime cohort study. *J Clin Oncol, 31*(36), 4496-4503.

Ogrodnik, M., Evans, S. A., Fielder, E., Victorelli, S., Kruger, P., Salmonowicz, H., et al. (2021). Whole-body senescent cell clearance alleviates age-related brain inflammation and cognitive impairment in mice. *Aging Cell, 20*(2), e13296.

Ogrodnik, M., Miwa, S., Tchkonia, T., Tiniakos, D., Wilson, C. L., Lahat, A., et al. (2017). Cellular senescence drives age-dependent hepatic steatosis. *Nat Commun, 8*, 15691.

Ogrodnik, M., Zhu, Y., Prata, L., Tchkonia, T., Krueger, P., Fielder, E., et al. (2018). Obesity-Induced Cellular Senescence Drives Anxiety-Like Behavior Via Impaired Neurogenesis. *Cell Metabolism, 29*, 1061-1077.

Orszaghova, Z., Mego, M., & Chovanec, M. (2021). Long-Term Cognitive Dysfunction in Cancer Survivors. *Front Mol Biosci, 8*, 770413.

Palacio, L., Goyer, M. L., Maggiorani, D., Espinosa, A., Villeneuve, N., Bourbonnais, S., et al. (2019). Restored immune cell functions upon clearance of senescence in the irradiated splenic environment. *Aging Cell, 18*(4), e12971.

Palacio, L., Krishnan, V., Le, N. L., Sharpless, N. E., & Beausejour, C. M. (2017). Sustained p16(INK4a) expression is required to prevent IR-induced tumorigenesis in mice. *Oncogene, 36*(9), 1309-1314.

Palliyaguru, D. L., Minor, R. K., Mitchell, S. J., Palacios, H. H., Licata, J. J., Ward, T. M., et al. (2020). Combining a High Dose of Metformin With the SIRT1 Activator, SRT1720, Reduces Life Span in Aged Mice Fed a High-Fat Diet. *J Gerontol A Biol Sci Med Sci, 75*(11), 2037-2041.

Palmer, A. K., Xu, M., Zhu, Y., Pirtskhalava, T., Weivoda, M. M., Hachfeld, C. M., et al. (2019). Targeting senescent cells alleviates obesity-induced metabolic dysfunction. *Aging Cell, 18*(3), e12950.

Passos, J. F., Nelson, G., Wang, C., Richter, T., Simillion, C., Proctor, C. J., et al. (2010). Feedback between p21 and reactive oxygen production is necessary for cell senescence. *Mol Syst Biol, 6*, 347.

Passos, J. F., Saretzki, G., Ahmed, S., Nelson, G., Richter, T., Peters, H., et al. (2007). Mitochondrial dysfunction accounts for the stochastic heterogeneity in telomere-dependent senescence. *PLoS Biol, 5*(5), e110.

Rezende, F., Schurmann, C., Schutz, S., Harenkamp, S., Herrmann, E., Seimetz, M., et al. (2017). Knock out of the NADPH oxidase Nox4 has no impact on life span in mice. *Redox Biol, 11*, 312-314.

Robison, L. L., & Hudson, M. M. (2014). Survivors of childhood and adolescent cancer: life-long risks and responsibilities. *Nat Rev Cancer, 14*(1), 61-70.

Rockwood, K., Mitnitski, A., & Howlett, S. E. (2015). Frailty: Scaling from Cellular Deficit Accumulation? *Interdiscip Top Gerontol Geriatr, 41*, 1-14.

Saleh, T., Tyutyunyk-Massey, L., & Gewirtz, D. A. (2019). Tumor Cell Escape from Therapy-Induced Senescence as a Model of Disease Recurrence after Dormancy. *Cancer Res, 79*(6), 1044-1046.

Sato, N., Takasaka, N., Yoshida, M., Tsubouchi, K., Minagawa, S., Araya, J., et al. (2016). Metformin attenuates lung fibrosis development via NOX4 suppression. *Respir Res, 17*(1), 107.

Schafer, M. J., White, T. A., Iijima, K., Haak, A. J., Ligresti, G., Atkinson, E. J., et al. (2017). Cellular senescence mediates fibrotic pulmonary disease. *Nature communications, 8*, 14532.

Selman, C., Tullet, J. M., Wieser, D., Irvine, E., Lingard, S. J., Choudhury, A. I., et al. (2009). Ribosomal protein S6 kinase 1 signaling regulates mammalian life span. *Science, 326*(5949), 140-144.

Selvarani, R., Mohammed, S., & Richardson, A. (2021). Effect of rapamycin on aging and age-related diseases-past and future. *Geroscience, 43*(3), 1135-1158.

Seol, M. A., Jung, U., Eom, H. S., Kim, S. H., Park, H. R., & Jo, S. K. (2012). Prolonged expression of senescence markers in mice exposed to gamma-irradiation. *J Vet Sci, 13*(4), 331-338.

Shi, Y., & Hou, S. A. (2021). Protective effects of metformin against myocardial ischemiareperfusion injury via AMPKdependent suppression of NOX4. *Mol Med Rep, 24*(4).

Shi, Y., Ma, Z., Cheng, Q., Wu, Y., Parris, A. B., Kong, L., et al. (2021). FGFR1 overexpression renders breast cancer cells resistant to metformin through activation of IRS1/ERK signaling. *Biochim Biophys Acta Mol Cell Res, 1868*(1), 118877.

Short, S., Fielder, E., Miwa, S., & von Zglinicki, T. (2019). Senolytics and senostatics as adjuvant tumour therapy. *EBioMedicine, 41*, 683-692.
Tarantini, S., Balasubramanian, P., Delfavero, J., Csipo, T., Yabluchanskiy, A., Kiss, T., et al. (2021). Treatment with the BCL-2/BCL-xL inhibitor senolytic drug ABT263/Navitoclax improves functional hyperemia in aged mice. *Geroscience, 43*(5), 2427-2440.
te Poele, R. H., Okorokov, A. L., Jardine, L., Cummings, J., & Joel, S. P. (2002). DNA damage is able to induce senescence in tumor cells in vitro and in vivo. *Cancer Res, 62*(6), 1876-1883.
von Zglinicki, T. (2021). Mechanisms of cell senescence in aging. In N. Musi & P. Hornsby (Eds.), *Handbook of the Biology of Aging* (9th ed., pp. 53-68): Academic Press.
Wang, C., Maddick, M., Miwa, S., Jurk, D., Czapiewski, R., Saretzki, G., et al. (2010). Adult-onset, short-term dietary restriction reduces cell senescence in mice. *Aging (Albany NY), 2*(9), 555-566.
Wang, C. P., Lorenzo, C., Habib, S. L., Jo, B., & Espinoza, S. E. (2017). Differential effects of metformin on age related comorbidities in older men with type 2 diabetes. *J Diabetes Complications, 31*(4), 679-686.
Weyemi, U., Lagente-Chevallier, O., Boufraqech, M., Prenois, F., Courtin, F., Caillou, B., et al. (2012). ROS-generating NADPH oxidase NOX4 is a critical mediator in oncogenic H-Ras-induced DNA damage and subsequent senescence. *Oncogene, 31*(9), 1117-1129.
Whitehead, J. C., Hildebrand, B. A., Sun, M., Rockwood, M. R., Rose, R. A., Rockwood, K., et al. (2014). A clinical frailty index in aging mice: comparisons with frailty index data in humans. *J Gerontol A Biol Sci Med Sci, 69*(6), 621-632.
Wilcock, C., & Bailey, C. J. (1994). Accumulation of metformin by tissues of the normal and diabetic mouse. *Xenobiotica, 24*(1), 49-57.
Wilson, W. H., O'Connor, O. A., Czuczman, M. S., LaCasce, A. S., Gerecitano, J. F., Leonard, J. P., et al. (2010). Navitoclax, a targeted high-affinity inhibitor of BCL-2, in lymphoid malignancies: a phase 1 dose-escalation study of safety, pharmacokinetics, pharmacodynamics, and antitumour activity. *Lancet Oncol, 11*(12), 1149-1159.
Xu, M., Pirtskhalava, T., Farr, J. N., Weigand, B. M., Palmer, A. K., Weivoda, M. M., et al. (2018). Senolytics improve physical function and increase lifespan in old age. *Nat Med*, doi: 10.1038/s41591-41018-40092-41599.
Yabluchanskiy, A., Tarantini, S., Balasubramanian, P., Kiss, T., Csipo, T., Fulop, G. A., et al. (2020). Pharmacological or genetic depletion of senescent astrocytes prevents whole brain irradiation-induced impairment of neurovascular coupling responses protecting cognitive function in mice. *Geroscience, 42*(2), 409-428.
Zhu, Y., Tchkonia, T., Fuhrmann-Stroissnigg, H., Dai, H. M., Ling, Y. Y., Stout, M. B., et al. (2016). Identification of a novel senolytic agent, navitoclax, targeting the Bcl-2 family of anti-apoptotic factors. *Aging Cell, 15*(3), 428-435.
Zhu, Y., Tchkonia, T., Pirtskhalava, T., Gower, A. C., Ding, H., Giorgadze, N., et al. (2015). The Achilles' heel of senescent cells: from transcriptome to senolytic drugs. *Aging Cell, 14*(4), 644-658.
Zou, Y., Sfeir, A., Gryaznov, S. M., Shay, J. W., & Wright, W. E. (2004). Does a sentinel or a subset of short telomeres determine replicative senescence? *Mol Biol Cell, 15*(8), 3709-3718.

Tables

Table 1: Immunostaining and blotting methods

Tissue	Thickness	Technique	Primary antibody	Cat No, vendor	Dilution	Secondary antibody	Cat No, vendor	Dilution	Detection
Liver	3	IF	Rabbit anti-HMGB1	Ab79823 (Abcam)	1:250	Goat Anti-Rabbit IgG H&L, Texas Red	Ab6719 (Abcam)	1:500	
	3	IF	Mouse anti-TOMM20	Ab56783 (Abcam)	1:200	Goat anti-mouse (Alexa Fluor 594)	Ab150116	1:1000	
Quads	3	IF	Rabbit anti-HMGB1	Ab79823 (Abcam)	1:250	Goat anti-rabbit (Alexa Fluor 594)	A32740 (Thermo Fisher)	1:1000	
Brain	10	IHC	Rabbit anti-Iba1	Ab178846 (Abcam)	1:2000	Biotinylated Goat anti-rabbit	BA-1000 (Vector labs)	1:250	VECTASTAIN ABC-HRP Kit, NovaRED (Vevtor labs)
	3	IF	Rabbit anti-γH2A.X primary antibody	9718 (Cell Signalling)	1:250	Biotinylated Goat anti-rabbit	BA-1000 (Vector labs)	1:250	Fluorescein Avidin DCS (1:500) (Vector labs)
	3	IF	Rabbit anti-Lamin B1	ab16048 (Abcam)	1:200	Biotinylated Goat anti-rabbit	BA-1000 (Vector labs)	1:250	Fluorescein Avidin DCS (1:500) (Vector labs)
MRC5 Cells	ICC		Anti-NADPH oxidase 4 antibody	ab109225 (Abcam)	1:200	Goat Anti-Rabbit IgG H&L (Alexa Fluor® 594)	ab150080 (Abcam)	1:1000	
			Anti-IL6 antibody	ab9324 (Abcam)	1:500	Anti-Mouse IgG (H+L) Alexa Fluor 488	A-11017 (vector labs)	1:1000	
			Rabbit anti-p21	ab109520 (Abcam)	1:100	Goat Anti-Rabbit IgG H&L (Alexa Fluor® 594)	ab150080 (Abcam)	1:1000	

		Rabbit anti-HMGB1	ab79823 (Abcam)	1:250	Goat Anti-Rabbit IgG H&L (Alexa Fluor® 594)	ab150080 (Abcam)	1:1000	
Protein	WB	Anti-NADPH oxidase 4 antibody	ab109225 (Abcam)	1:2000	Goat Anti-Rabbit IgG H&L (HRP)	ab6721 (Abcam)	1:10000	
		Anti-β-Actin antibody	5125 (Cell Signaling)	1:1000	Goat Anti-Rabbit IgG H&L (HRP)	ab6721 (Abcam)	1:10000	

Table 2. List of metal conjugated antibodies for stress response pathway analysis by CyTOF

Antibody	Metal	cat #	Vendor
SOD2/MnSOD [9E2BD2]	176Yb	ab110300	Abcam
GSTM2 (9E975)	167Er	H00002946-M03	Novus Biologicals
HSF1	153Eu	825801	BioLegend
Hsp-70 (2A4)	154Sm	ab5442	Abcam
Nrf2 (phospho S40) [EP1809Y]	142Nd	ab180844	Abcam
NR1L2/PXR (6H11D8)	164Dy	LS-C682408-LSP	Stratech Scientific Ltd.
GRP78 BiP [EPR4041(2)]	161Dy	ab108615	Abcam
EIF2S1 (phospho S51) (E90)	169Tm	ab214434	Abcam
ATF-6 (-Carboxy terminal end)	175Lu	ab62576	Abcam
GADD153/CHOP	141Pr	NBP2-13172	Novus Biologicals
CLPP [EPR7133]	165Ho	ab236064	Abcam
Hsp-60 (LK1)	144Nd	ab212454	Abcam
pS6 [S235/S236]	172Yb	3172008A	Fluidigm
p21 Waf1/Cip1	159Tb	3159026A	Fluidigm
Phospho-Acetyl-CoA Carboxylase (Ser79) (10HCLC)	170Er	711289	ThermoFisher
p62 / SQSTM1 (C-terminus)	146Nd	GP62-C	Progen
p-p38 [T180/Y182]	156Gd	3156002A	Fluidigm
DNA/RNA damage	173Yb	ab62623	Abcam
pHistone H2A.X [Ser139]	147Sm	NB100-384	Novus Biologicals
PHB	151Eu	NBP2-32305	Novus Biologicals
p16INK4	174Yb	ab54210	Abcam
Cell-ID™ Intercalator-Ir—500µM		201192B	Fluidigm

A)

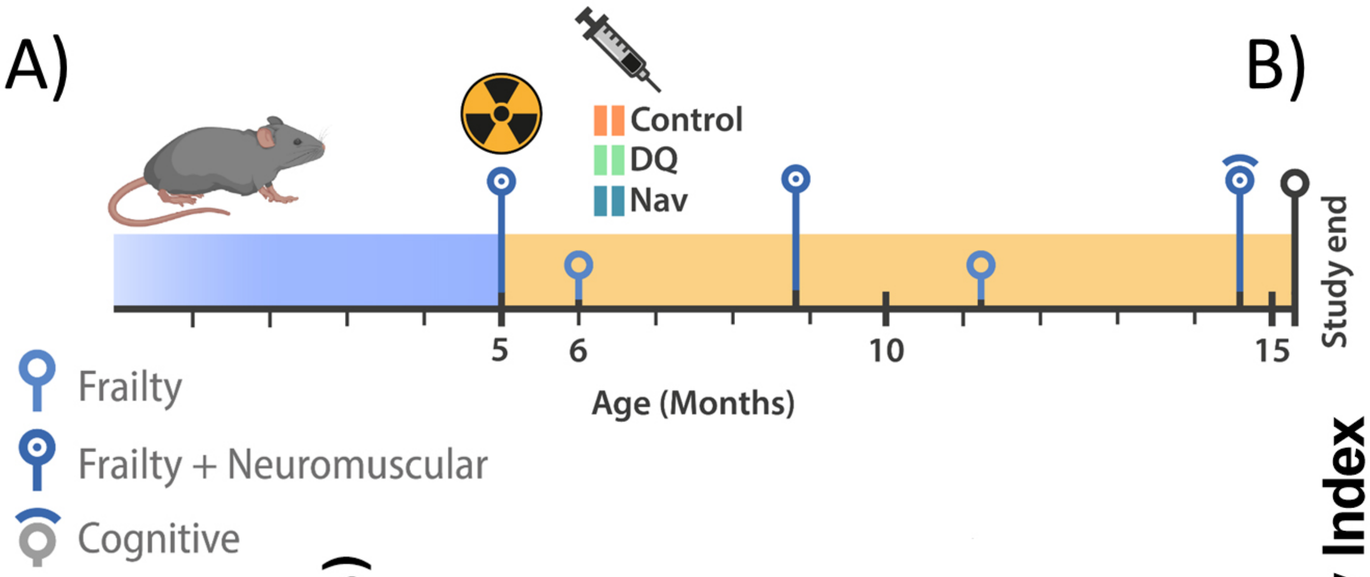

B)

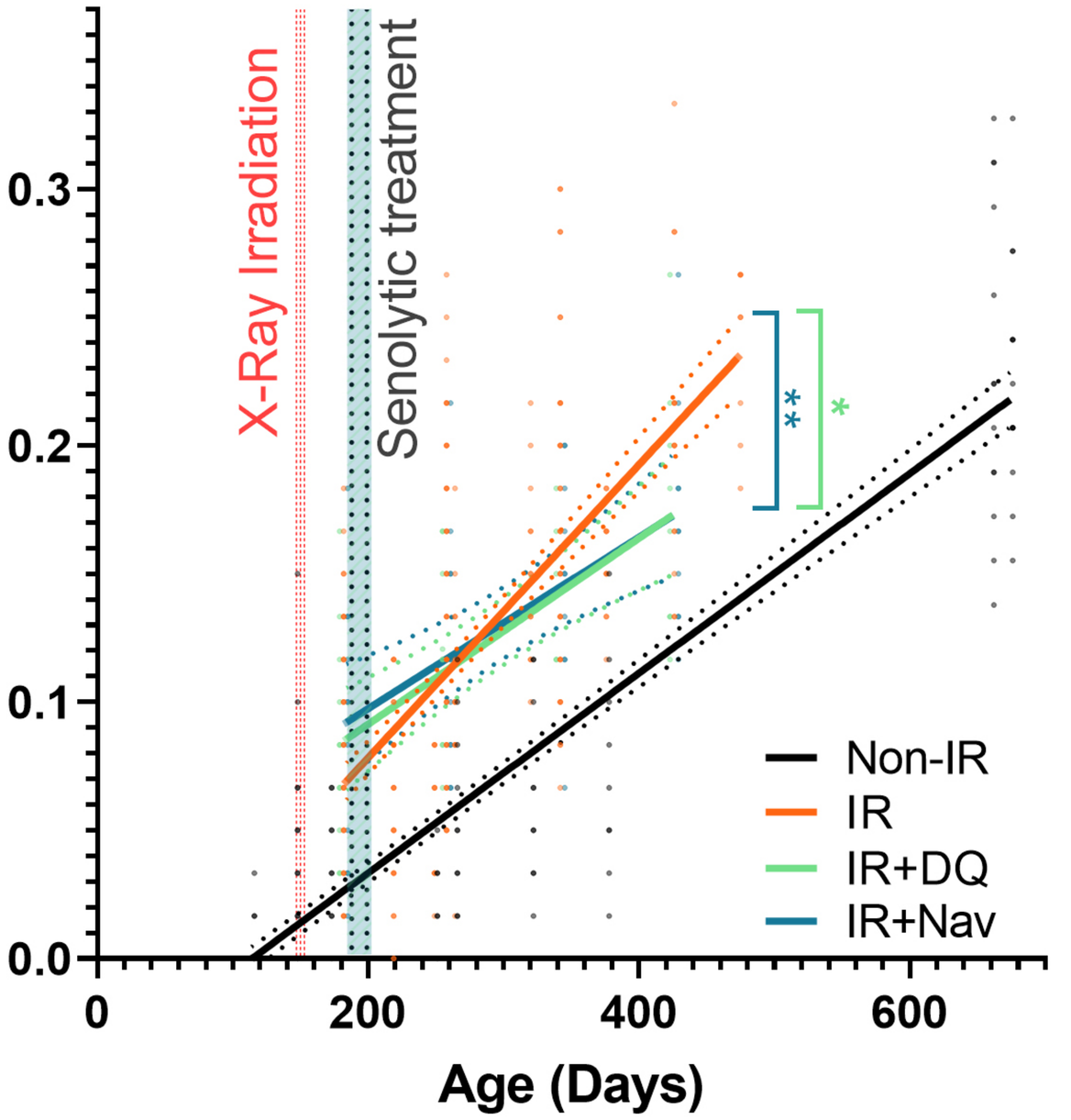

C)

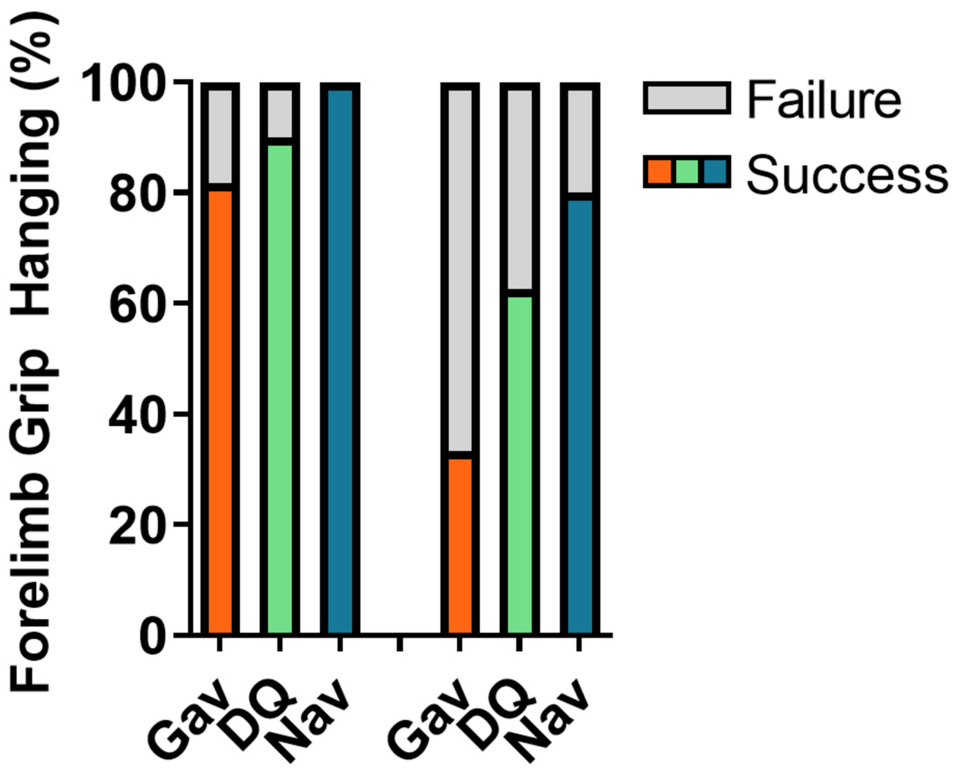

Age (months): 9m 15m

D)

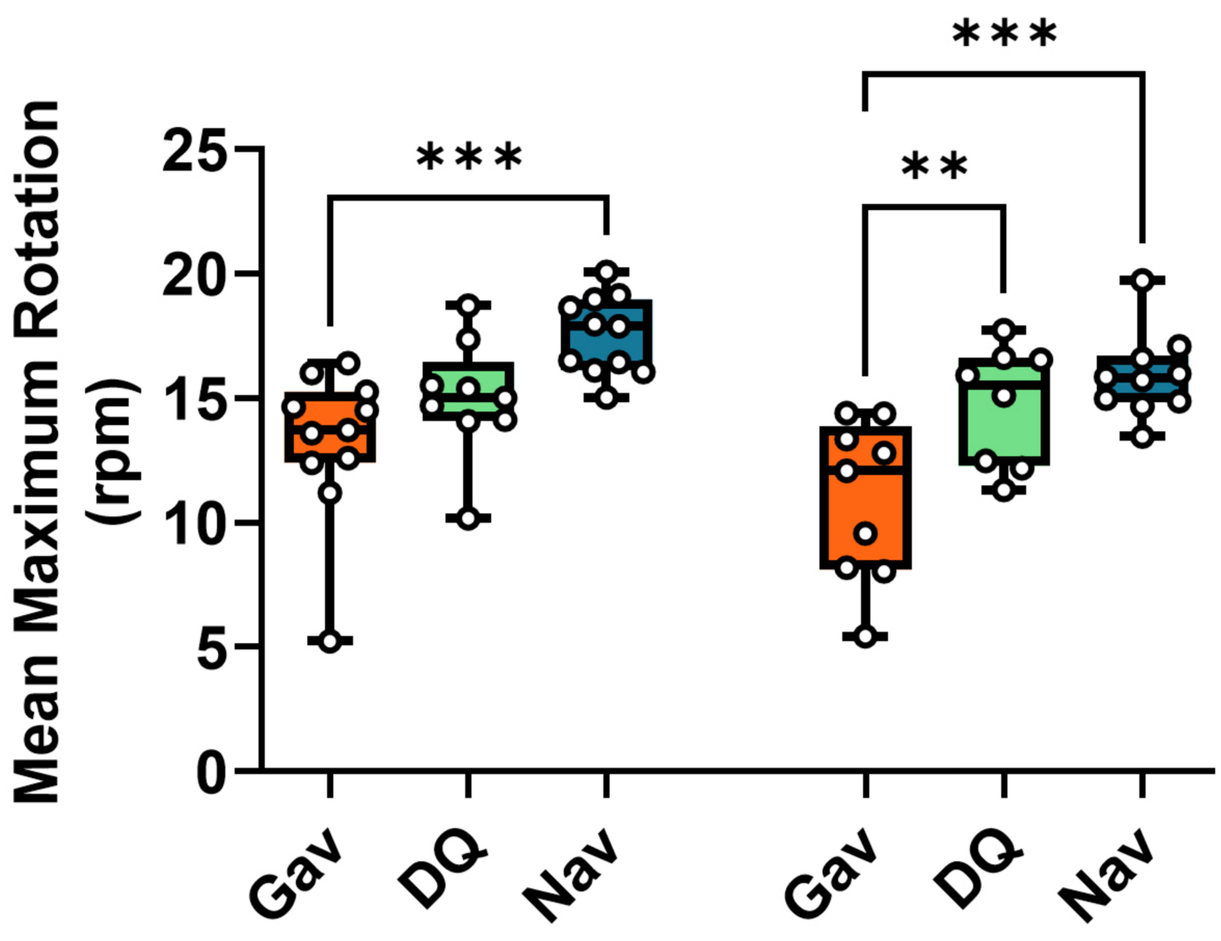

Age (months): 9m 15m

E)

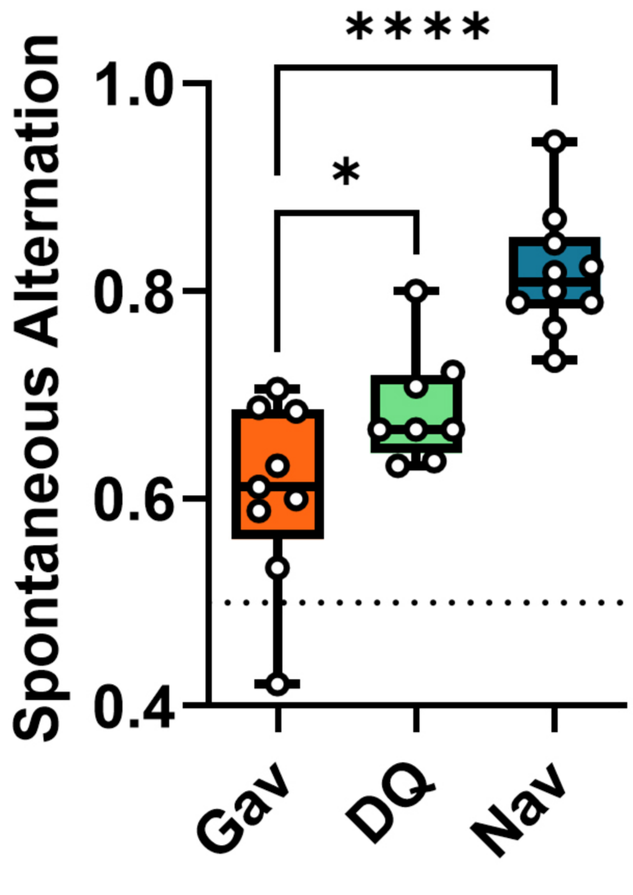

Age (months): 15m

F)

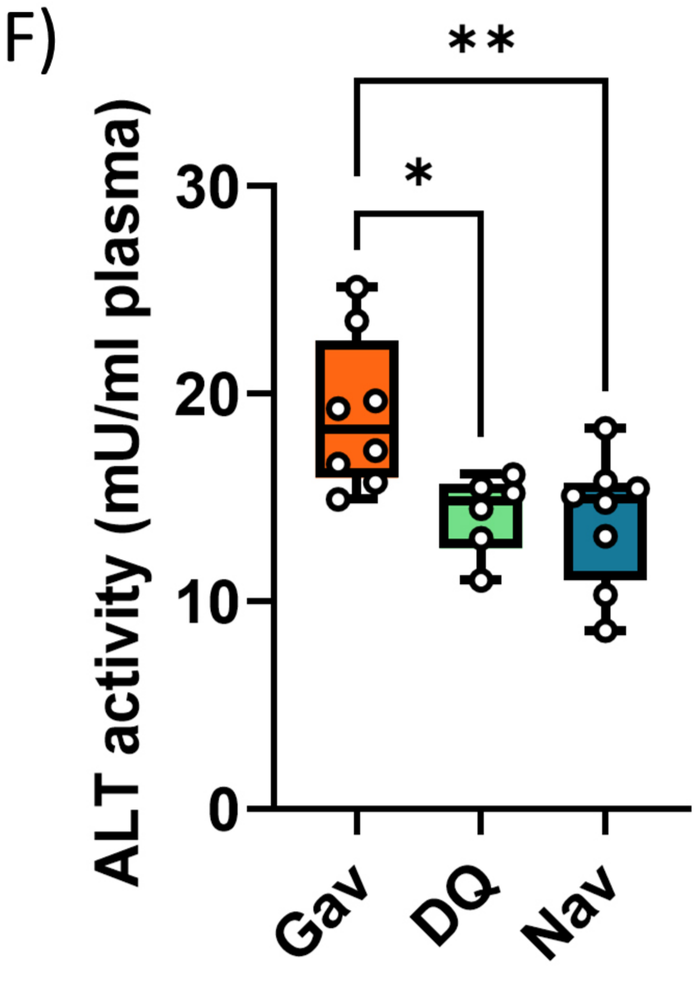

G)

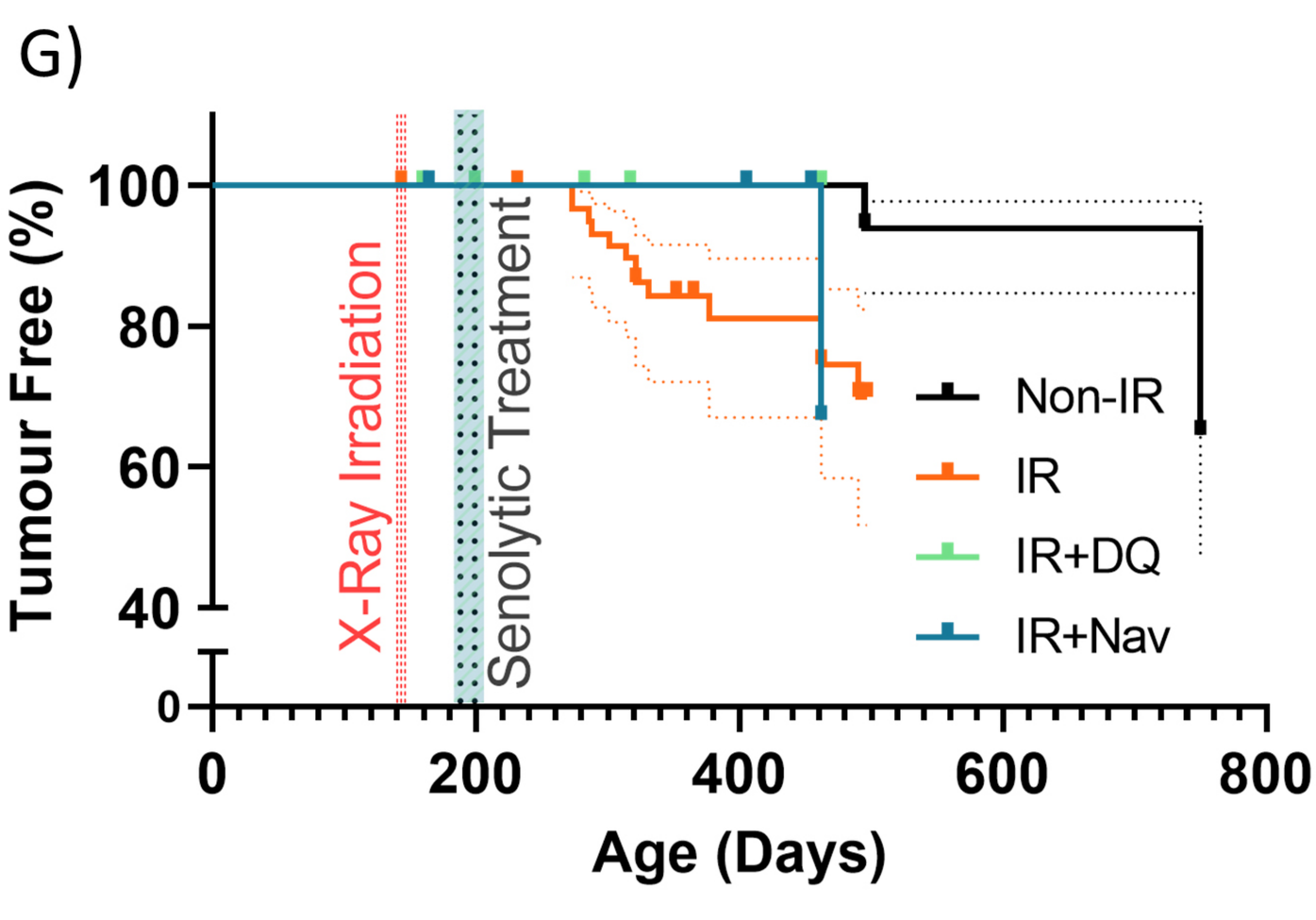

A)

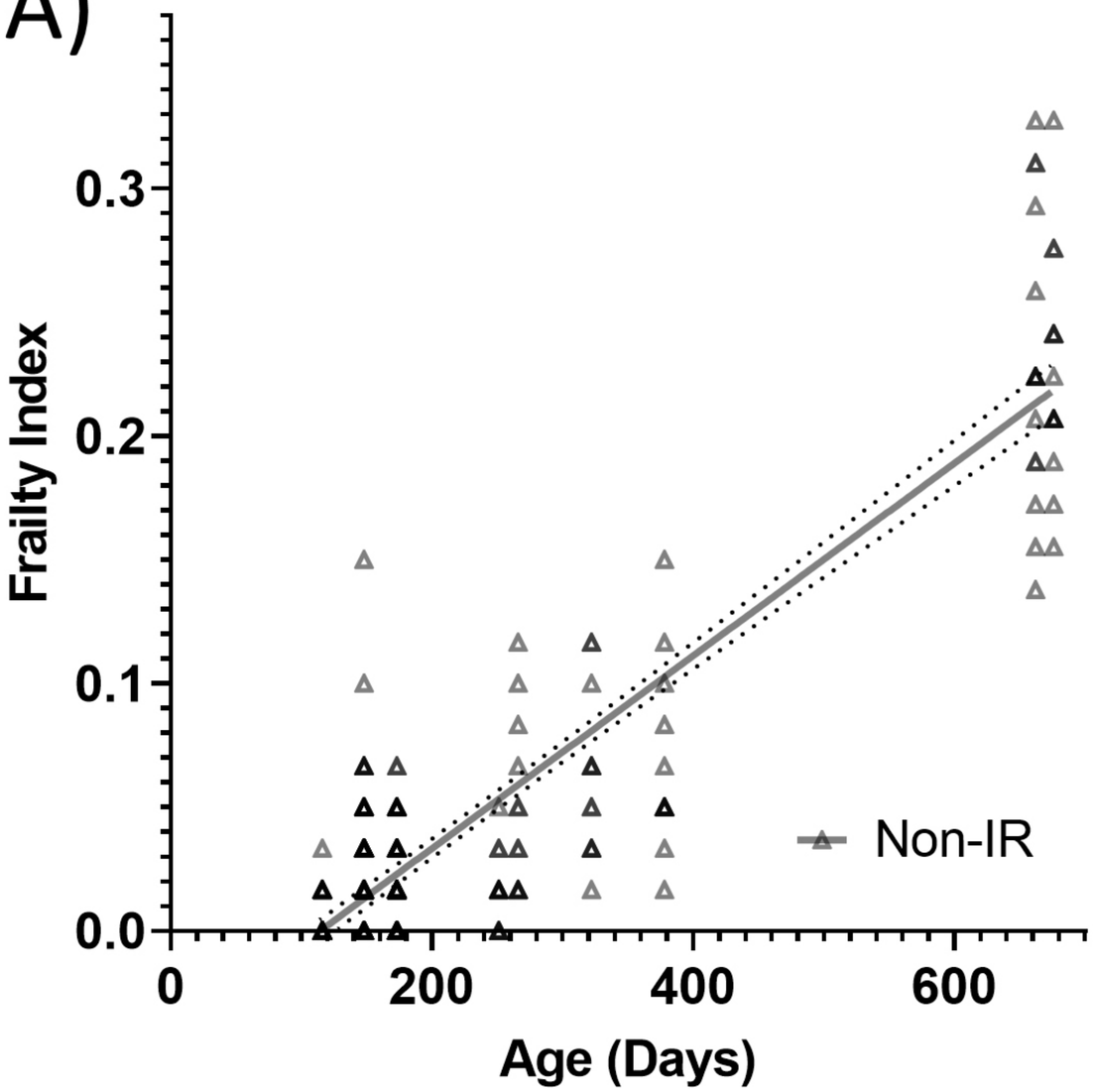
Frailty Index
0.0
0.1
0.2
0.3
0
200
400
600
Age (Days)
Non-IR

B)

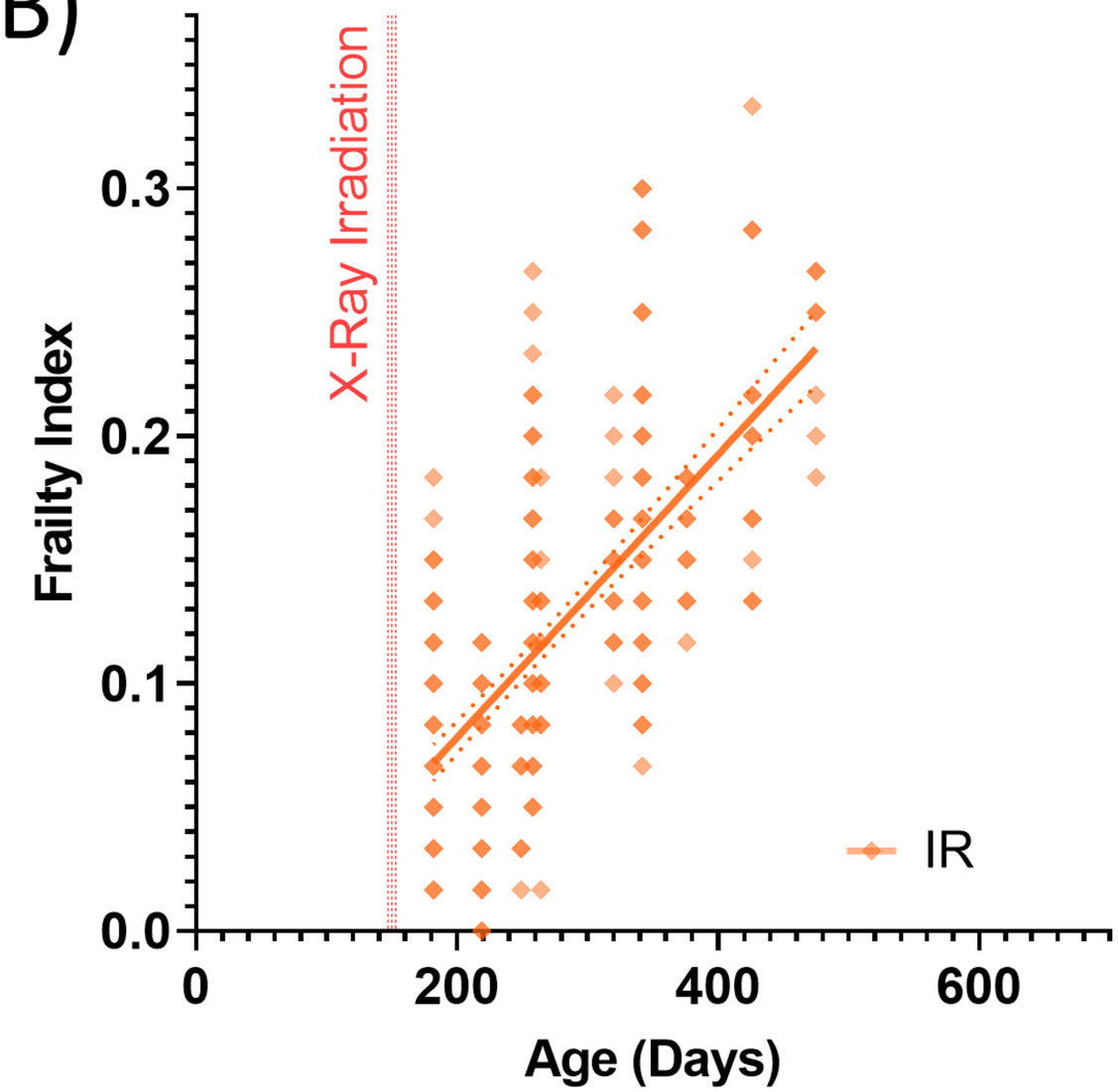
X-Ray Irradiation
Frailty Index
0.0
0.1
0.2
0.3
0
200
400
600
Age (Days)
IR

C)

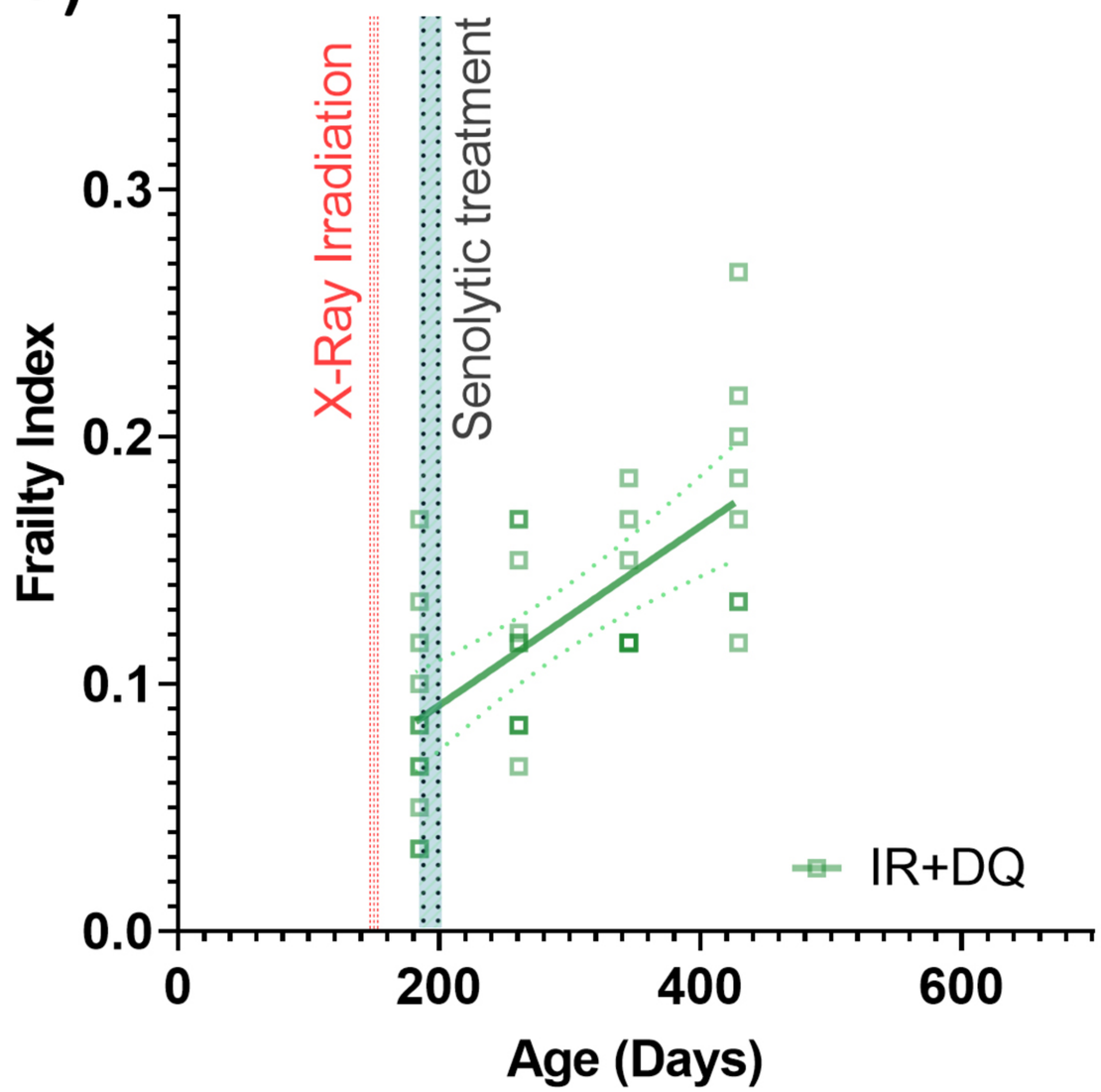
X-Ray Irradiation
Senolytic treatment
Frailty Index
0.0
0.1
0.2
0.3
0
200
400
600
Age (Days)
IR+DQ

D)

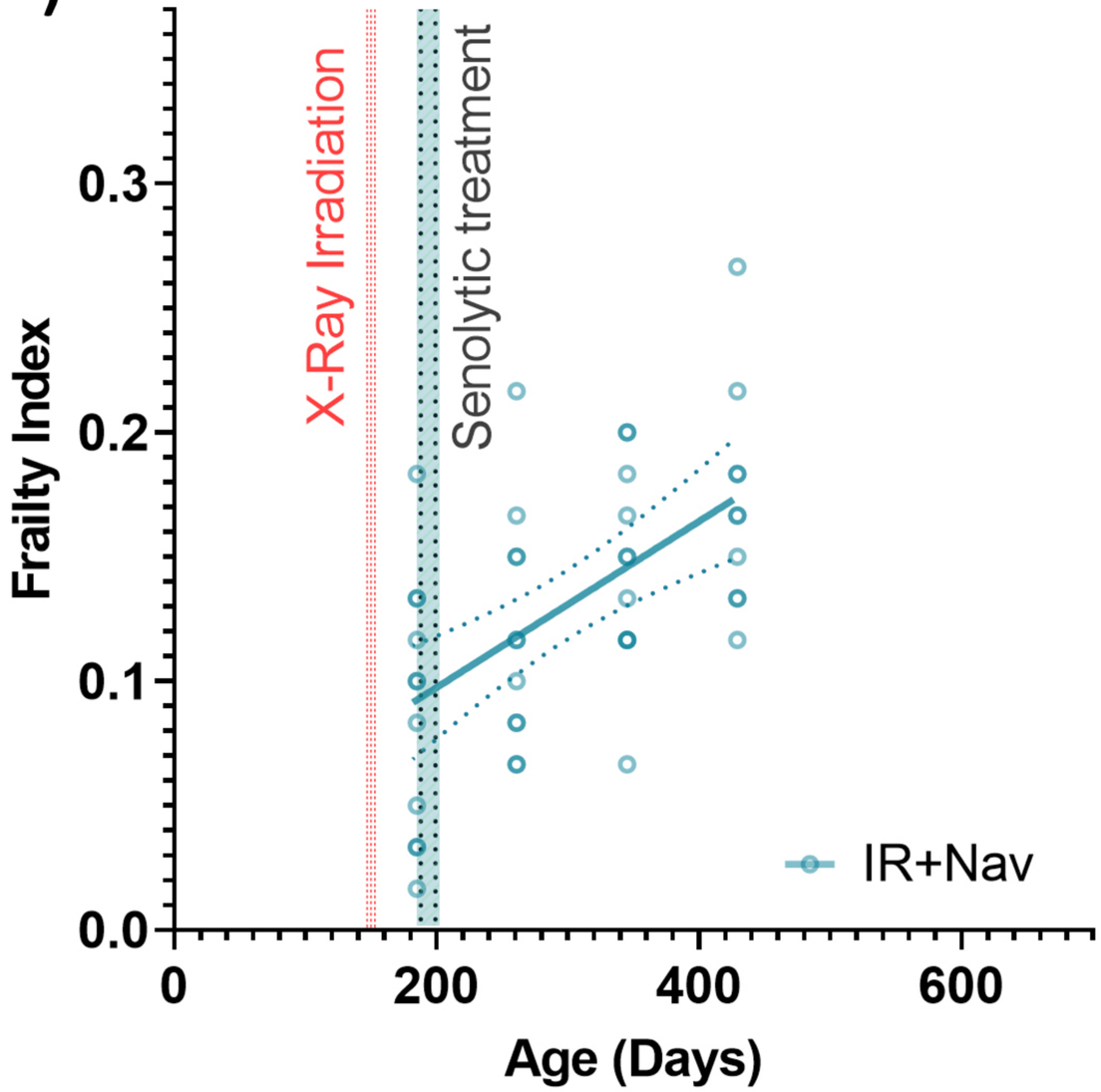
X-Ray Irradiation
Senolytic treatment
Frailty Index
0.0
0.1
0.2
0.3
0
200
400
600
Age (Days)
IR+Nav

Mean FI

0

0.5

1

Control

Metformin

D+Q

Navitoclax

D+Q

Navitoclax

Baseline

+1 month

+4 month

+6 month

+9 month

+11 month

+4 month

+6 month

+9 month

+11 month

+4 month

+6 month

+9 month

+4 month

+6 month

+9 month

+9 month

+11 month

+9 month

+11 month

Tail stiffening

Vestibular disturbance

Vision loss

Mouse Grimace Scale

Piloerrection

Loss of fur colour

Coat condition

Body condition

Kyphosis

Gait disorder

Breathing rate

Tremour

Alopecia

Dermatitis

Cataracts

Corneal Opacity

Eye discharge/swelling

Microphtalmia

Nasal discharge

Tumours

Distended abdomen

Penile prolapse

Rectal prolapse

Diarrhoea

Malocclusions

Loss of whiskers

Hearing loss

Forelimb grip strenght

Bodyweight

Body temperature

Irradiation

Intervention

Intervention

Early Intervention

Late Intervention

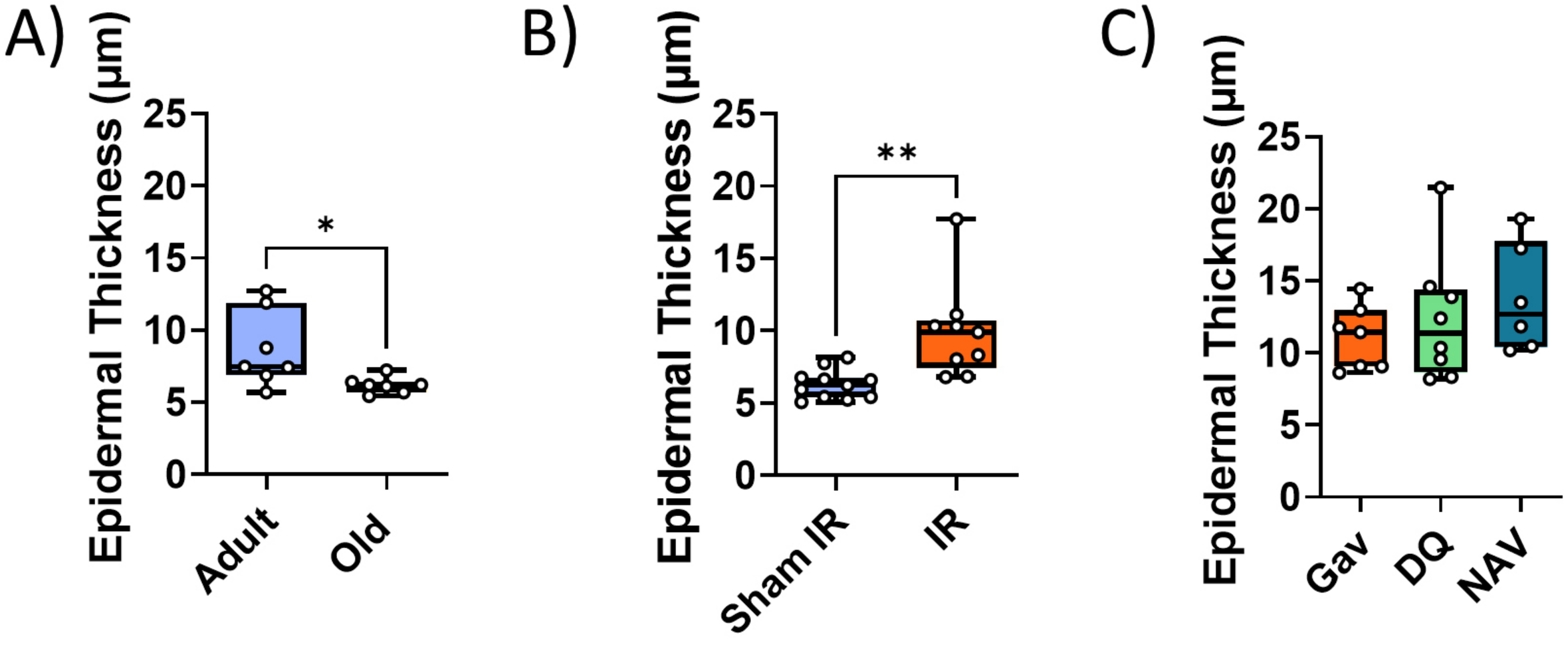
A)
Epidermal Thickness (µm)
25
20
15
10
5
0
*
Adult
Old
B)
Epidermal Thickness (µm)
25
20
15
10
5
0
**
Sham IR
IR
C)
Epidermal Thickness (µm)
25
20
15
10
5
0
Gav
DQ
NAV

A)

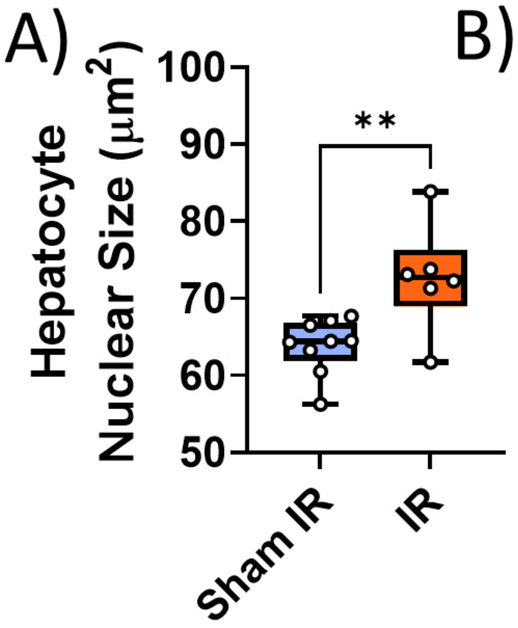

B)

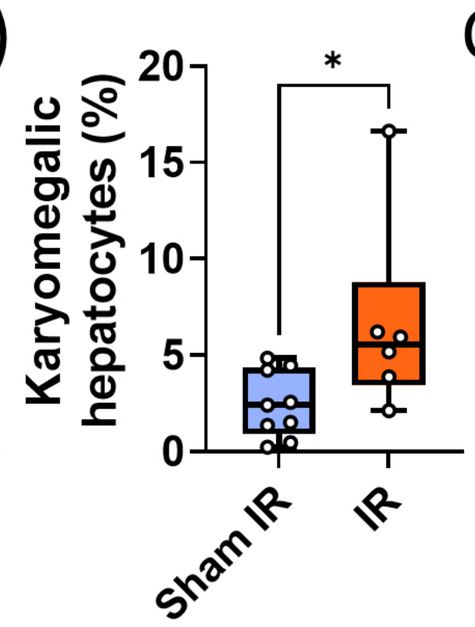

C)

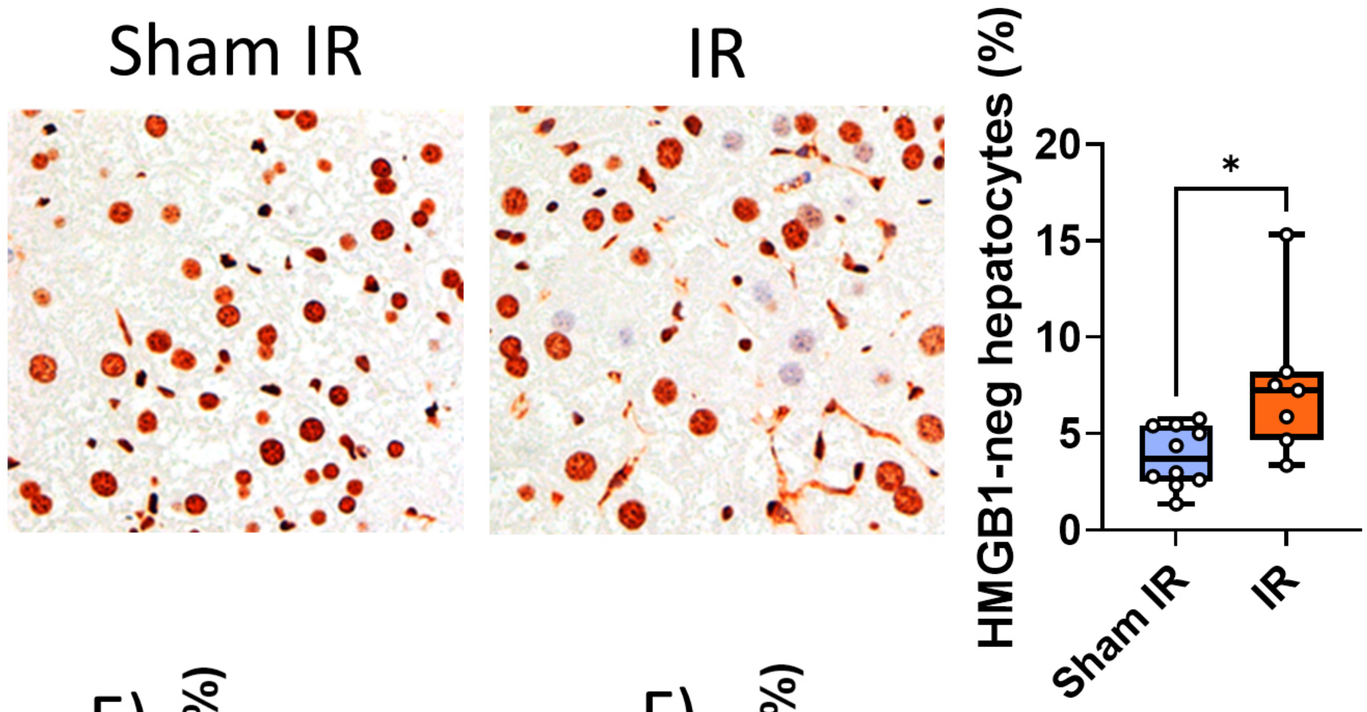

D)

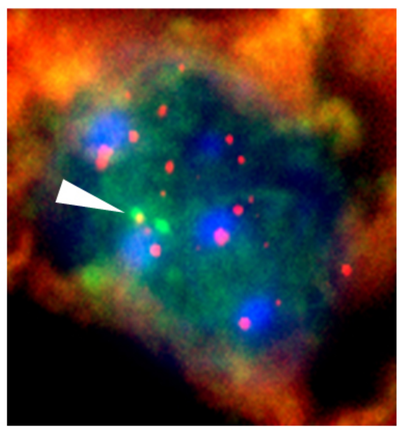

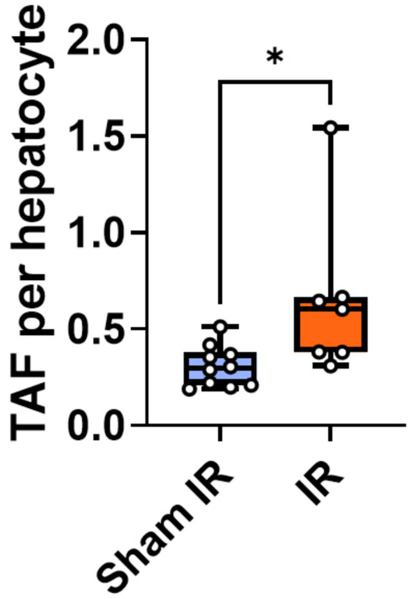

E)

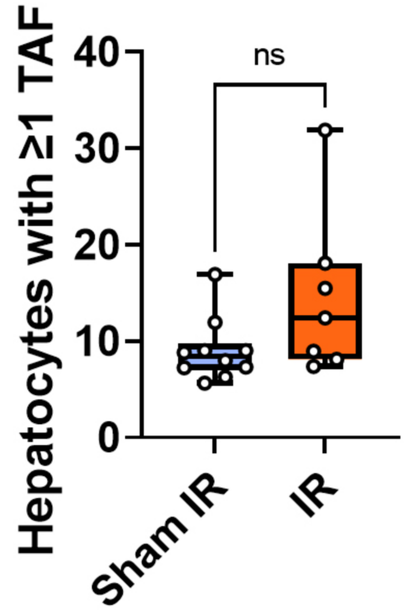

F)

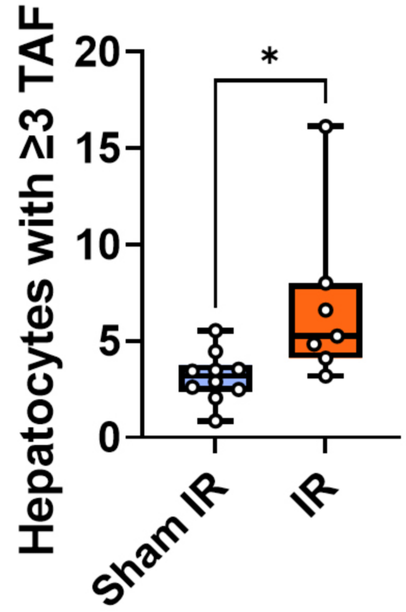

G)

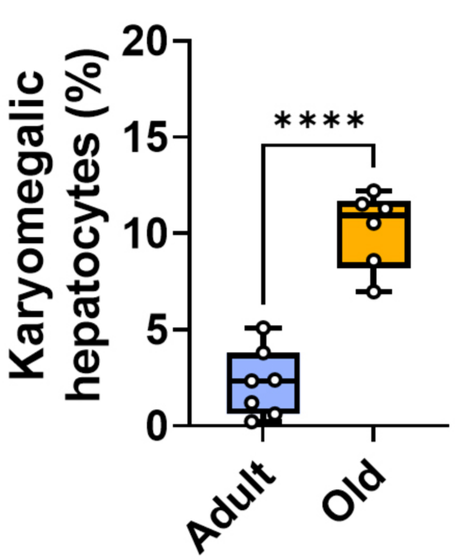

H)

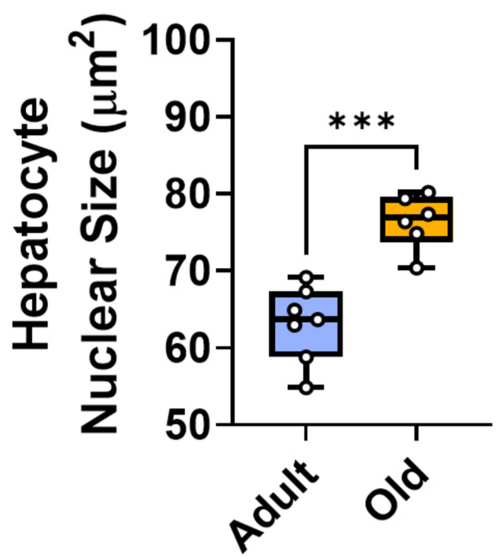

I)

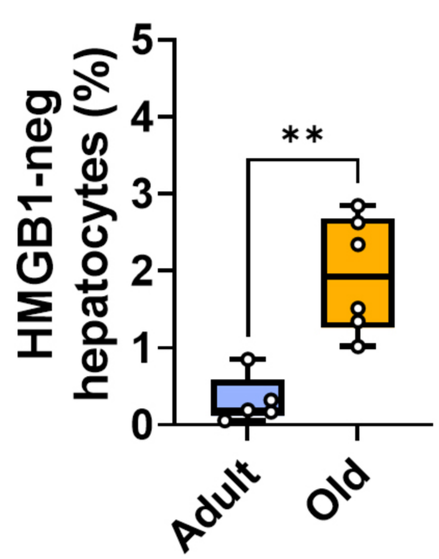

J)

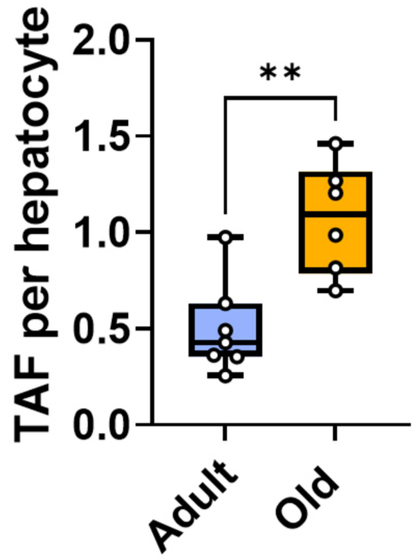

K)

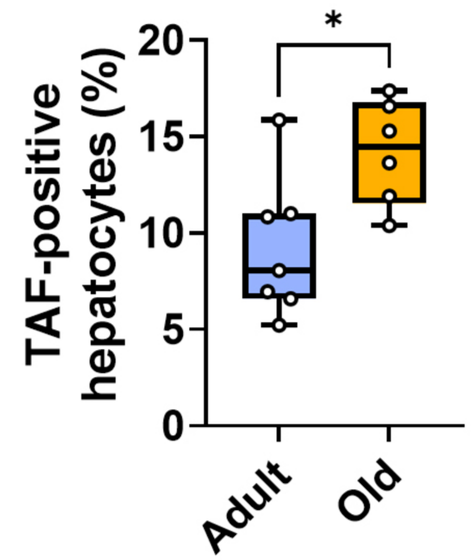

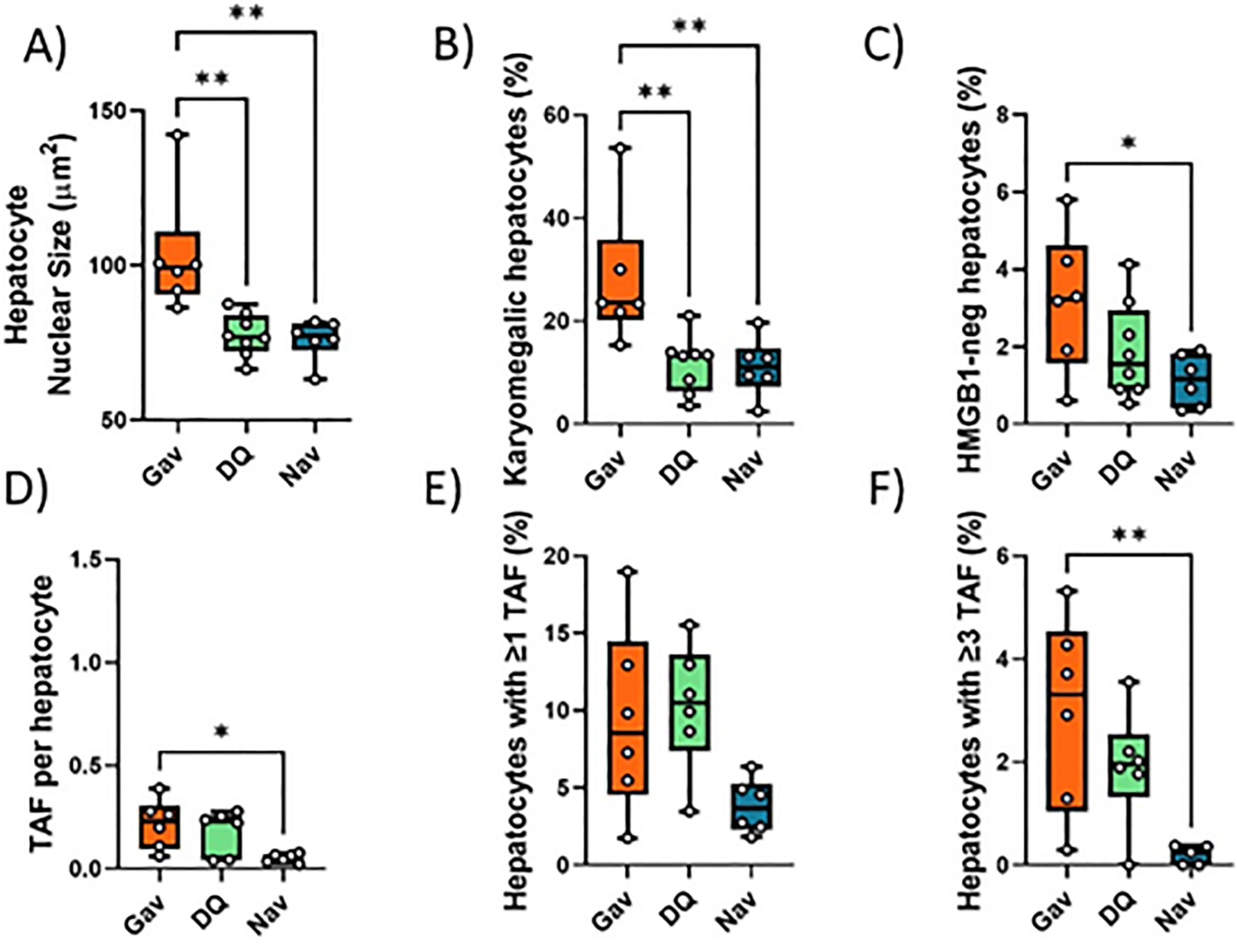
A)
Hepatocyte Nuclear Size (µm²)
150
100
50
**
**
Gav
DQ
Nav
B)
Karyomegalic hepatocytes (%)
60
40
20
0
**
**
Gav
DQ
Nav
C)
HMGB1-neg hepatocytes (%)
8
6
4
2
0
*
Gav
DQ
Nav
D)
TAF per hepatocyte
1.5
1.0
0.5
0.0
*
Gav
DQ
Nav
E)
Hepatocytes with ≥1 TAF (%)
20
15
10
5
0
Gav
DQ
Nav
F)
Hepatocytes with ≥3 TAF (%)
6
4
2
0
**
Gav
DQ
Nav

A)

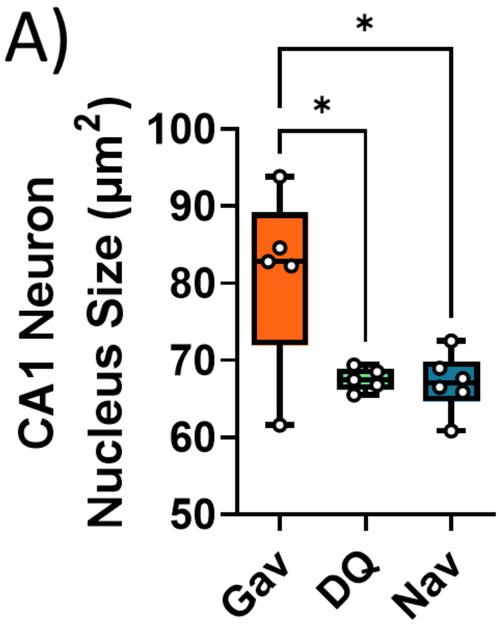

B)

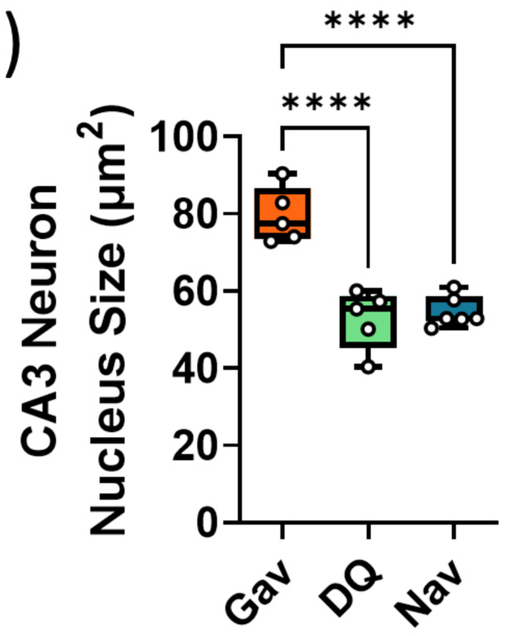

C)

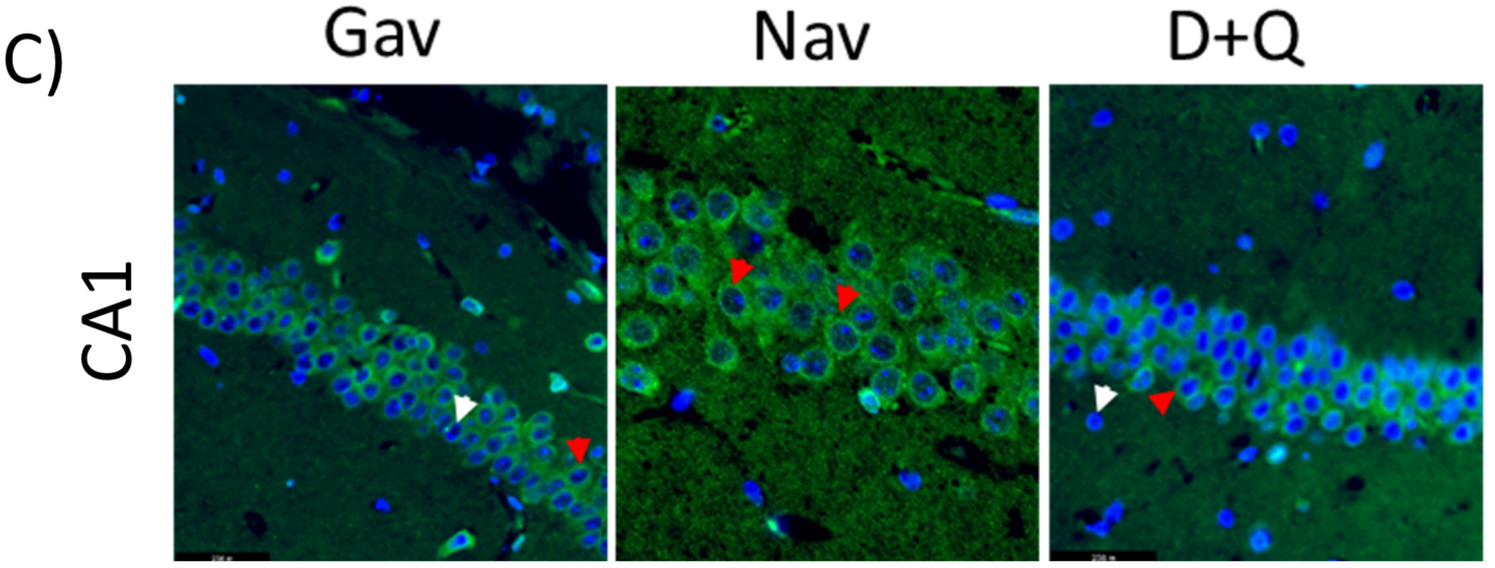

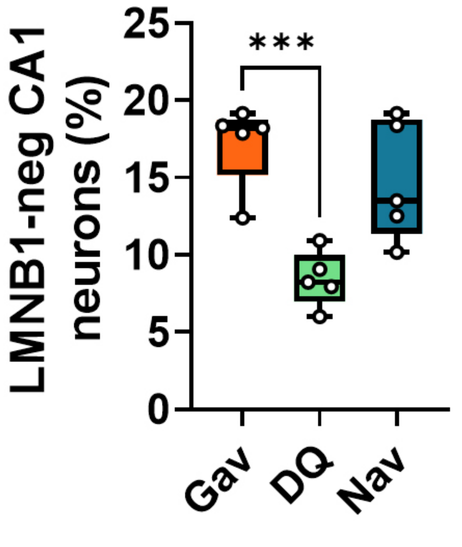

D)

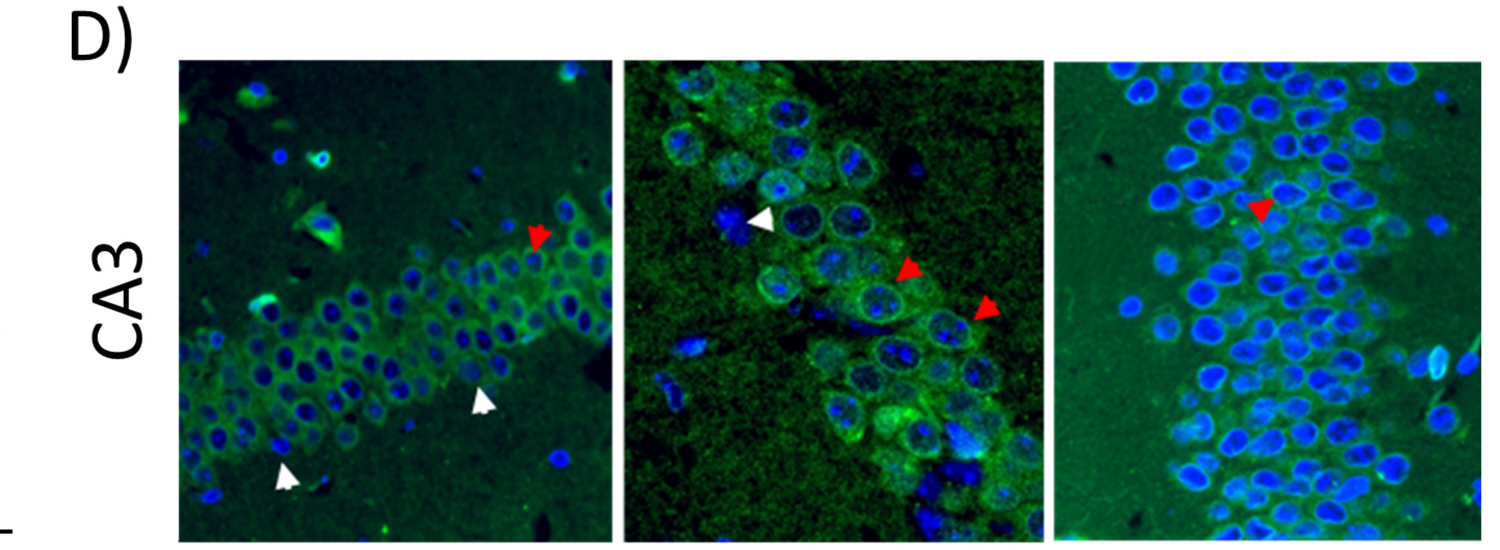

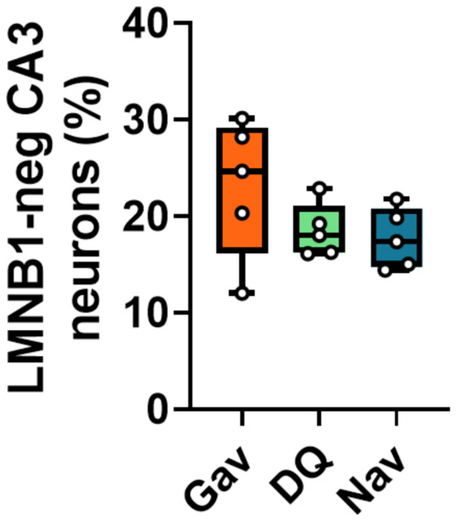

E)

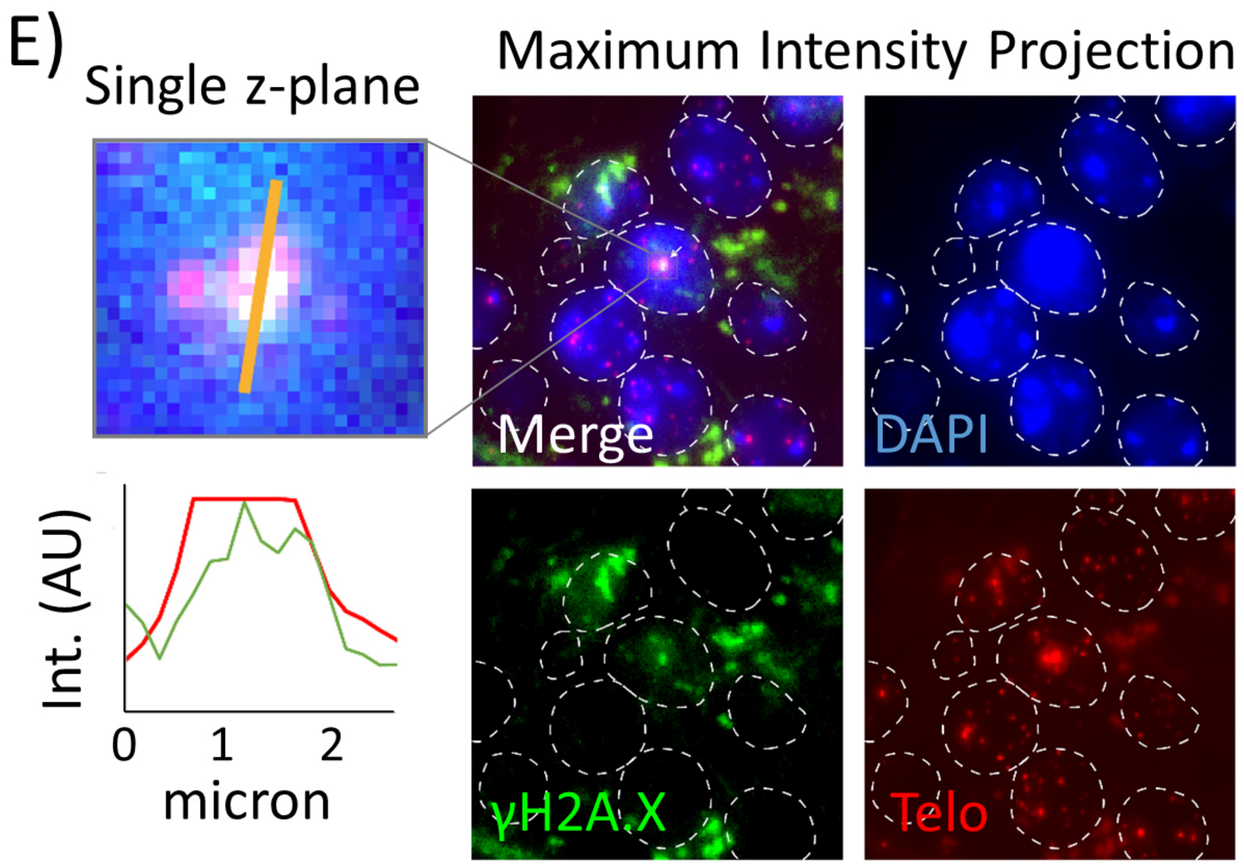

F)

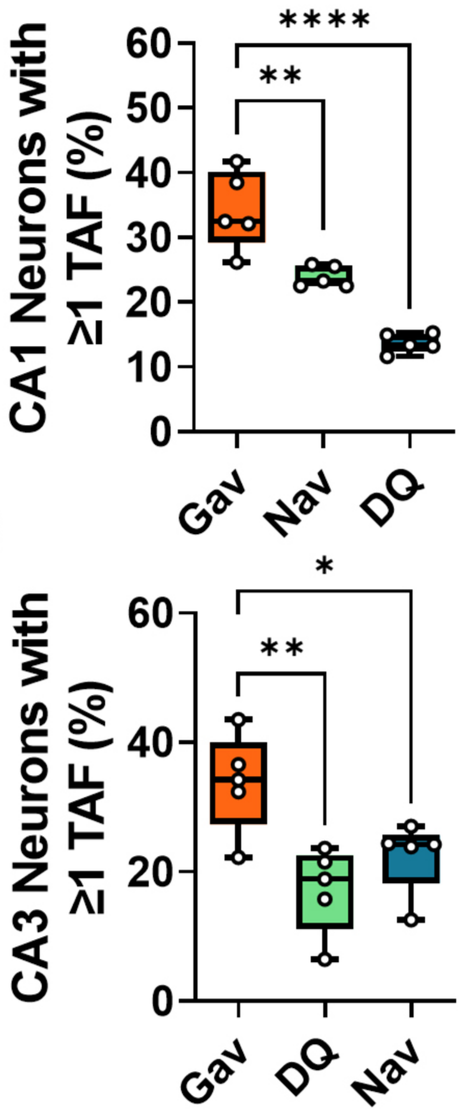

G)

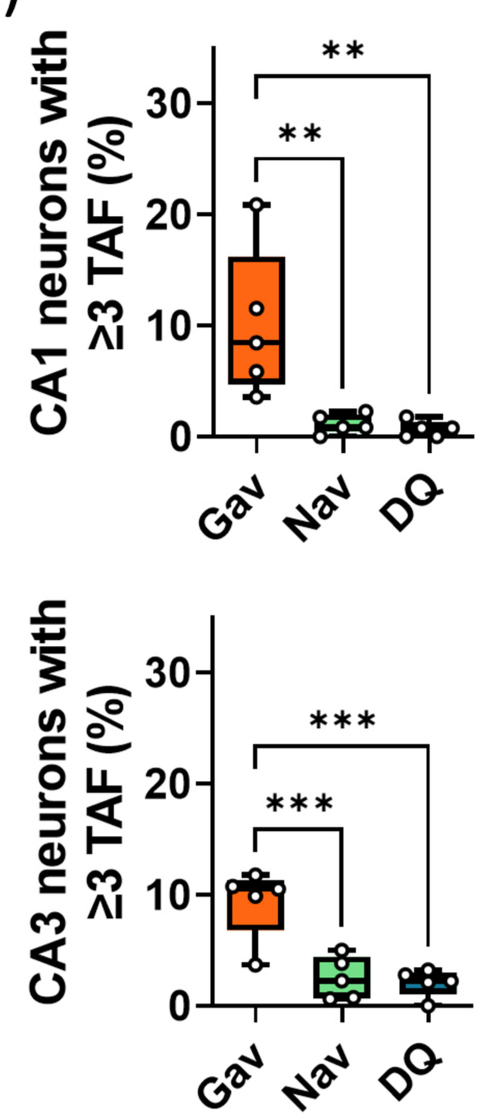

H)

I)

J)

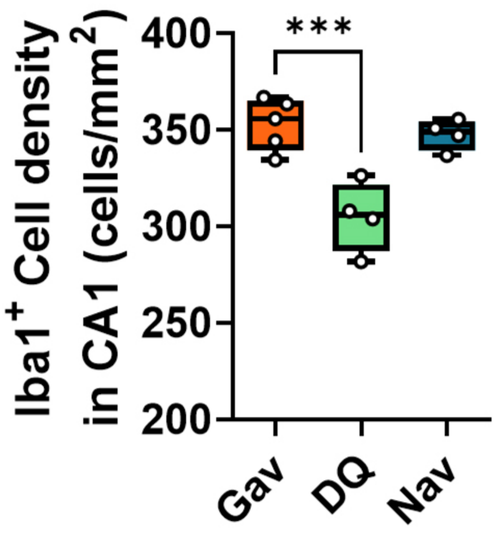

K)

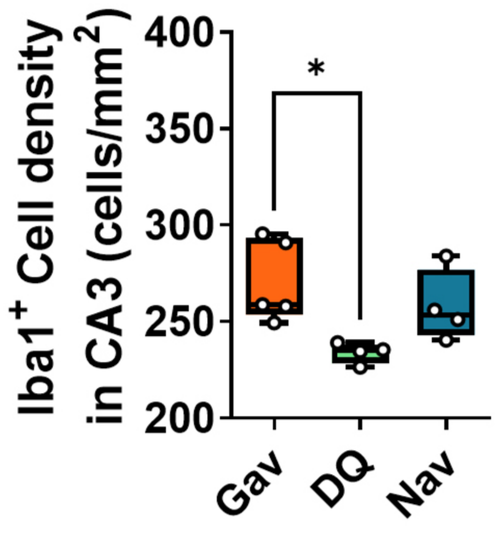

L)

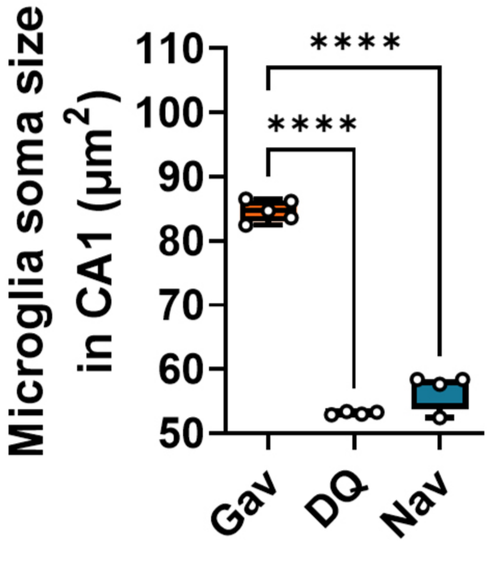

M)

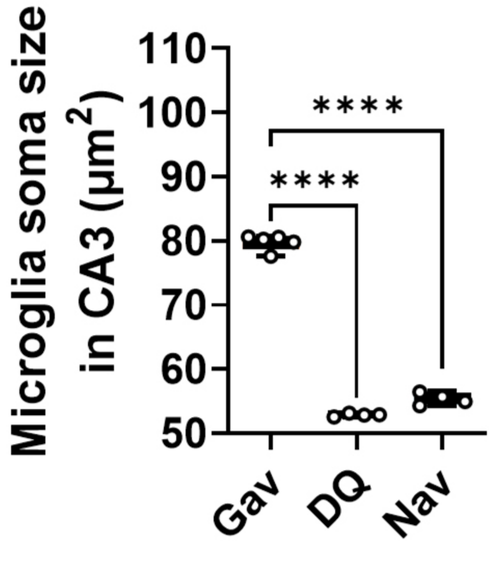

A)

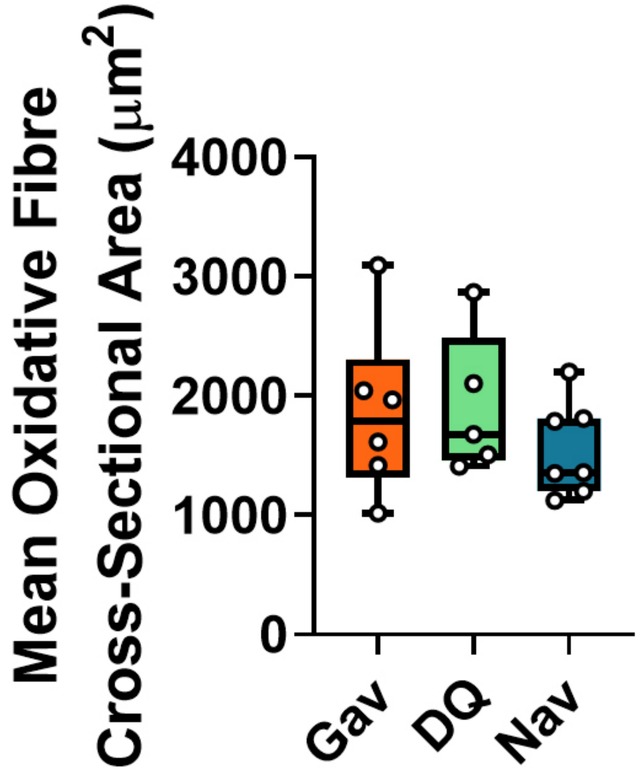
Mean Oxidative Fibre Cross-Sectional Area (μm²)
4000
3000
2000
1000
0
Gav
DQ
Nav

B)

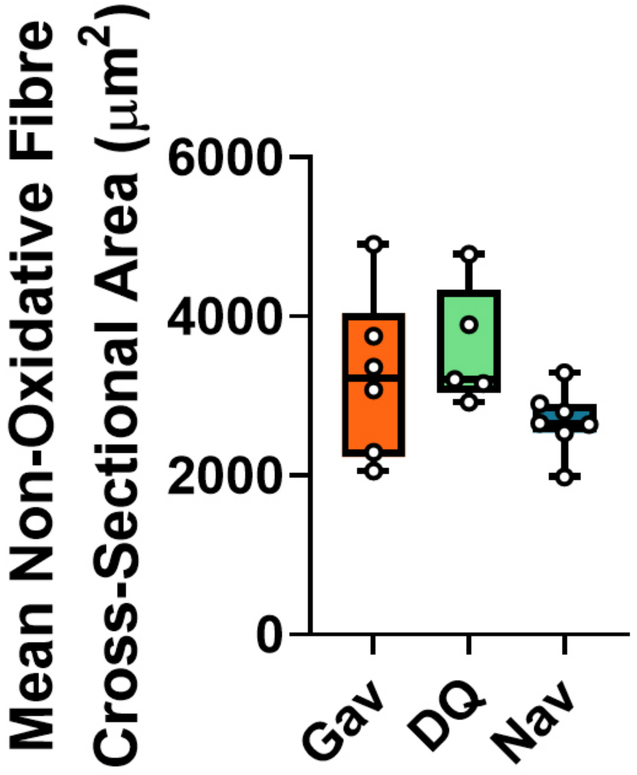
Mean Non-Oxidative Fibre Cross-Sectional Area (μm²)
6000
4000
2000
0
Gav
DQ
Nav

C)

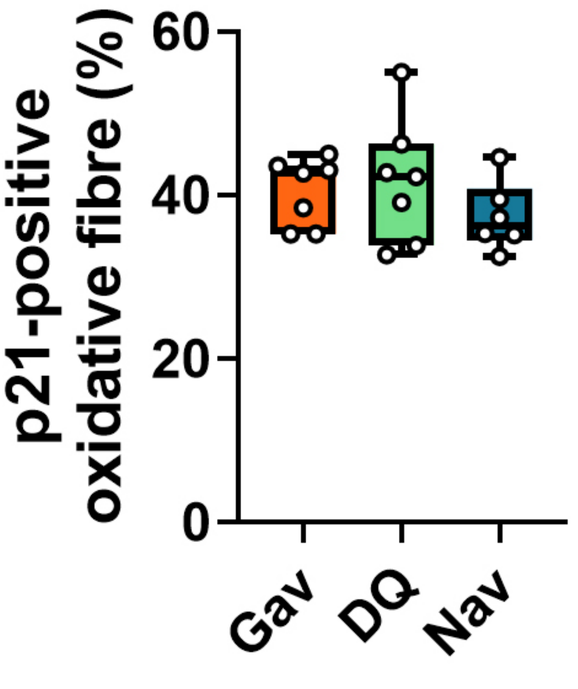
p21-positive oxidative fibre (%)
60
40
20
0
Gav
DQ
Nav

D)

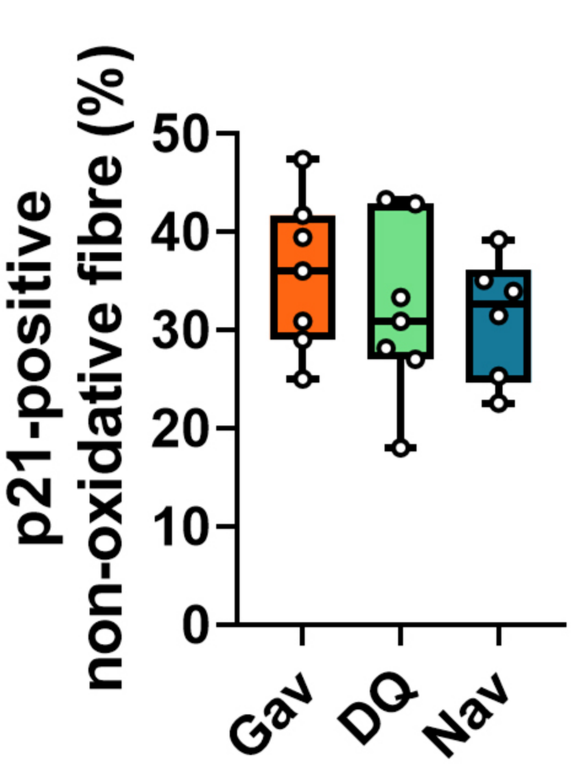
p21-positive non-oxidative fibre (%)
50
40
30
20
10
0
Gav
DQ
Nav

E)

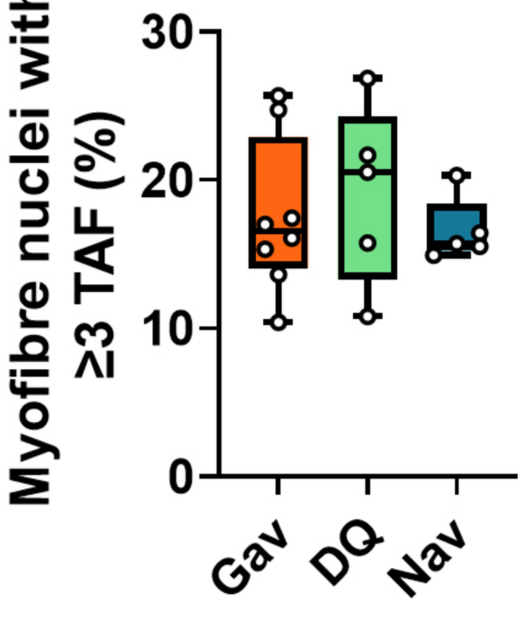
Myofibre nuclei with ≥3 TAF (%)
30
20
10
0
Gav
DQ
Nav

Control

D+Q

Nacitoclax

IL1a
IL2
IL5
IL6
IL7
IL10
IL12
IL13
LIX
IL17A
CXCL1
CCL2
CXCL2
TNFa

-2

0

+2

A)

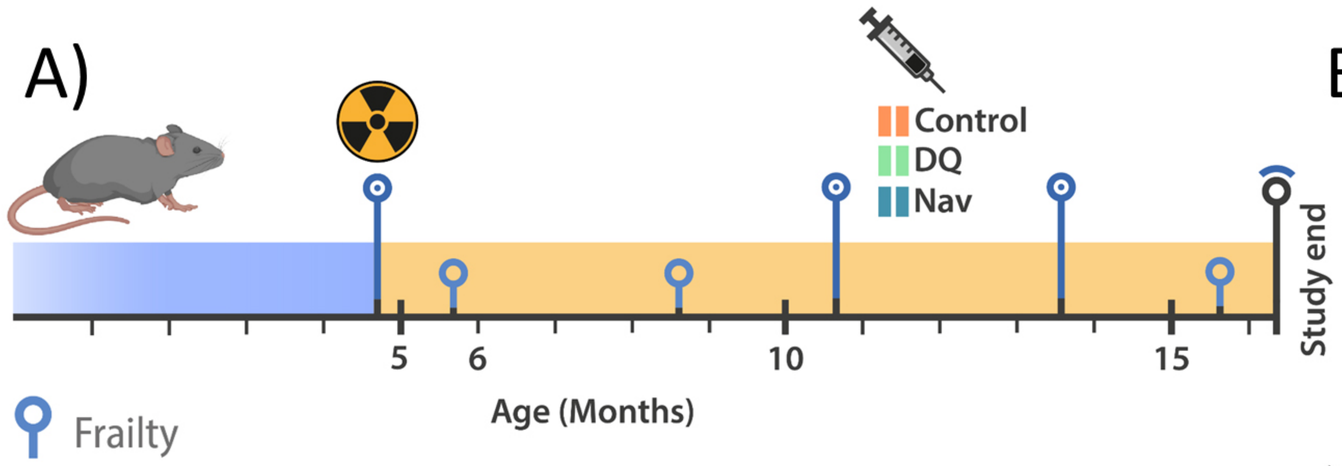

B)

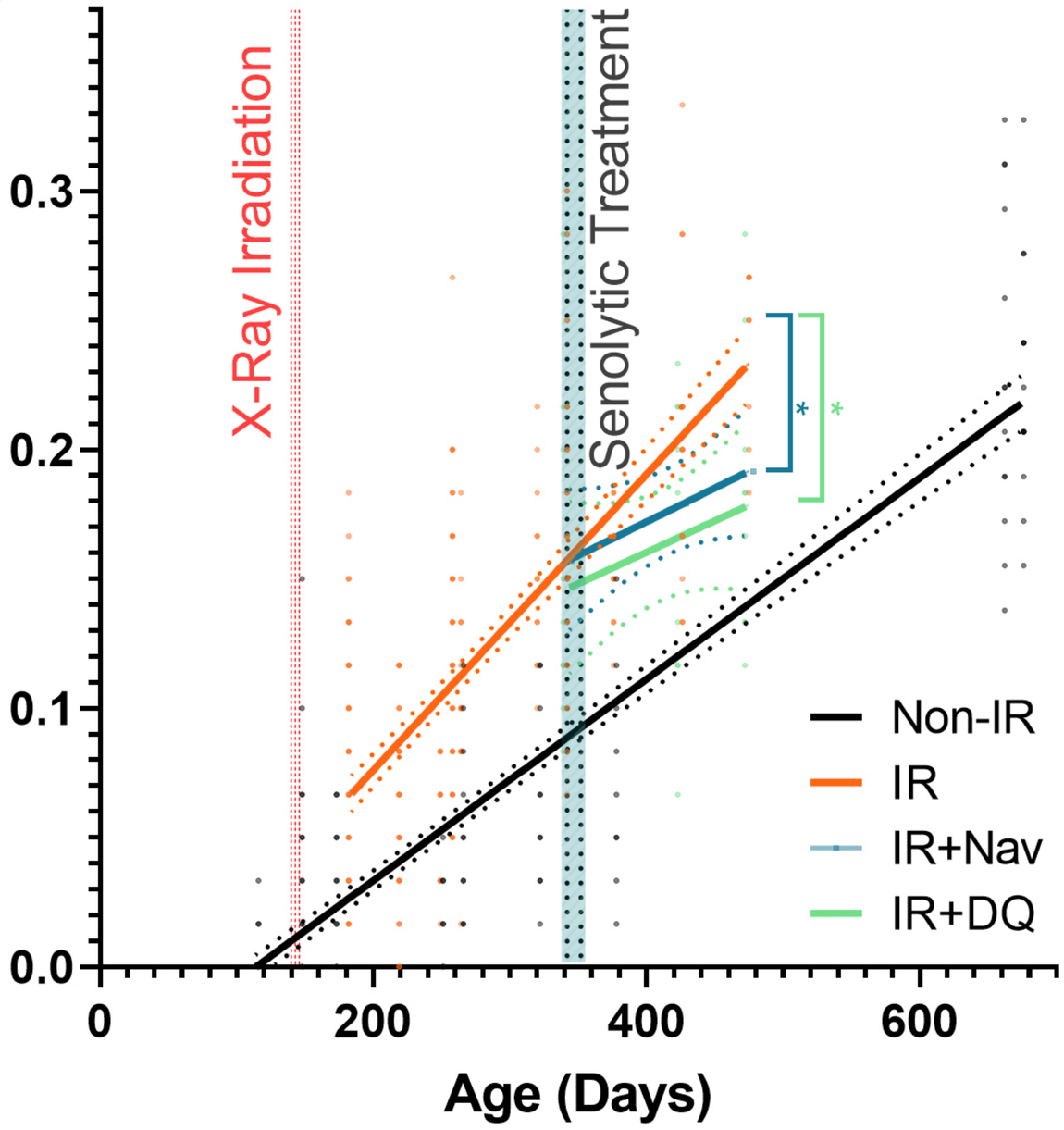

C)

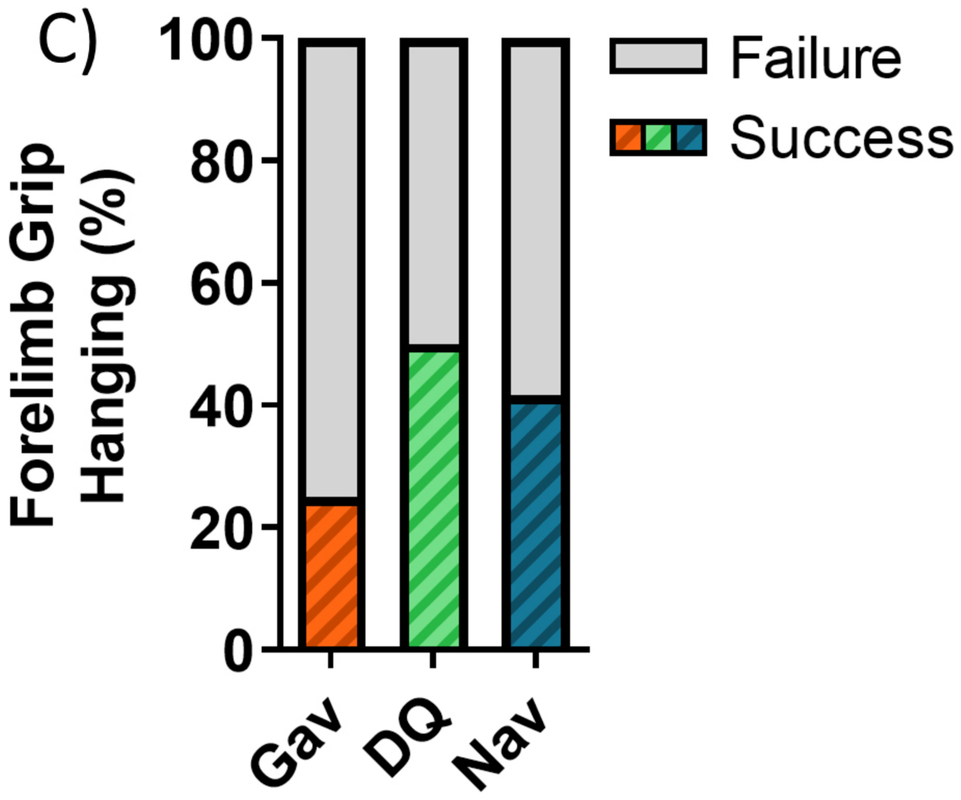

Age (months): 14m

D)

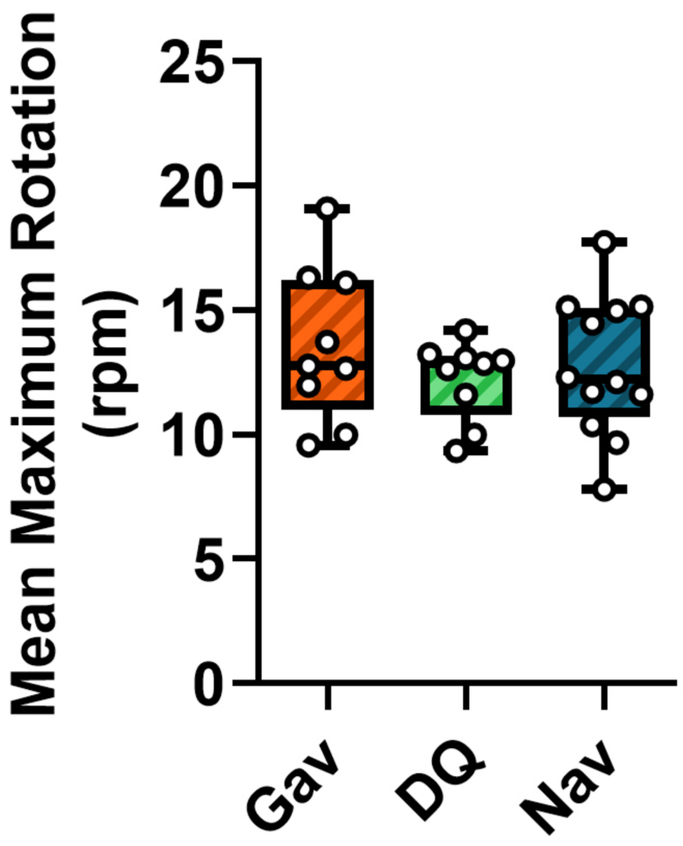

Age (months): 14m

E)

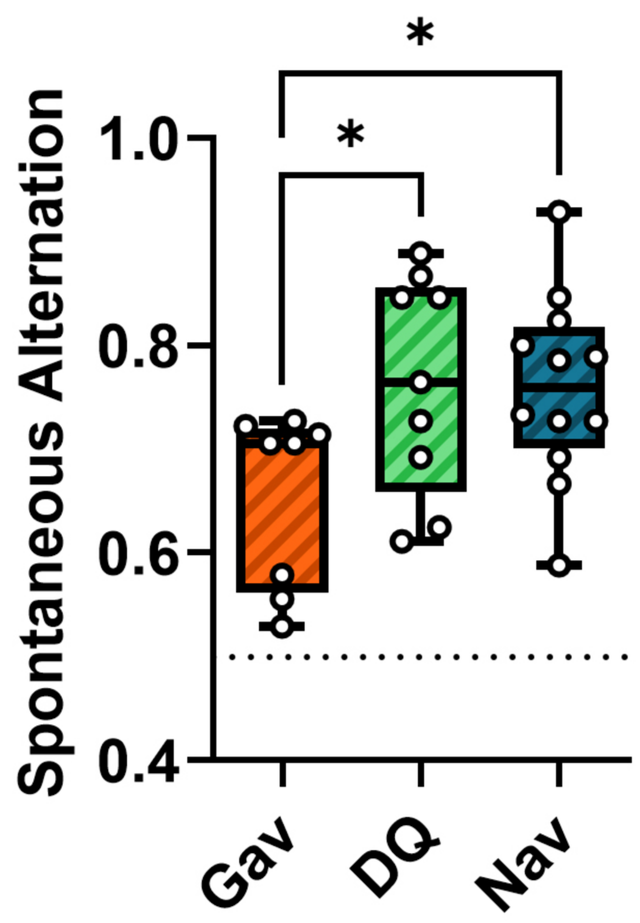

Age (months): 16m

F)

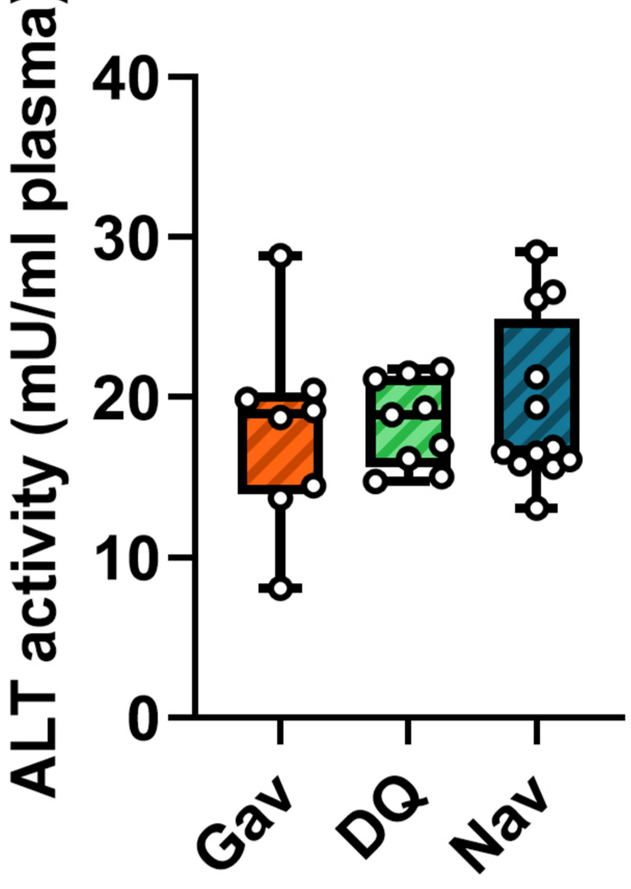

G)

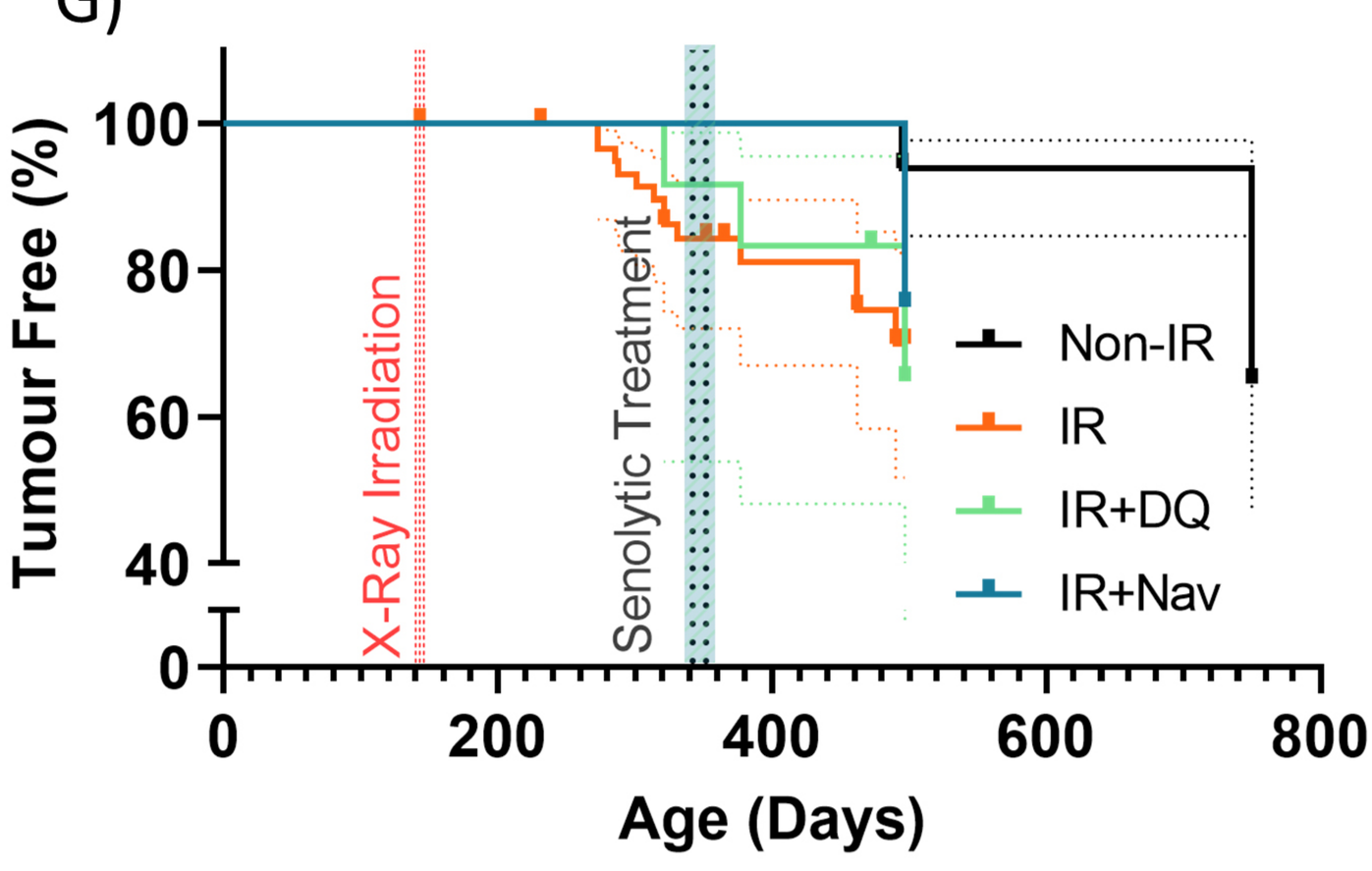

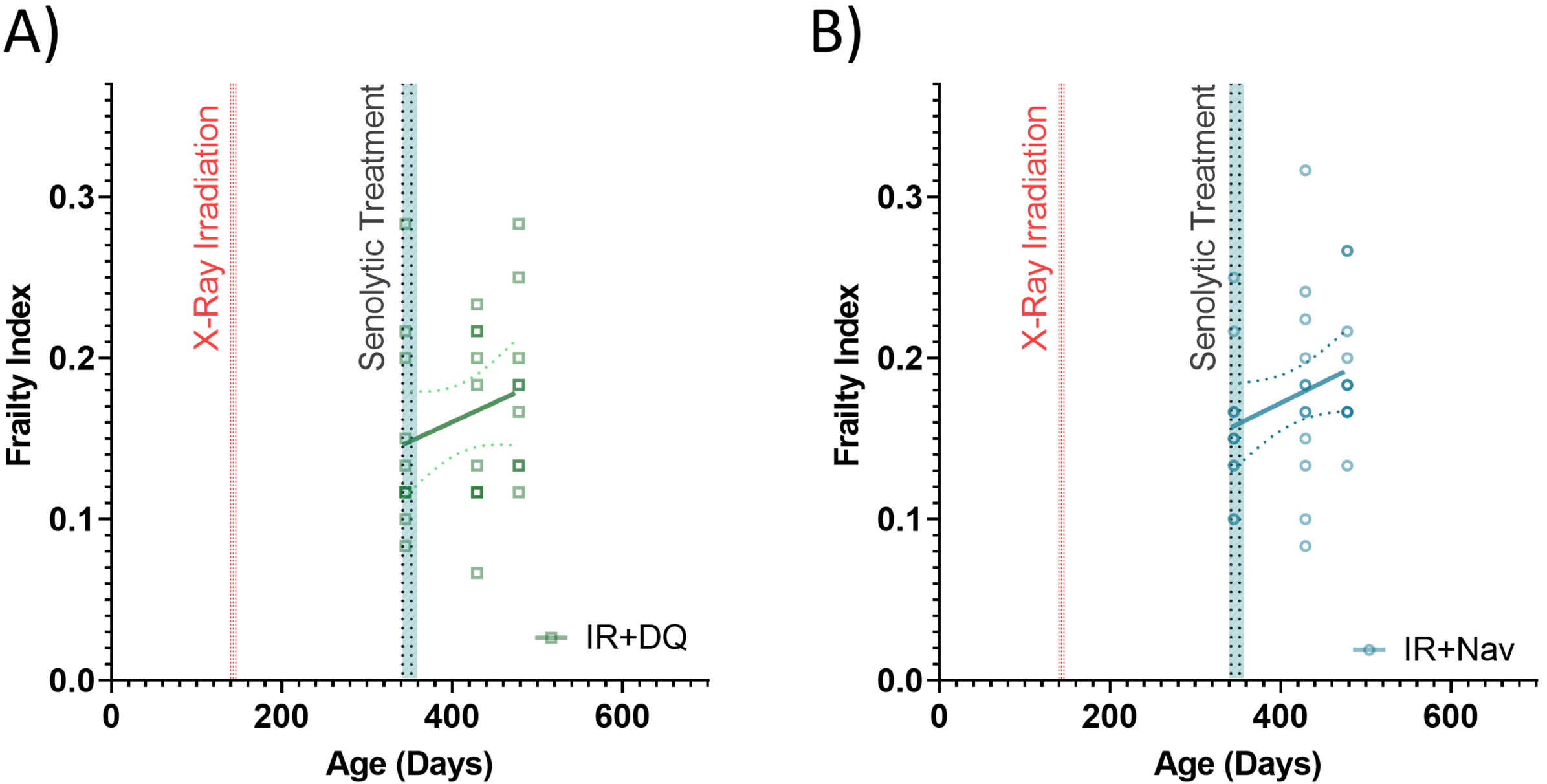
A)
X-Ray Irradiation
Senolytic Treatment
Frailty Index
0.0
0.1
0.2
0.3
0
200
400
600
Age (Days)
IR+DQ
B)
X-Ray Irradiation
Senolytic Treatment
Frailty Index
0.0
0.1
0.2
0.3
0
200
400
600
Age (Days)
IR+Nav

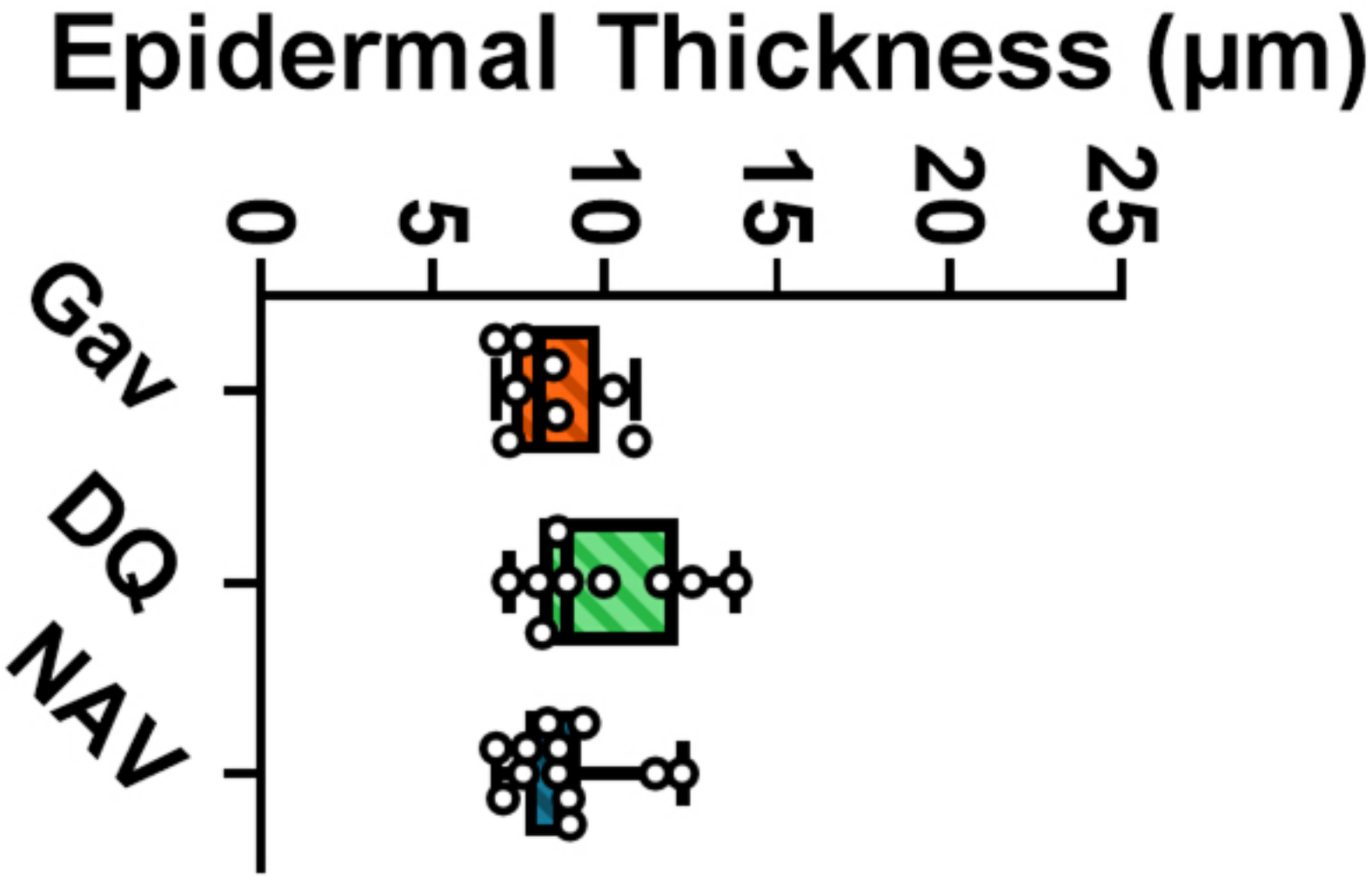
Epidermal Thickness (µm)
0
5
10
15
20
25
Gav
DQ
NAV

A)

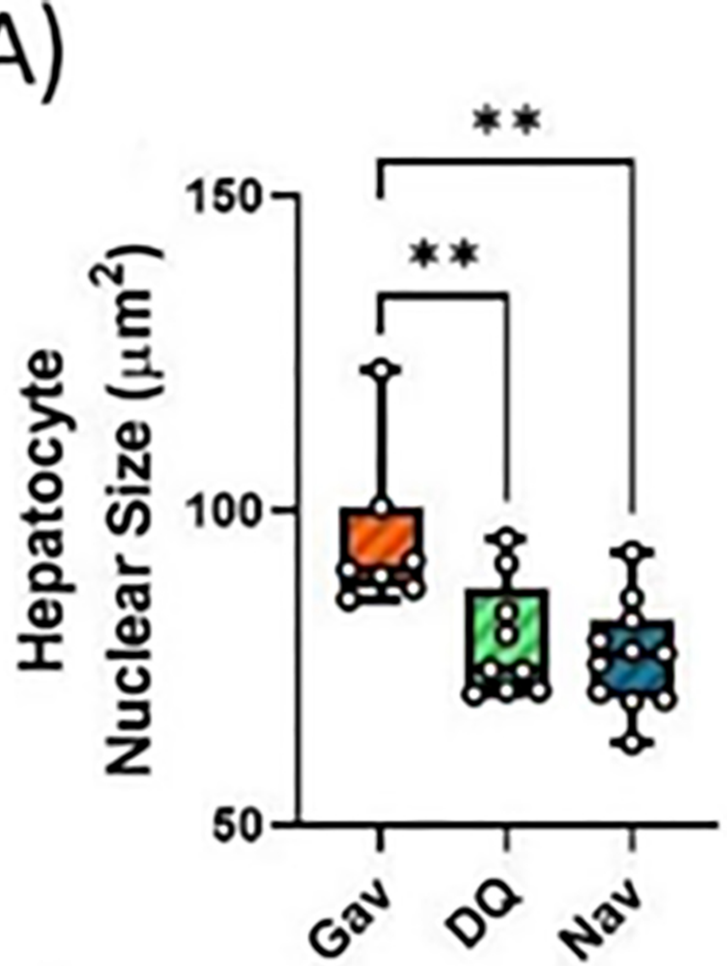
**
**
Hepatocyte Nuclear Size (µm²)
150
100
50
Gav
DQ
Nav

B)

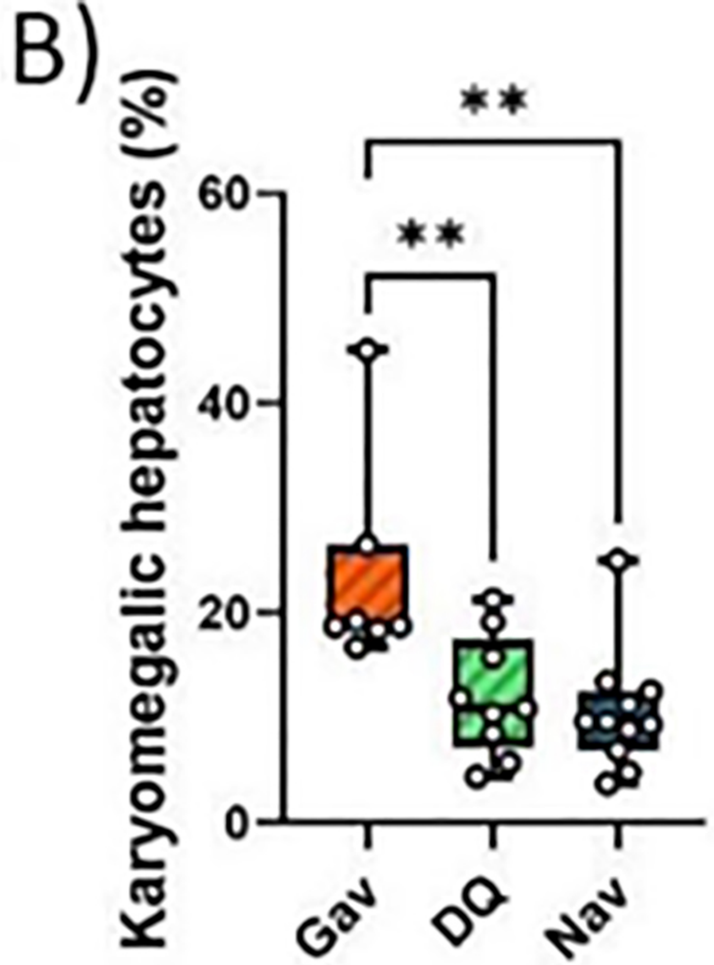
**
**
Karyomegalic hepatocytes (%)
60
40
20
0
Gav
DQ
Nav

C)

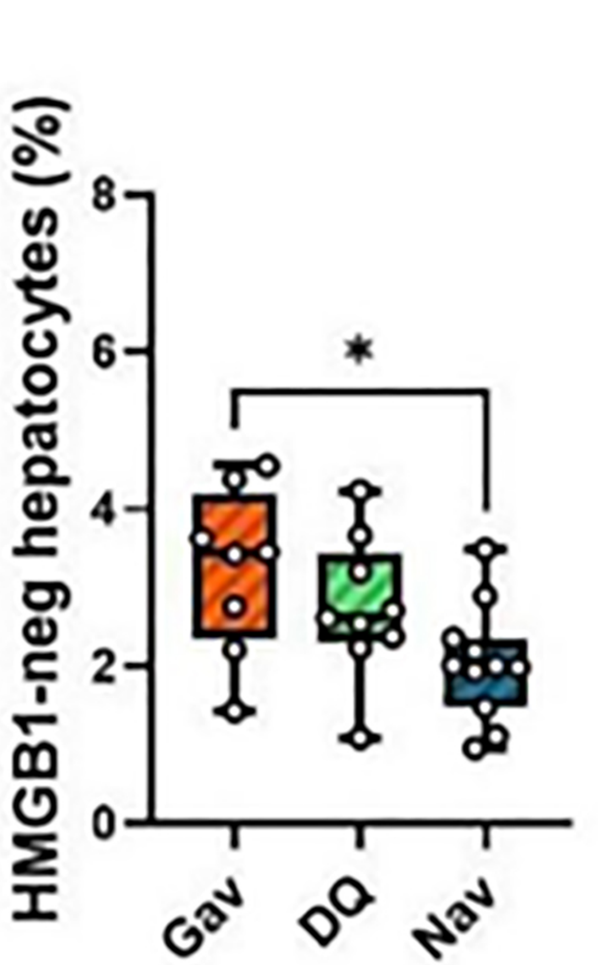
*
HMGB1-neg hepatocytes (%)
8
6
4
2
0
Gav
DQ
Nav

D)

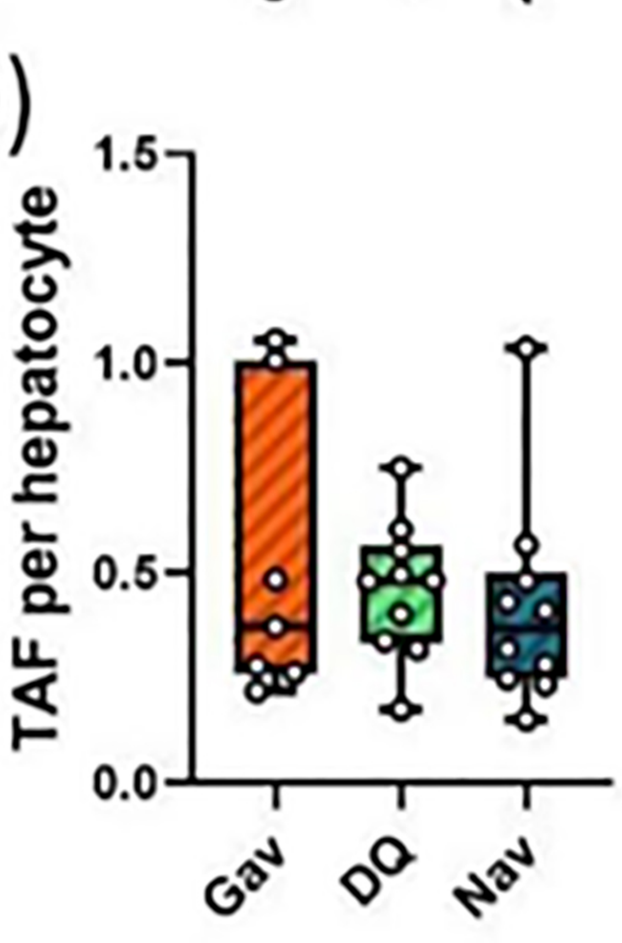
TAF per hepatocyte
1.5
1.0
0.5
0.0
Gav
DQ
Nav

E)

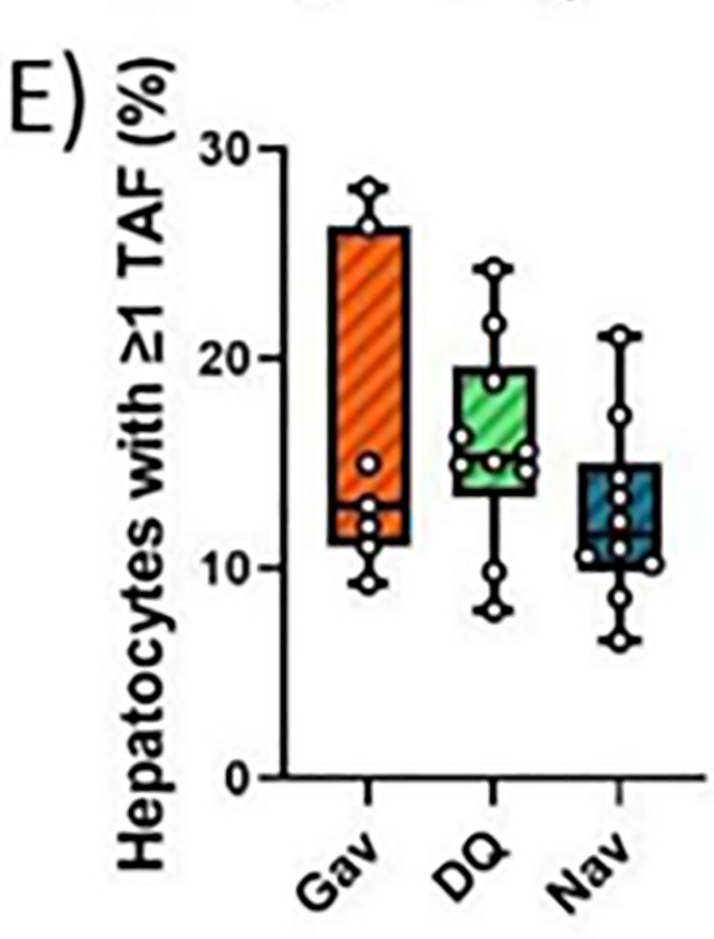
Hepatocytes with ≥1 TAF (%)
30
20
10
0
Gav
DQ
Nav

F)

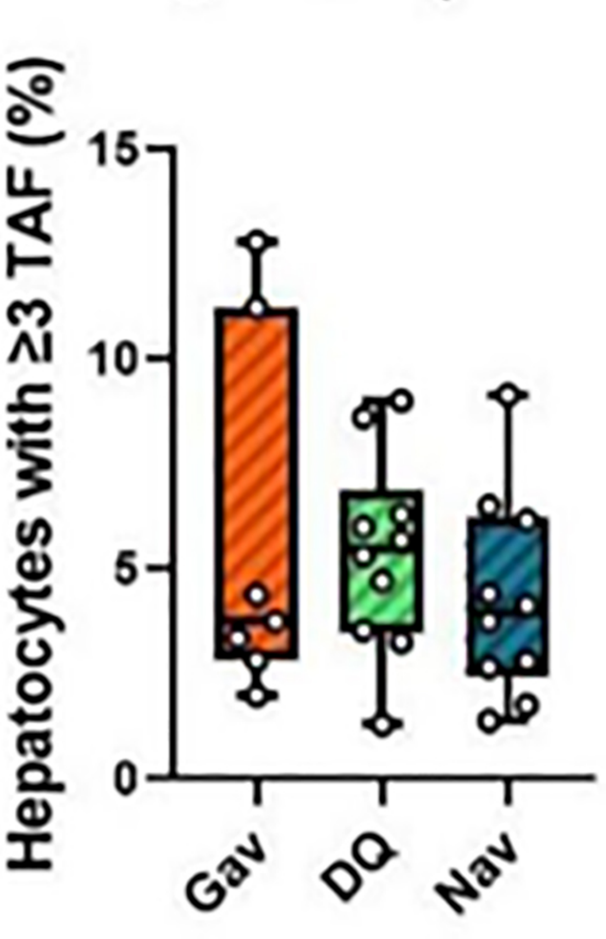
Hepatocytes with ≥3 TAF (%)
15
10
5
0
Gav
DQ
Nav

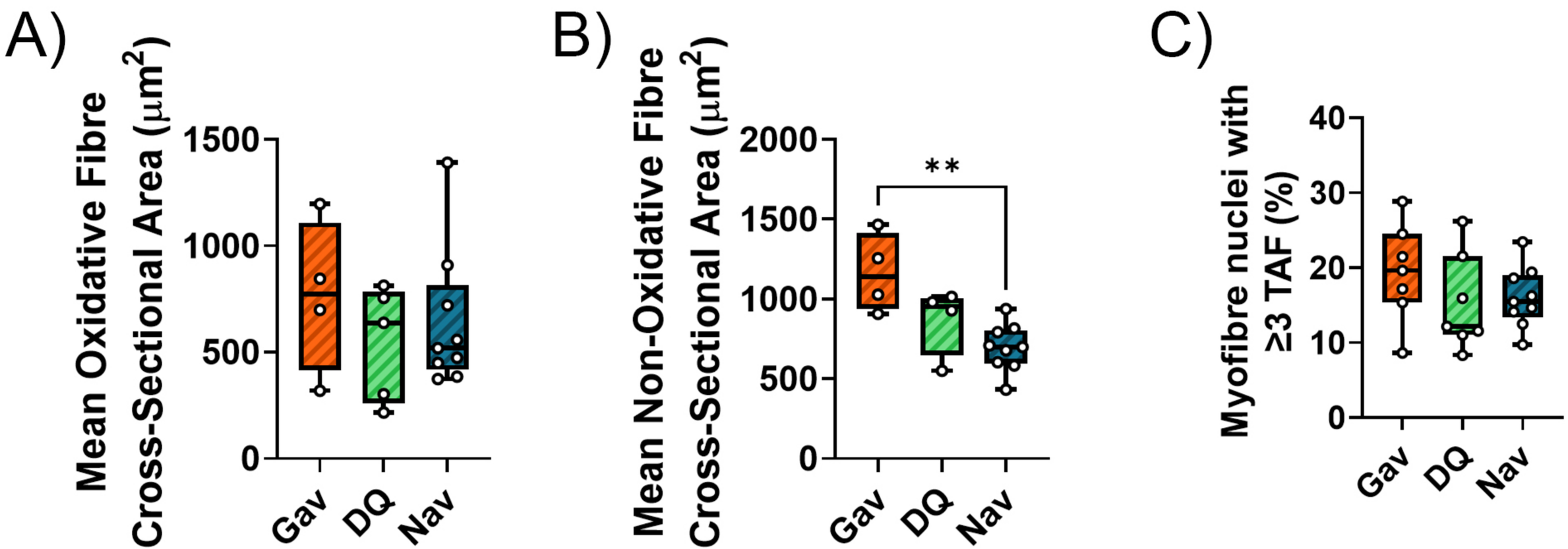
A)
Mean Oxidative Fibre Cross-Sectional Area (μm²)
1500
1000
500
0
Gav
DQ
Nav
B)
Mean Non-Oxidative Fibre Cross-Sectional Area (μm²)
2000
1500
1000
500
0
**
Gav
DQ
Nav
C)
Myofibre nuclei with ≥3 TAF (%)
40
30
20
10
0
Gav
DQ
Nav

CA1

A)

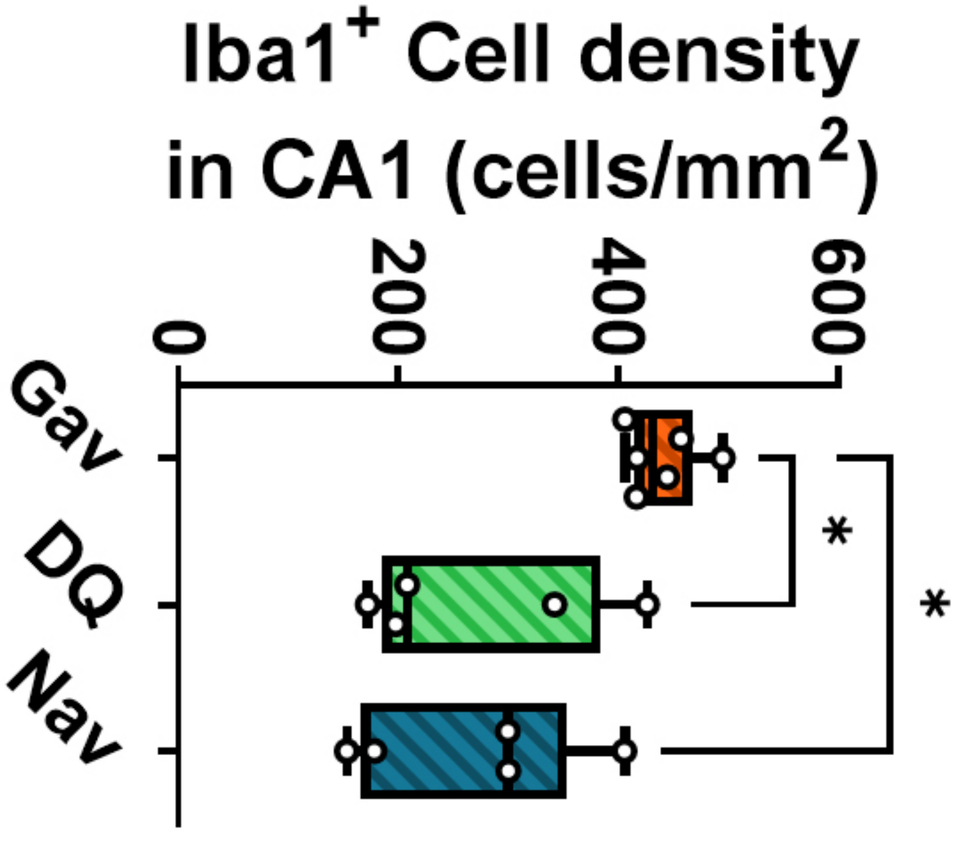
Iba1+ Cell density in CA1 (cells/mm2)
0
200
400
600
Gav
DQ
Nav
*
*

B)

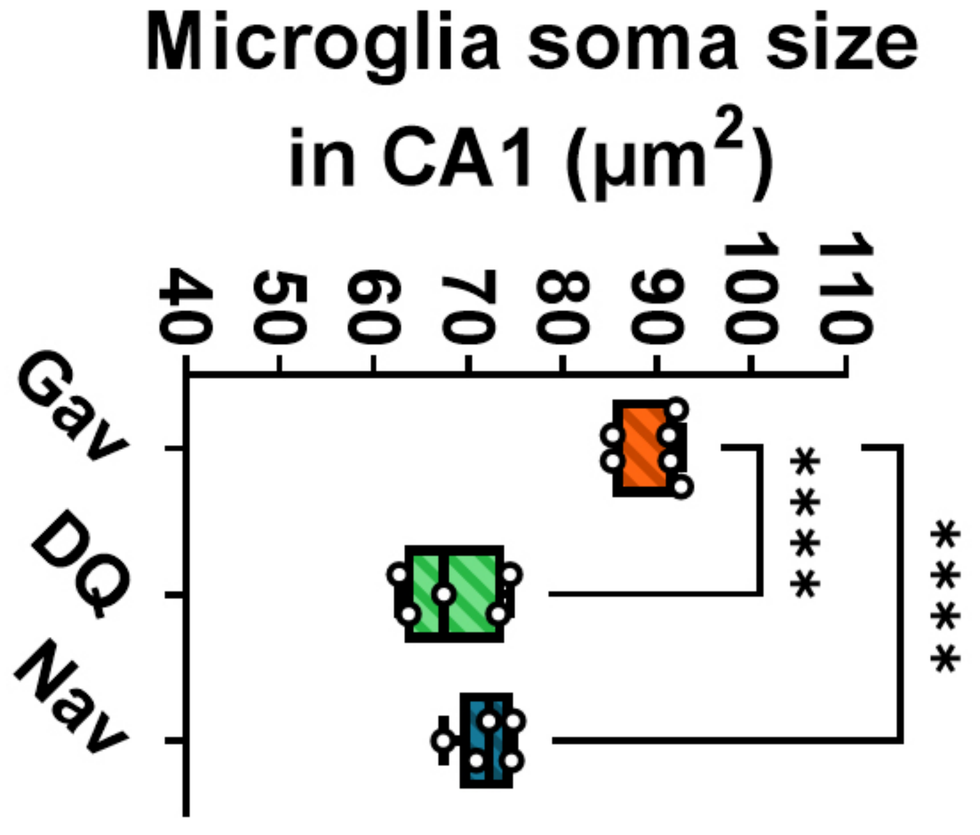
Microglia soma size in CA1 (µm2)
40
50
60
70
80
90
100
110
Gav
DQ
Nav
****
****

CA3

C)

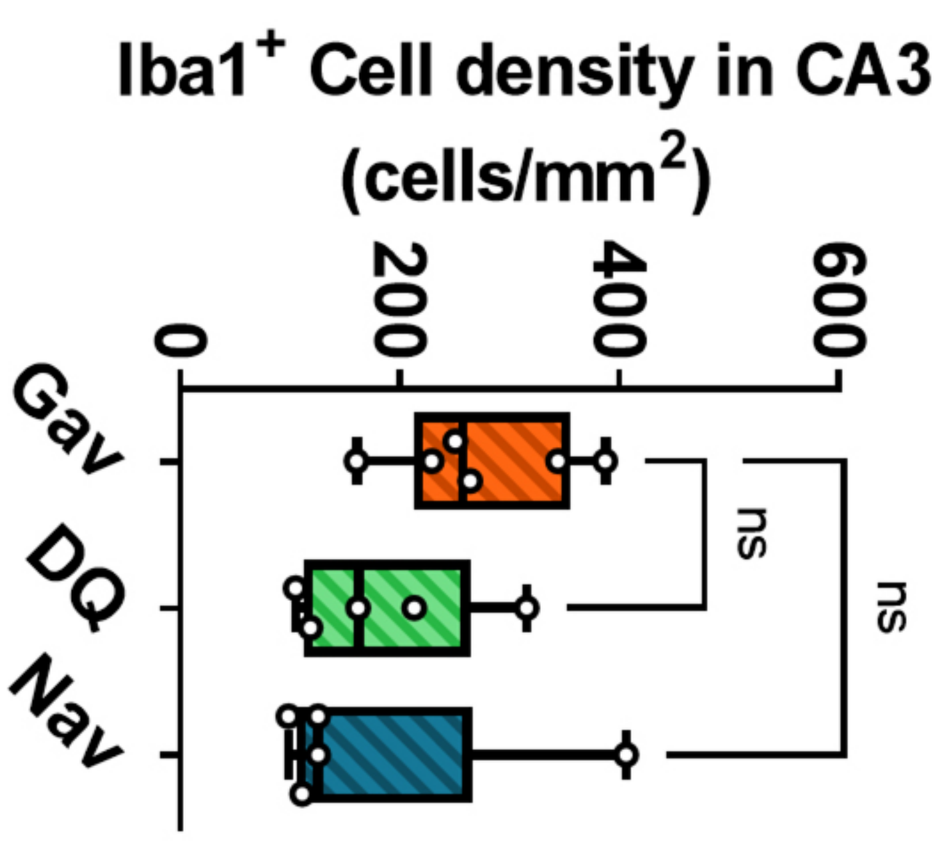
Iba1+ Cell density in CA3 (cells/mm2)
0
200
400
600
Gav
DQ
Nav
ns
ns

D)

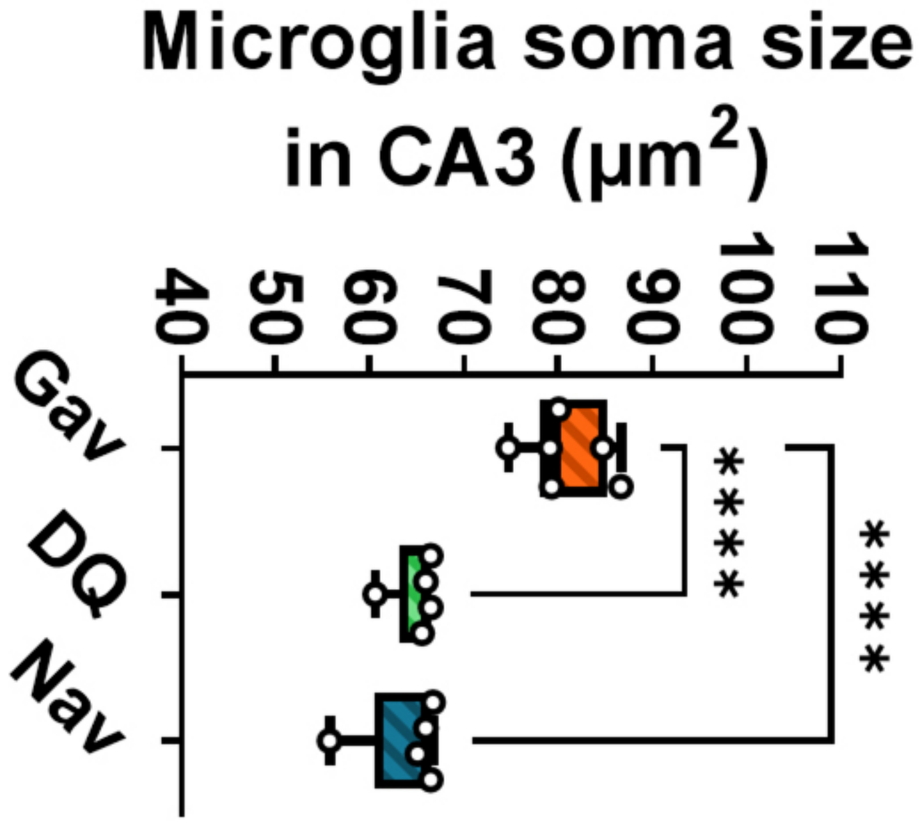
Microglia soma size in CA3 (µm2)
40
50
60
70
80
90
100
110
Gav
DQ
Nav
****
****

A)

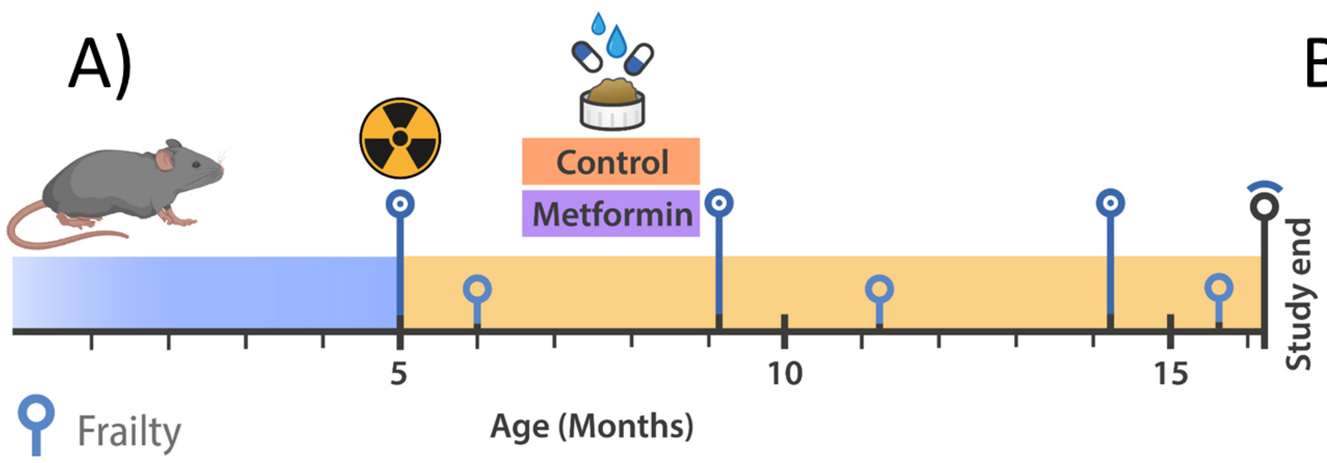

B)

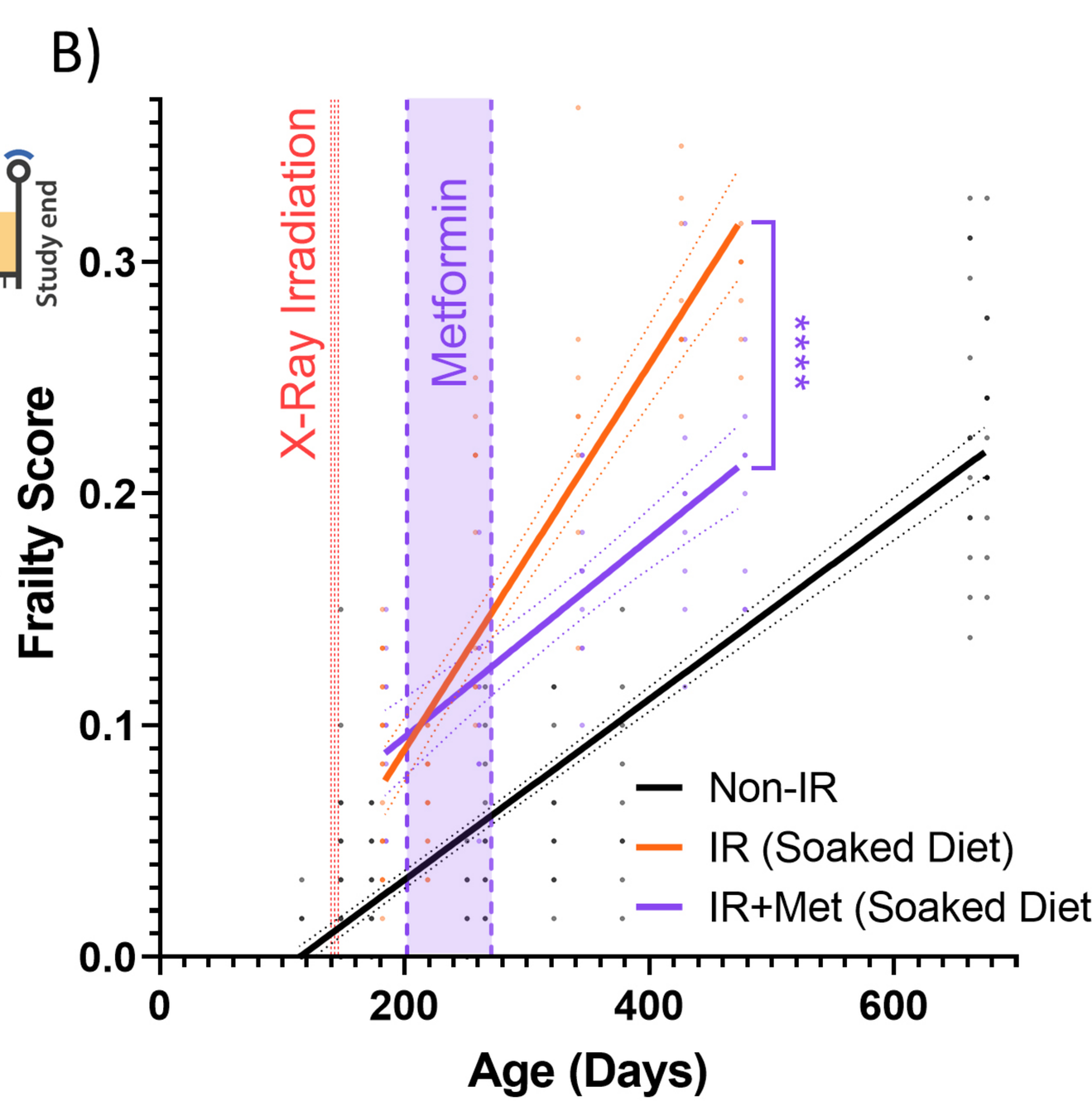

C)

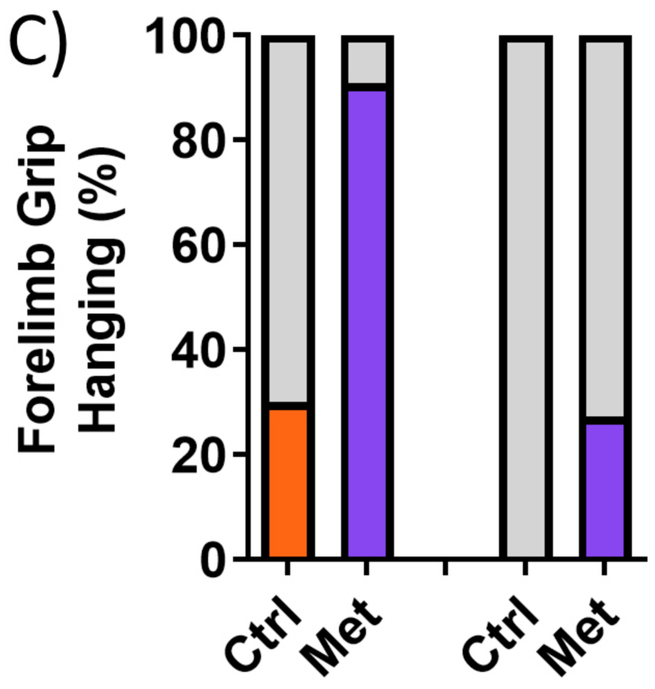

Age (months): 9m 14m

D)

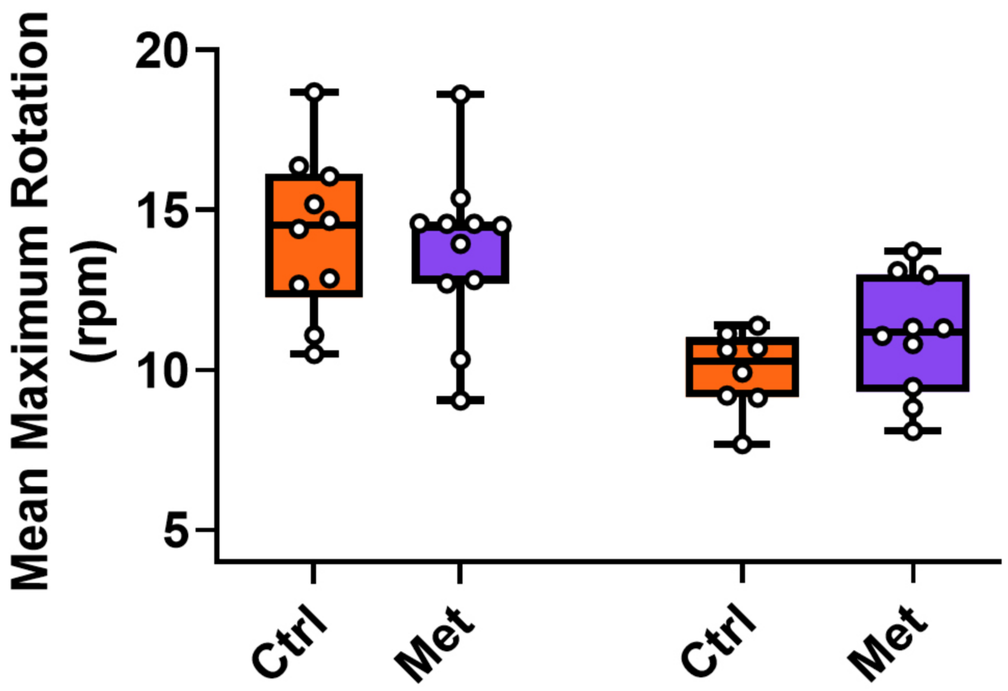

Age (months): 10m 15m

E)

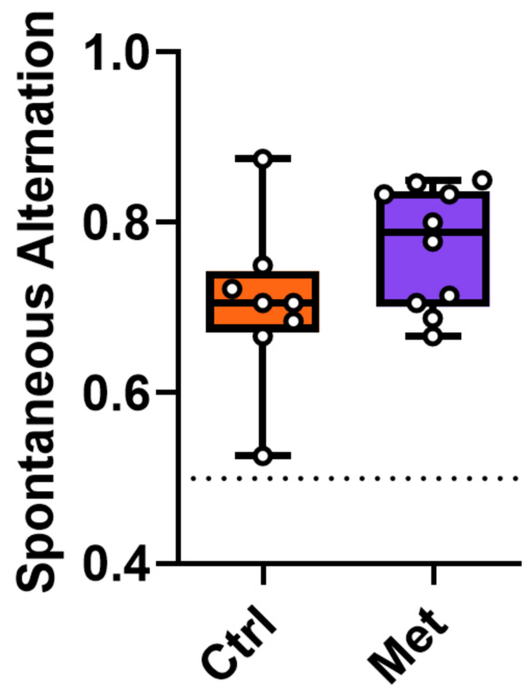

Age (months): 16m

F)

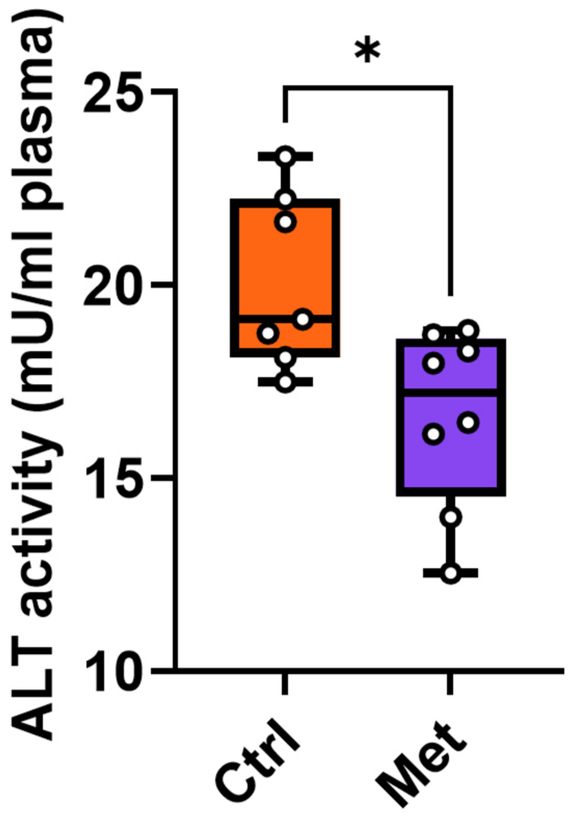

G)

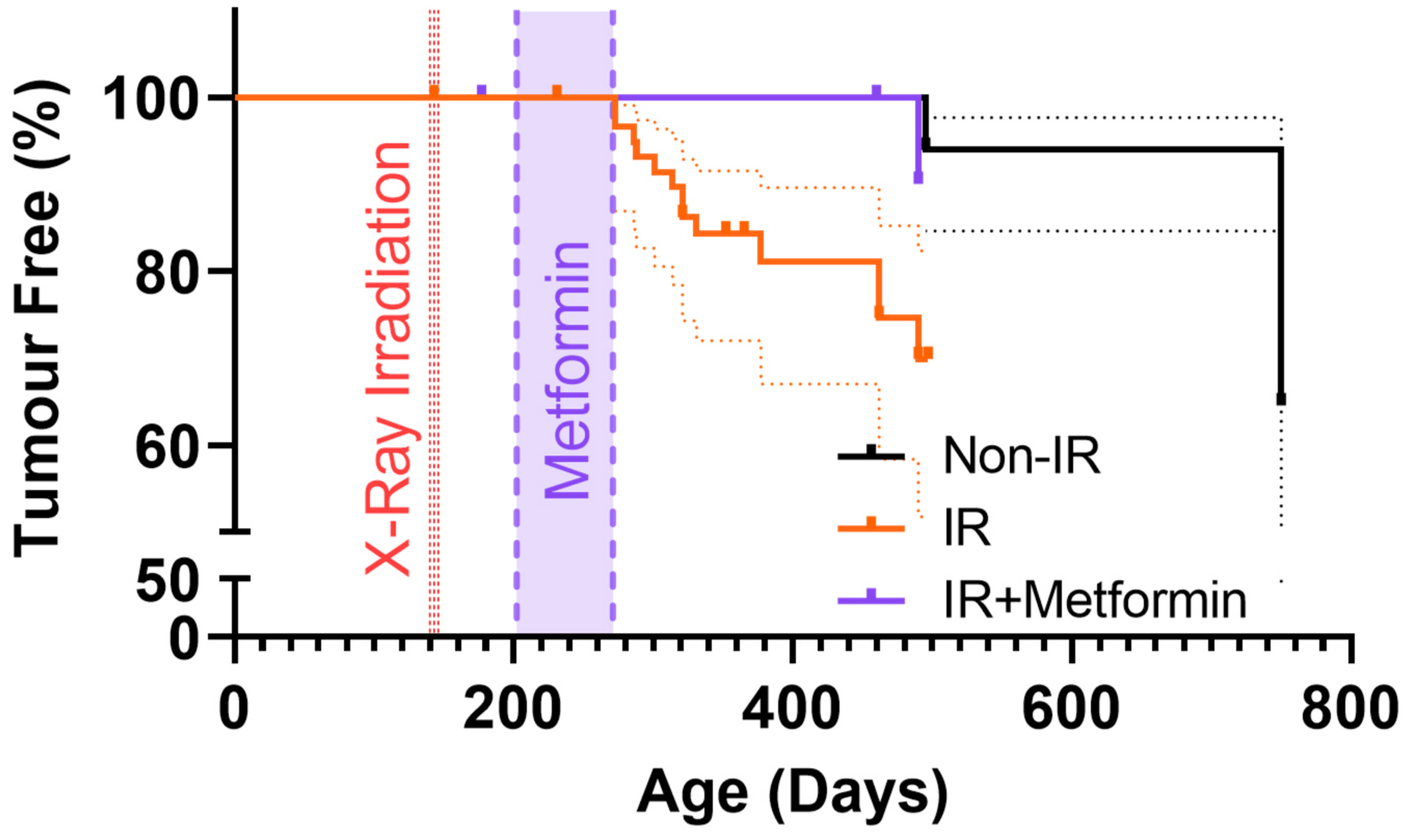

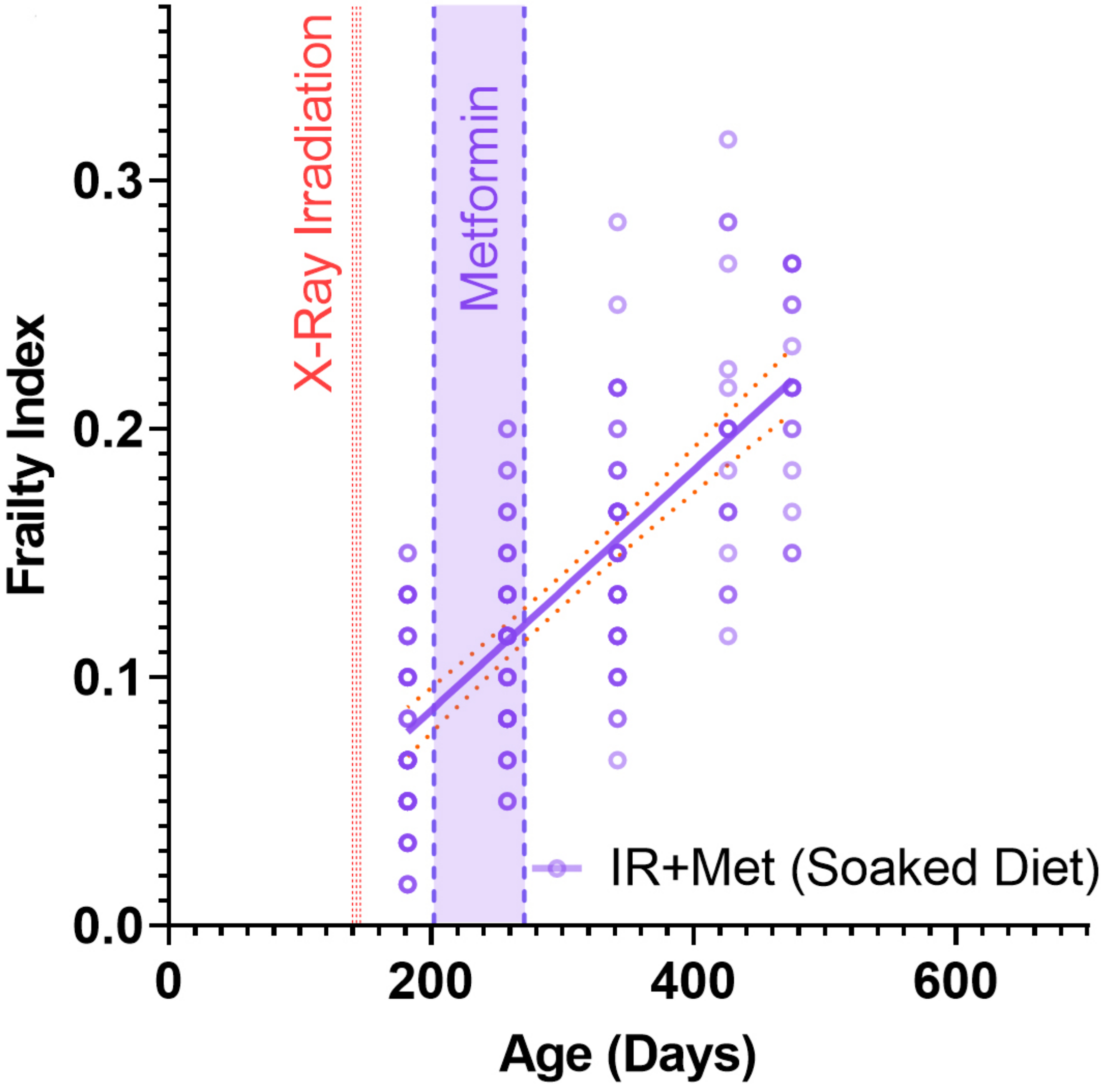
Frailty Index
0.0
0.1
0.2
0.3
0
200
400
600
Age (Days)
X-Ray Irradiation
Metformin
IR+Met (Soaked Diet)

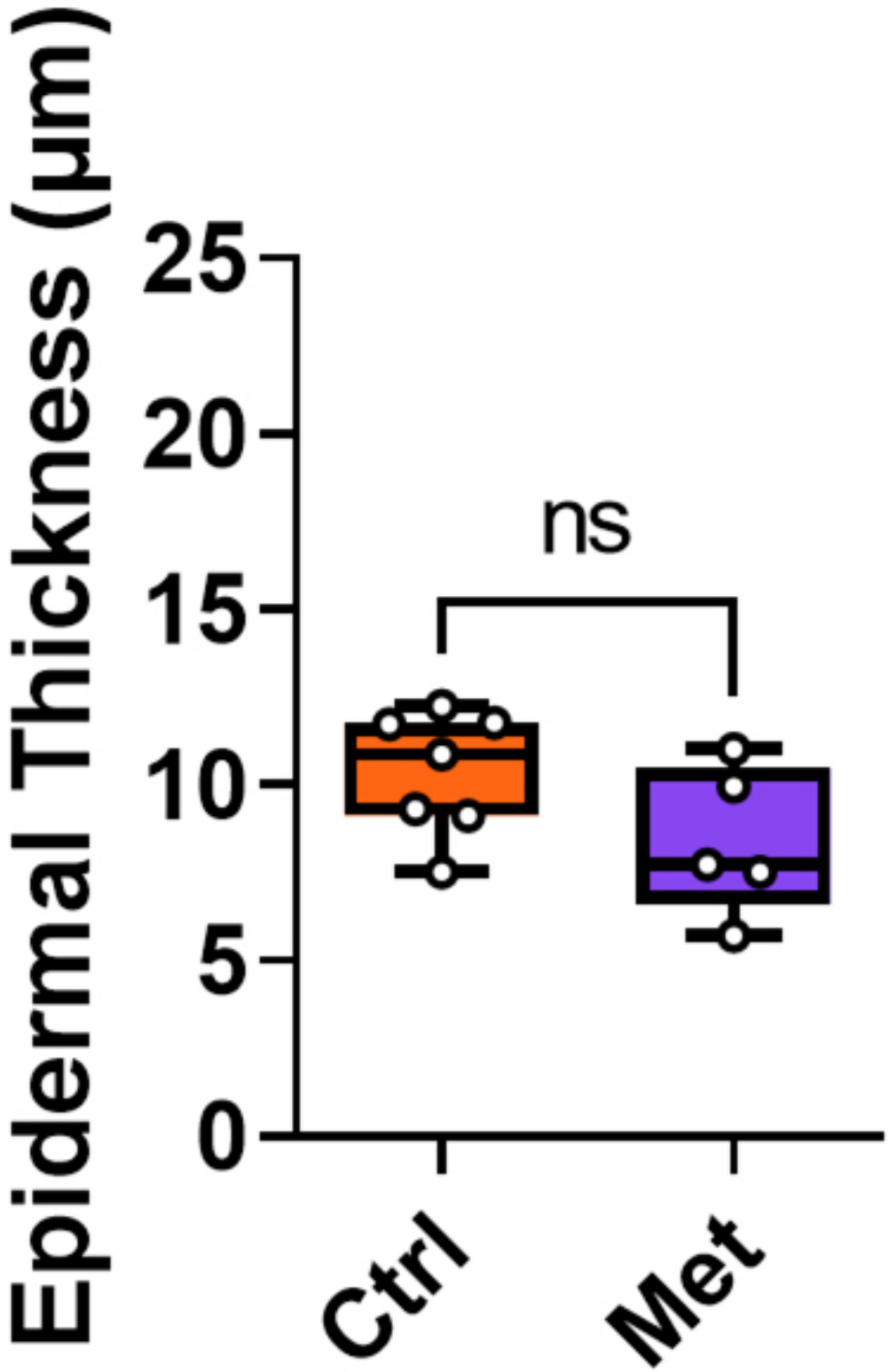
Epidermal Thickness (µm)
25
20
15
10
5
0
ns
Ctrl
Met

A)

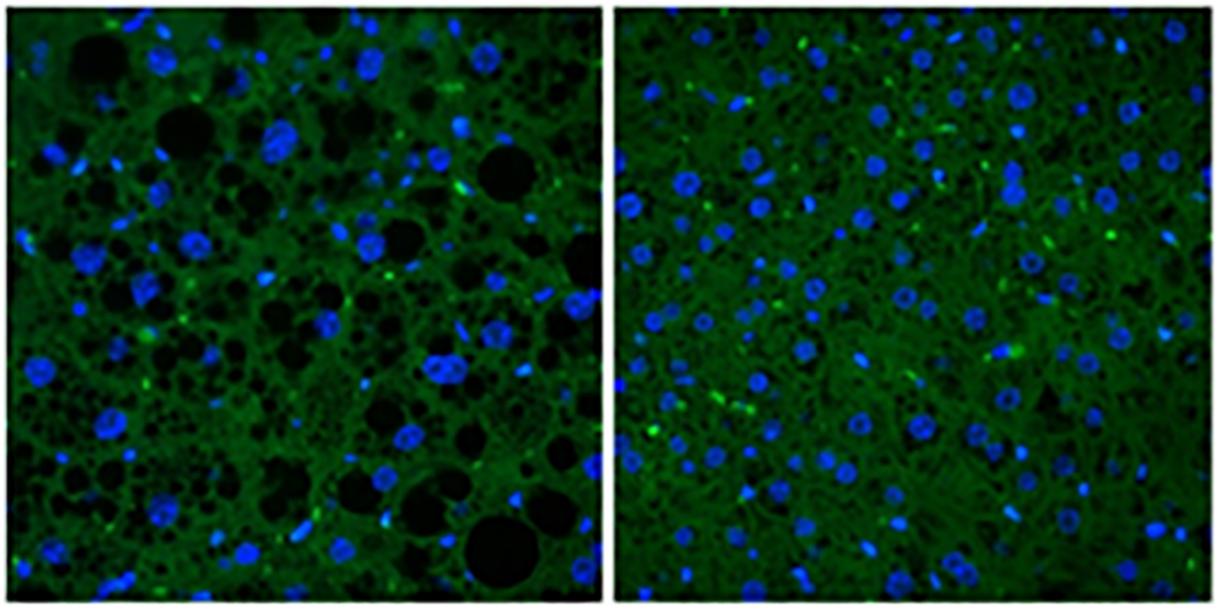
Control
Metformin

B)

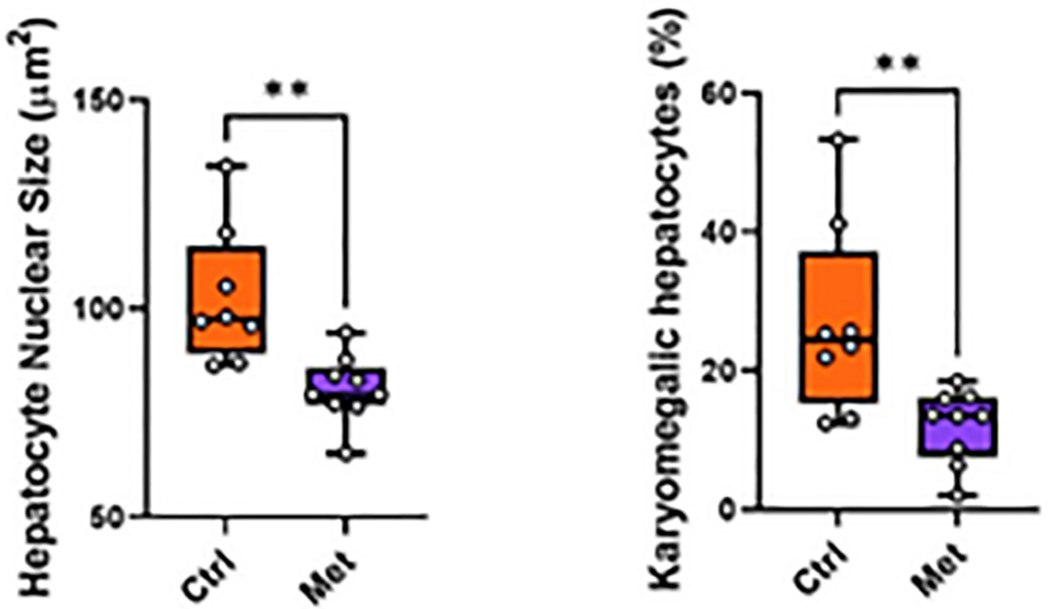
Hepatocyte Nuclear Size (µm²)
150
100
50
**
Ctrl
Met
Karyomegalic hepatocytes (%)
60
40
20
0
**
Ctrl
Met

C)

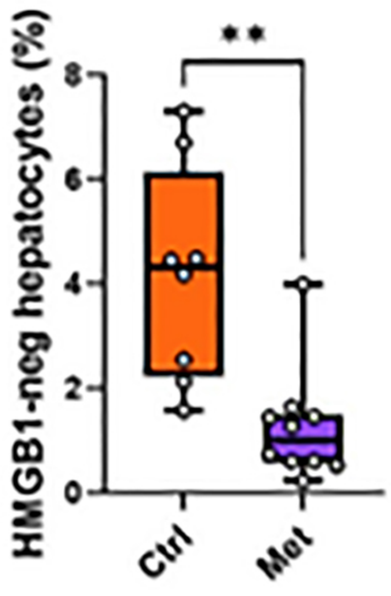
HMGB1-neg hepatocytos (%)
8
6
4
2
0
**
Ctrl
Met

D)

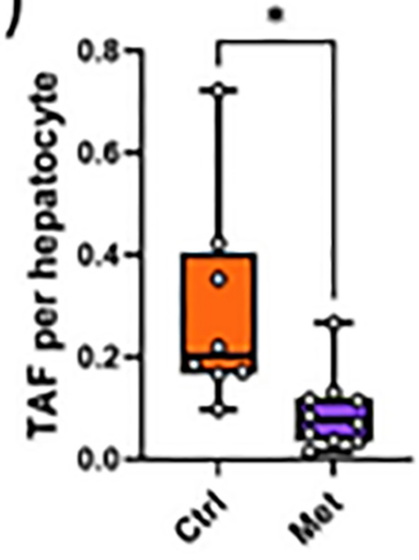
TAF per hepatocyte
0.8
0.6
0.4
0.2
0.0
*
Ctrl
Met

E)

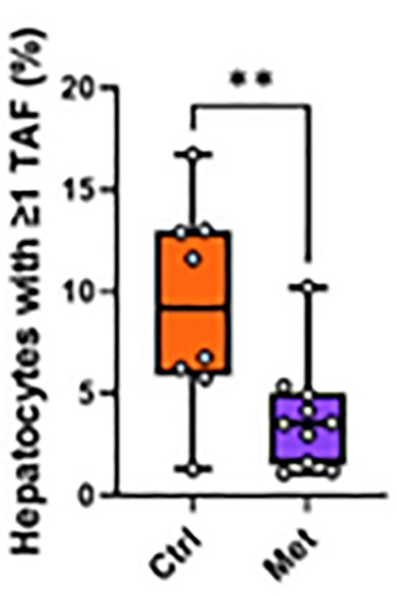
Hepatocytes with ≥1 TAF (%)
20
15
10
5
0
**
Ctrl
Met

F)

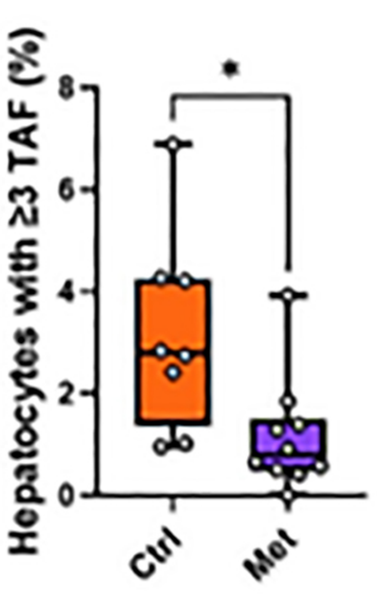
Hepatocytes with ≥3 TAF (%)
8
6
4
2
0
*
Ctrl
Met

A)

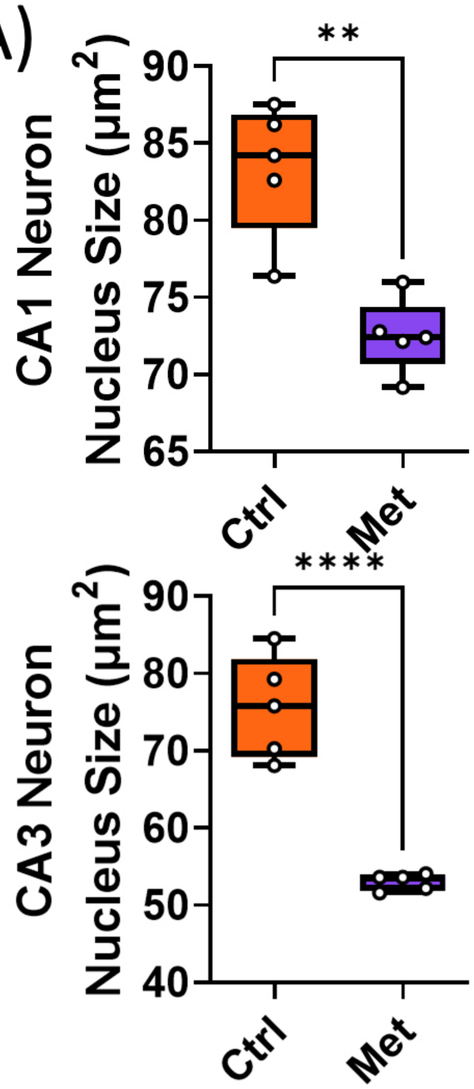
CA1 Neuron Nucleus Size (μm²)
90
85
80
75
70
65
**
Ctrl
Met

CA3 Neuron Nucleus Size (μm²)
90
80
70
60
50
40
****
Ctrl
Met

B)

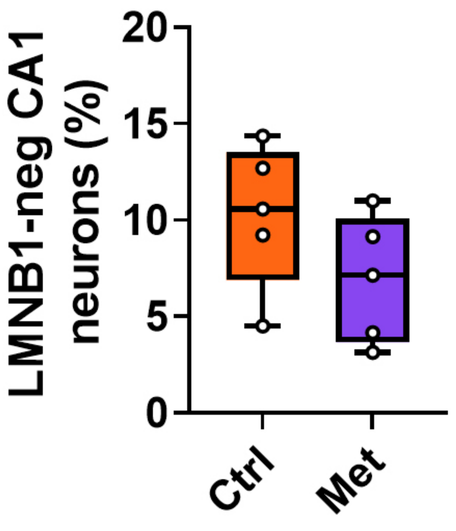
LMNB1-neg CA1 neurons (%)
20
15
10
5
0
Ctrl
Met

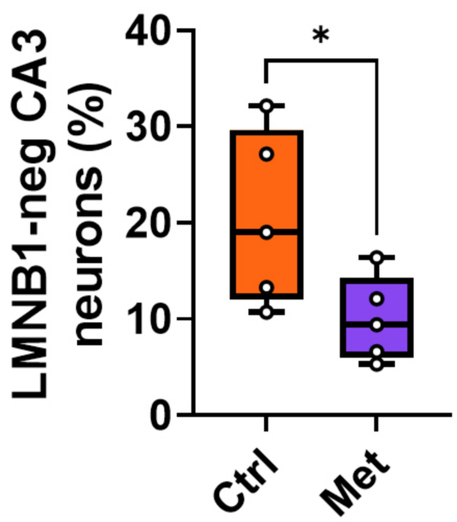
LMNB1-neg CA3 neurons (%)
40
30
20
10
0
*
Ctrl
Met

C)

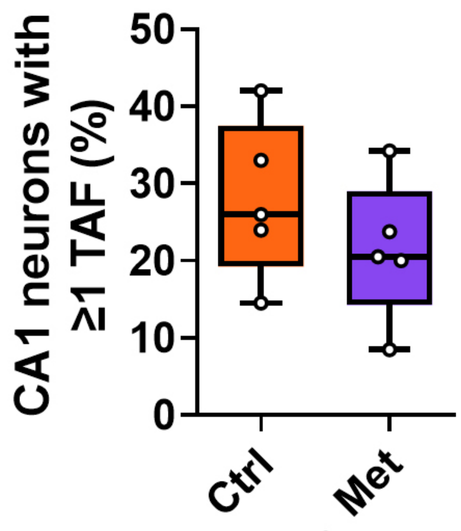
CA1 neurons with ≥1 TAF (%)
50
40
30
20
10
0
Ctrl
Met

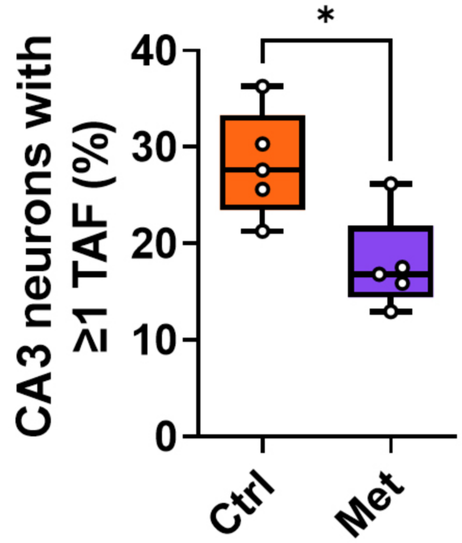
CA3 neurons with ≥1 TAF (%)
40
30
20
10
0
*
Ctrl
Met

D)

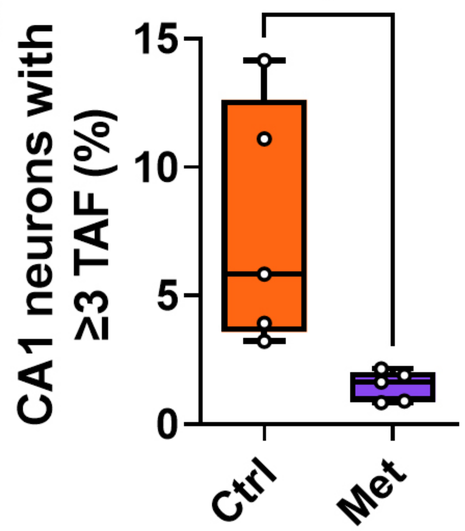
CA1 neurons with ≥3 TAF (%)
15
10
5
0
*
Ctrl
Met

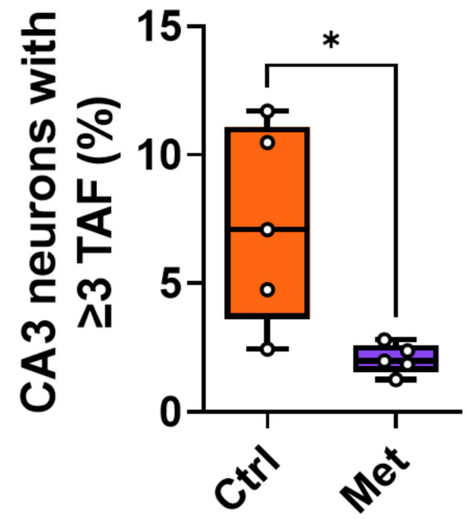
CA3 neurons with ≥3 TAF (%)
15
10
5
0
*
Ctrl
Met

E)

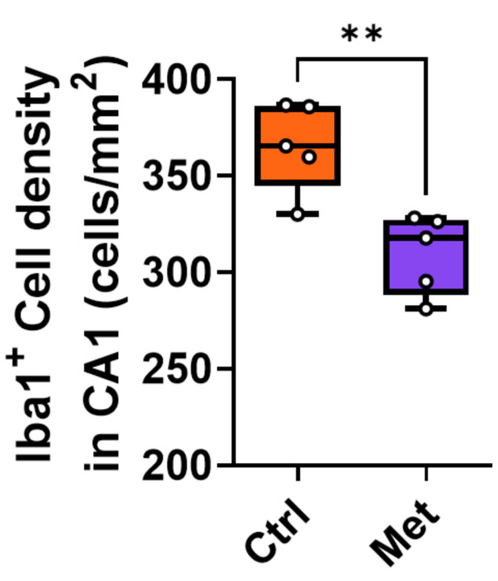
Iba1⁺ Cell density in CA1 (cells/mm²)
400
350
300
250
200
**
Ctrl
Met

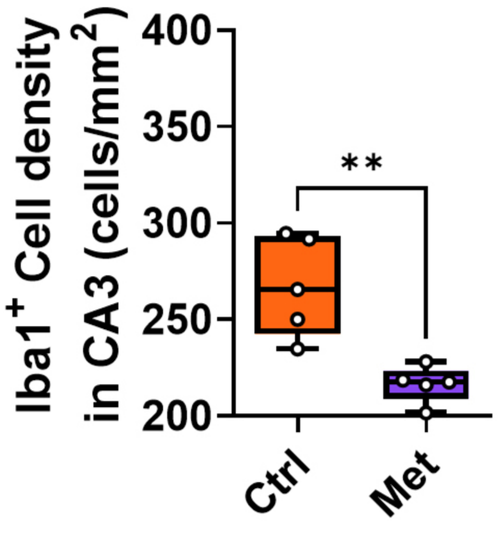
Iba1⁺ Cell density in CA3 (cells/mm²)
400
350
300
250
200
**
Ctrl
Met

F)

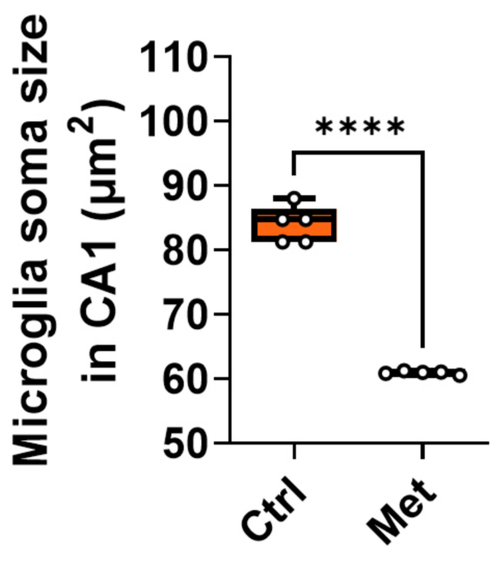
Microglia soma size in CA1 (μm²)
110
100
90
80
70
60
50
****
Ctrl
Met

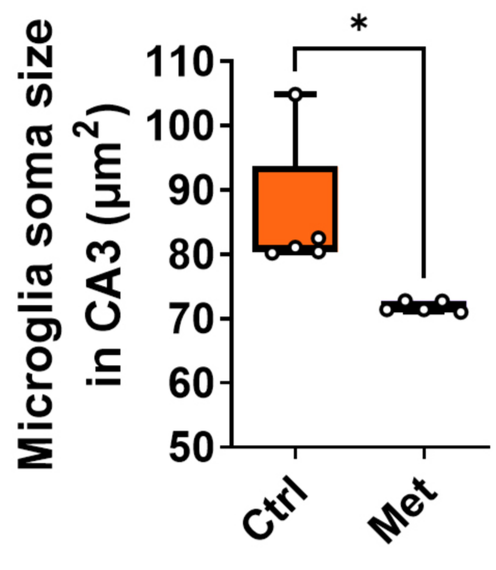
Microglia soma size in CA3 (μm²)
110
100
90
80
70
60
50
*
Ctrl
Met

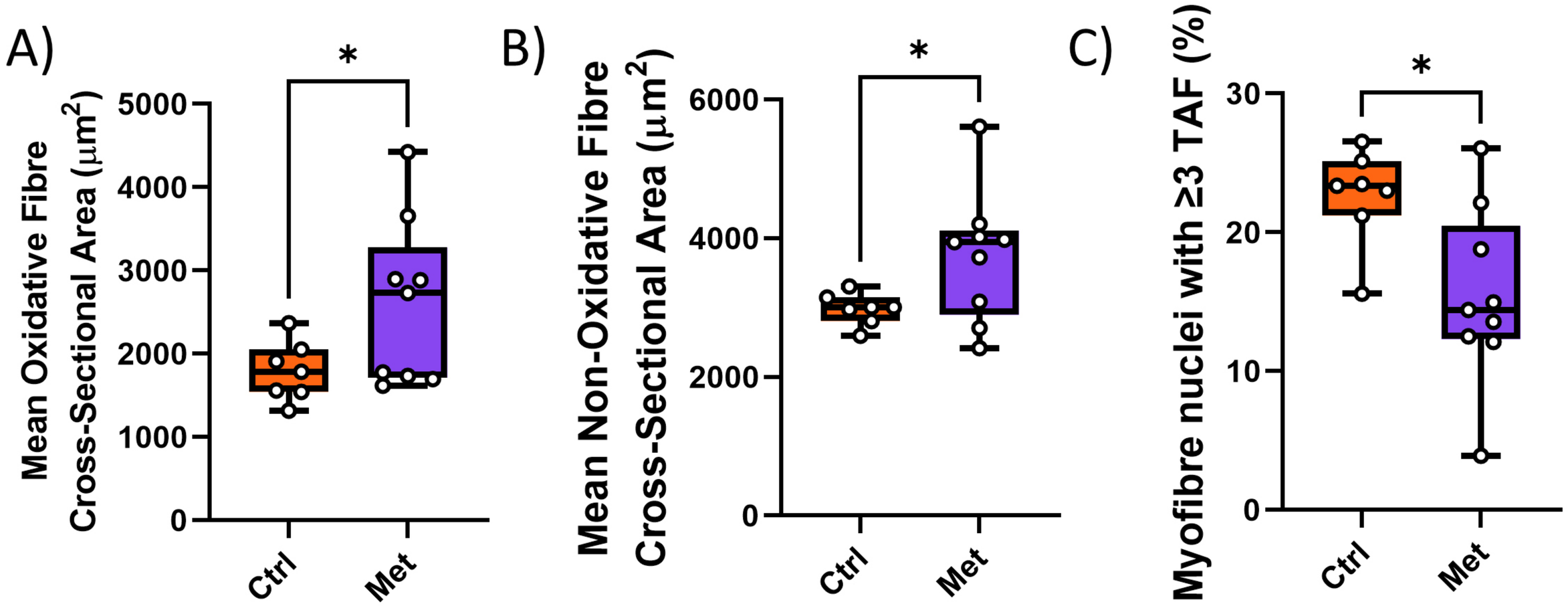
A)
Mean Oxidative Fibre Cross-Sectional Area (µm²)
5000
4000
3000
2000
1000
0
*
Ctrl
Met
B)
Mean Non-Oxidative Fibre Cross-Sectional Area (µm²)
6000
4000
2000
0
*
Ctrl
Met
C)
Myofibre nuclei with ≥3 TAF (%)
30
20
10
0
*
Ctrl
Met

Control

Metformin

IL1a
IL2
IL5
IL6
IL7
IL10
IL12
IL13
LIX
IL17A
CXCL1
CCL2
CXCL2
TNFa

+
*
+

-2 0 +2

A)

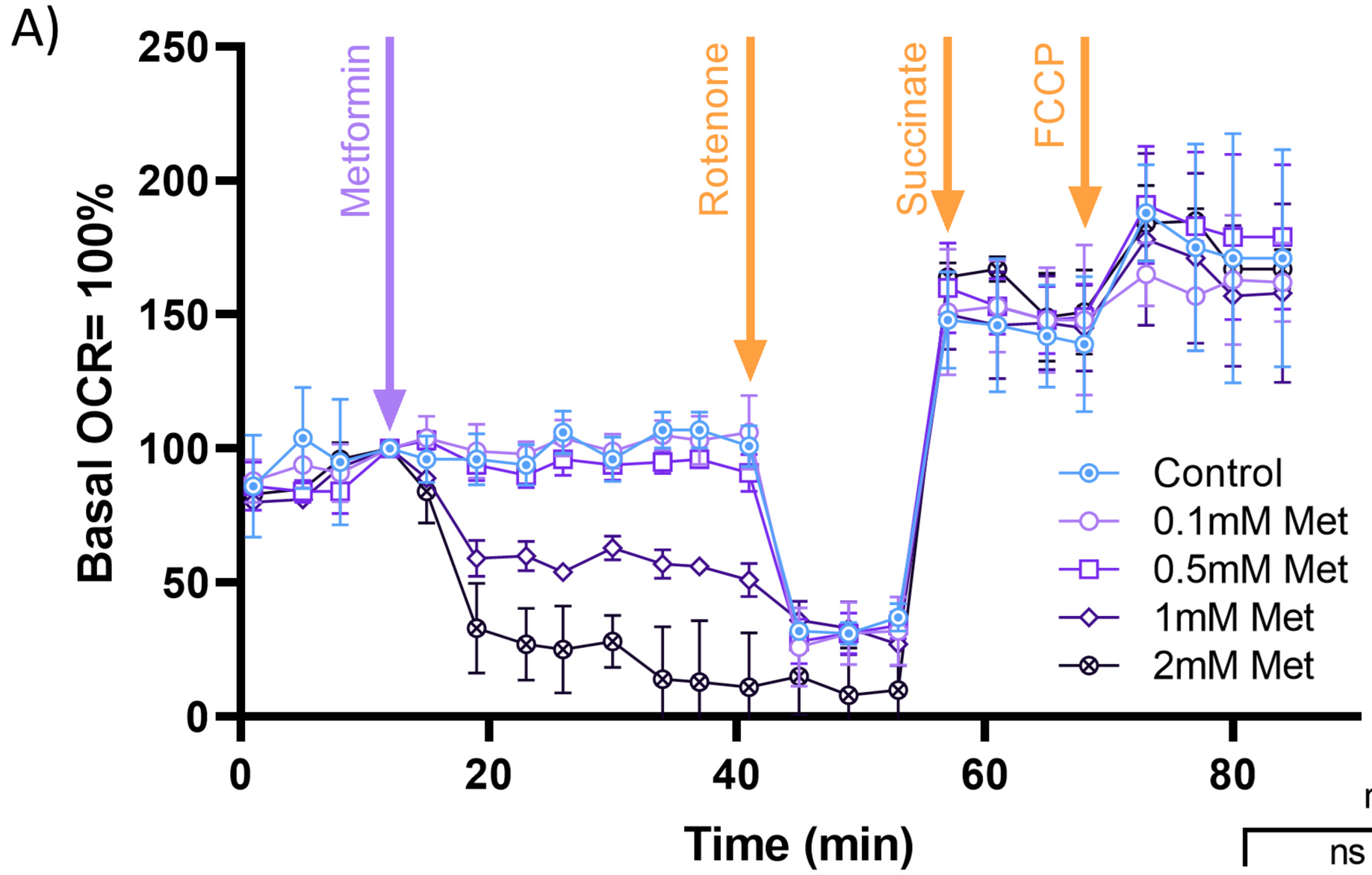
Basal OCR= 100%
250
200
150
100
50
0
Metformin
Rotenone
Succinate
FCCP
Control
0.1mM Met
0.5mM Met
1mM Met
2mM Met
0
20
40
60
80
Time (min)

B)

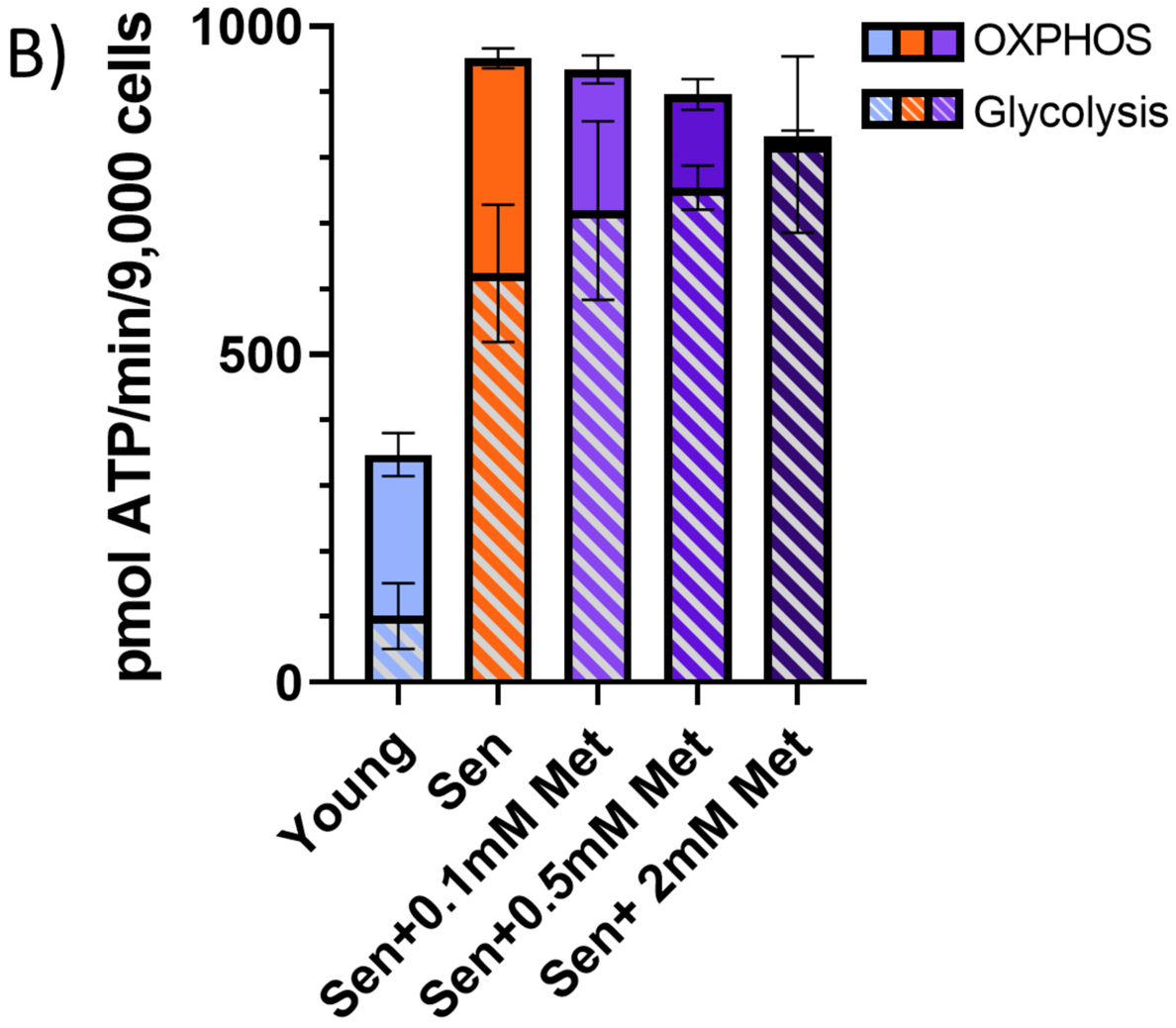
pmol ATP/min/9,000 cells
1000
500
0
OXPHOS
Glycolysis
Young
Sen
Sen+0.1mM Met
Sen+0.5mM Met
Sen+ 2mM Met

C)

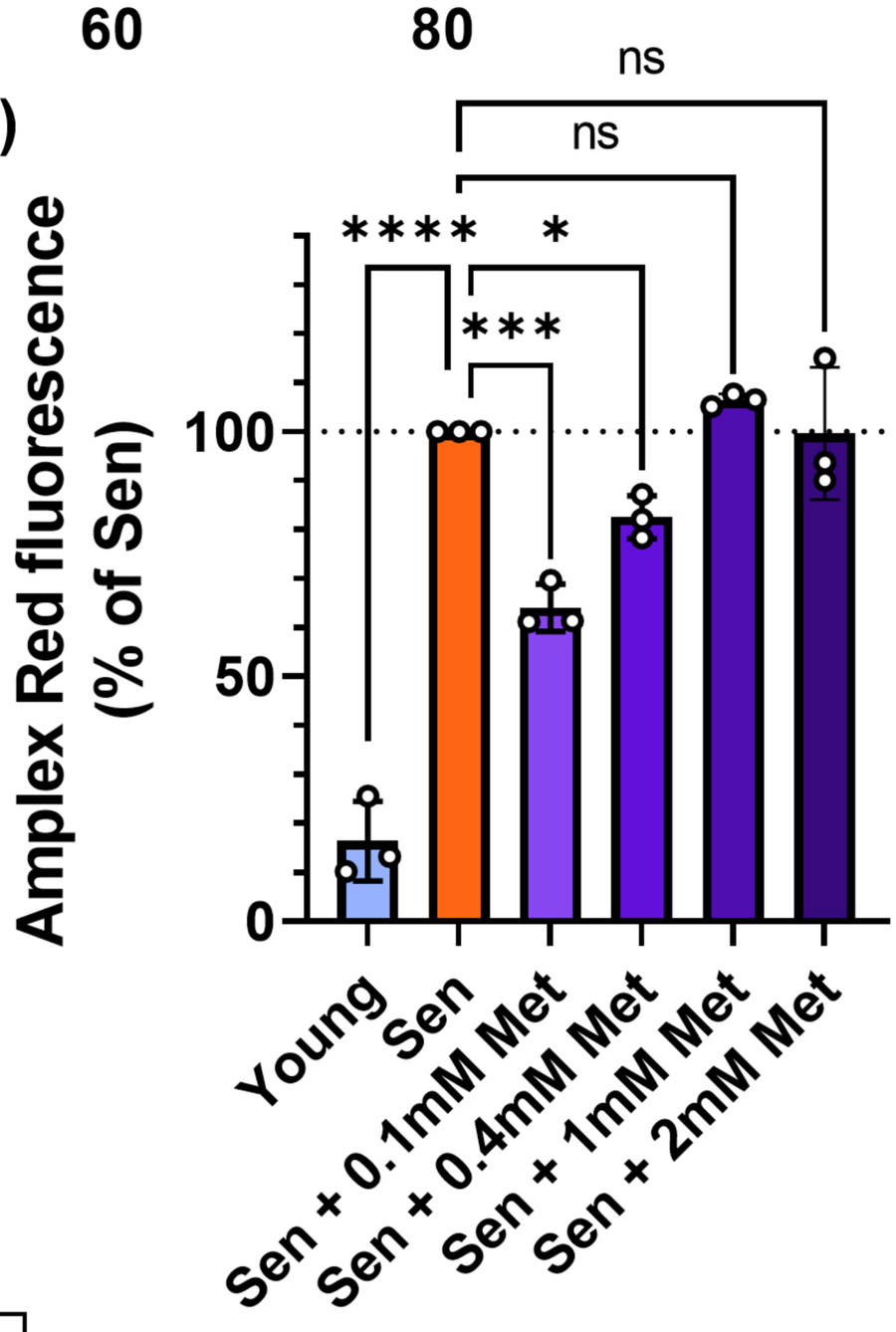
Amplex Red fluorescence (% of Sen)
ns
ns
****
*
***
100
50
0
Young
Sen
Sen + 0.1mM Met
Sen + 0.4mM Met
Sen + 1mM Met
Sen + 2mM Met

D)

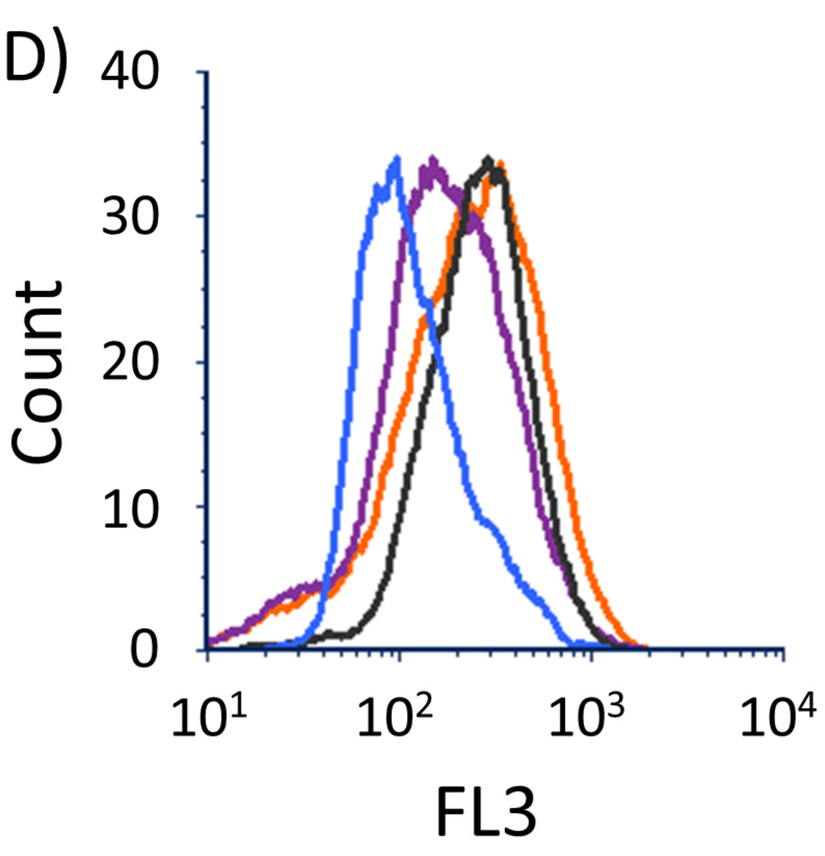
Count
40
30
20
10
0
10^1
10^2
10^3
10^4
FL3

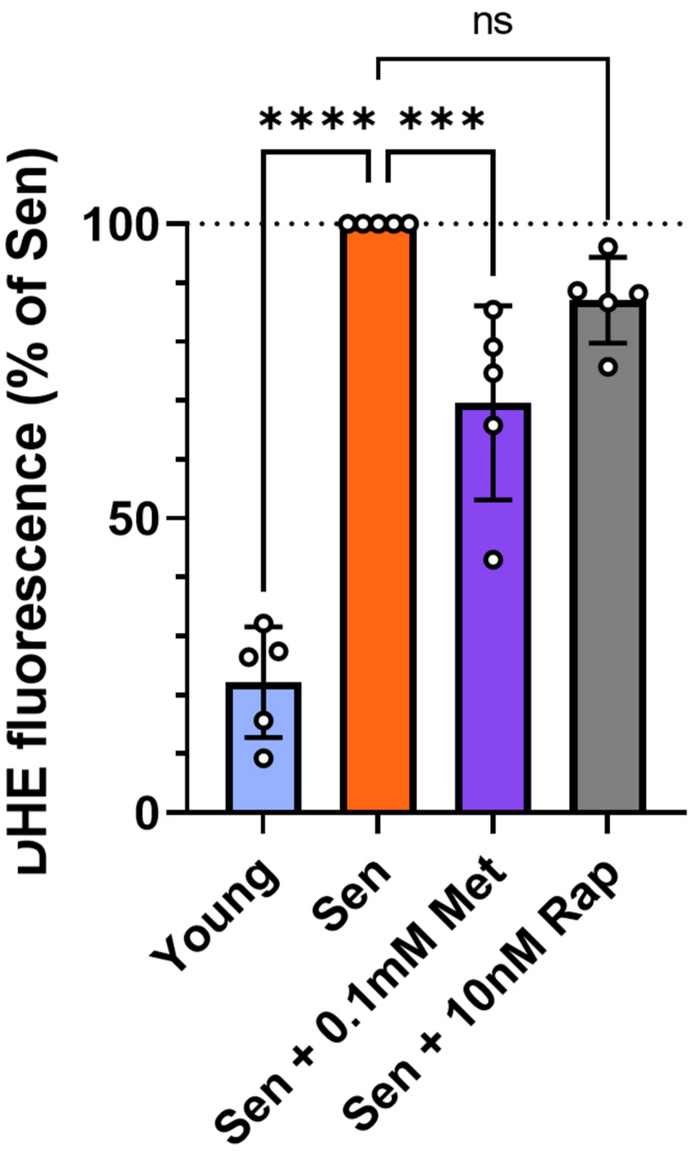
DHE fluorescence (% of Sen)
ns
**** ***
100
50
0
Young
Sen
Sen + 0.1mM Met
Sen + 10nM Rap

E)

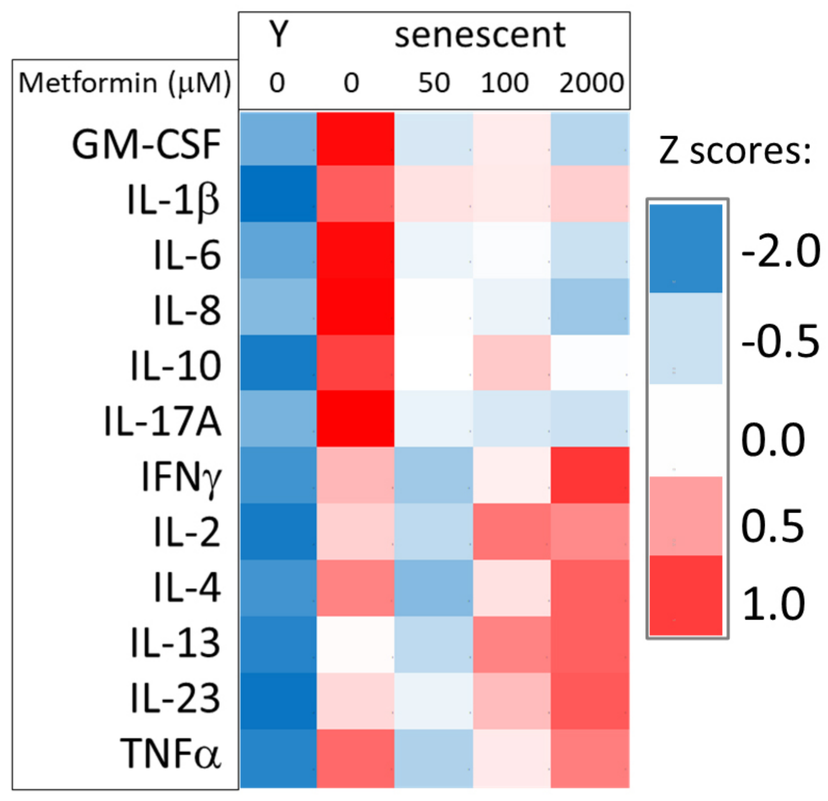
Y
senescent
Metformin (μM)
0
0
50
100
2000
GM-CSF
IL-1β
IL-6
IL-8
IL-10
IL-17A
IFNγ
IL-2
IL-4
IL-13
IL-23
TNFα
Z scores:
-2.0
-0.5
0.0
0.5
1.0

A)

	Heat shock			Stress	Oxid Stress			Xeno detox		ER-UPR			Mito-UPR			mTOR			DDR, senescence		
	HSF1	HSP60	HSP70	p-p38	NRF2	SOD2	8oxoG	GSTM2	NR1|2	ATF6a	p-eIF2a	GRP78	HSP60	CLpP	CHOP	pACoA	pS6RP	p62	gH2AX	p21	p16
2mM Metformin																					
0.1mM Metformin																					
starvation																					
heat shock																					
H_2O_2																					

B)

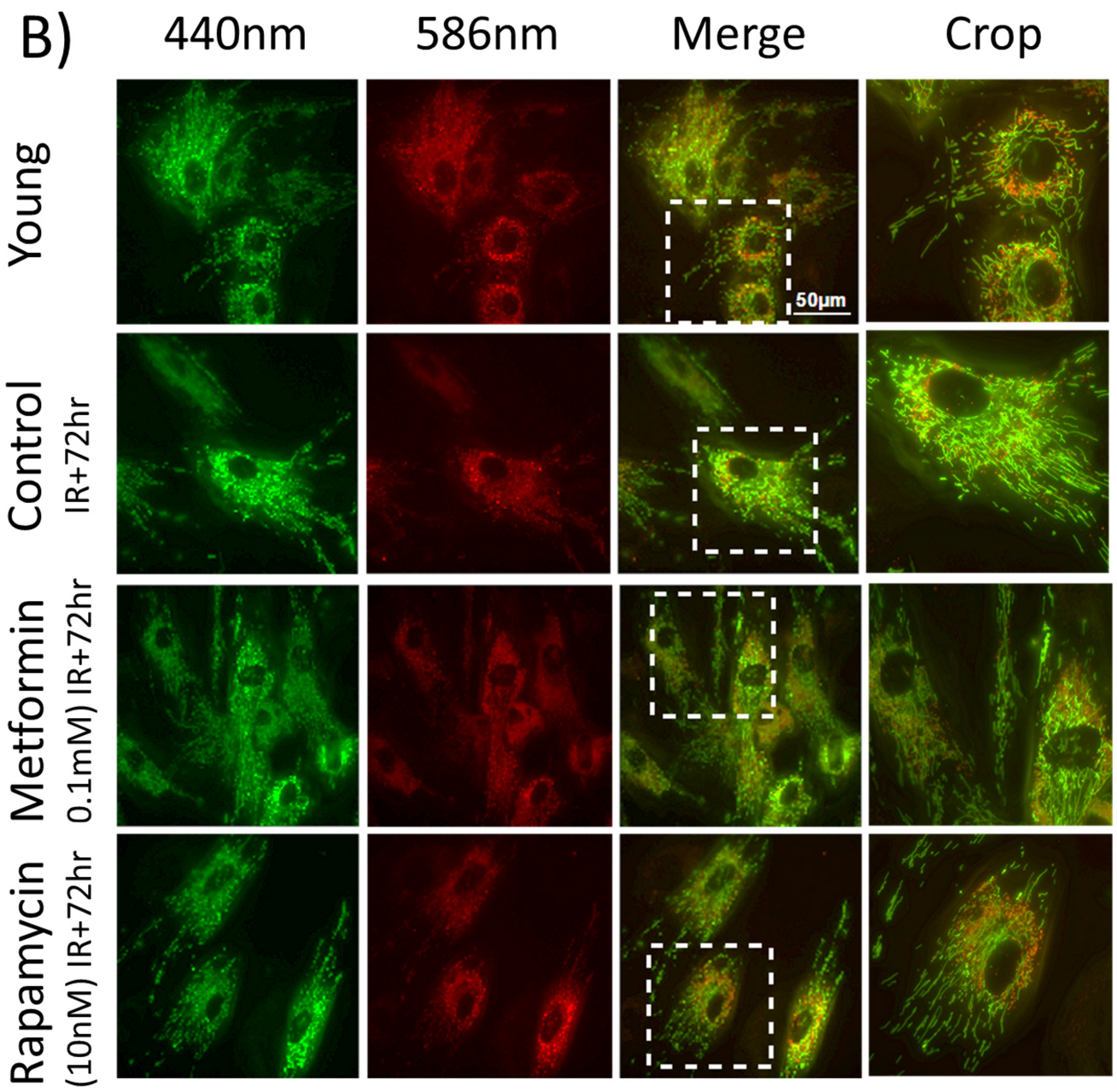

C)

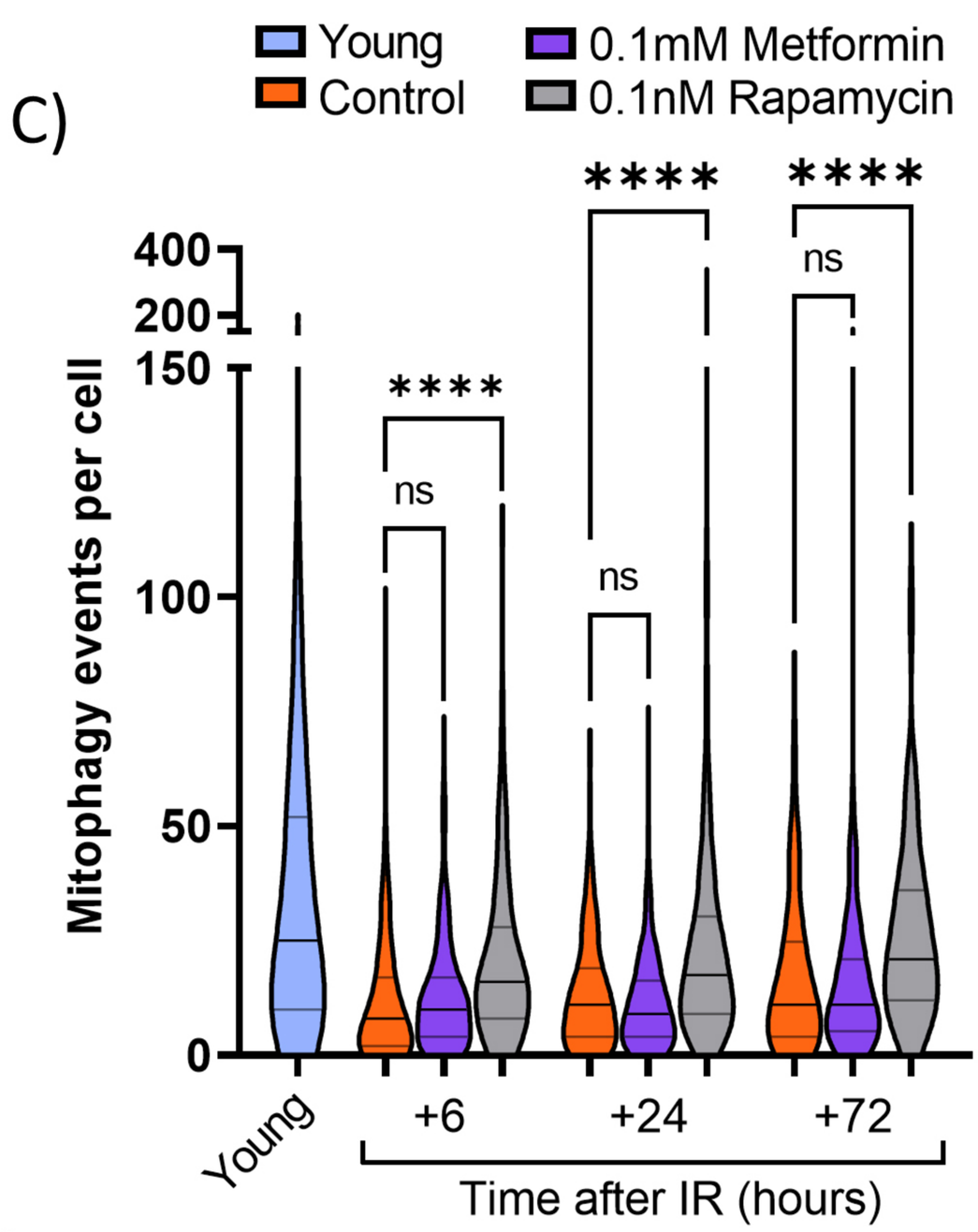

D)

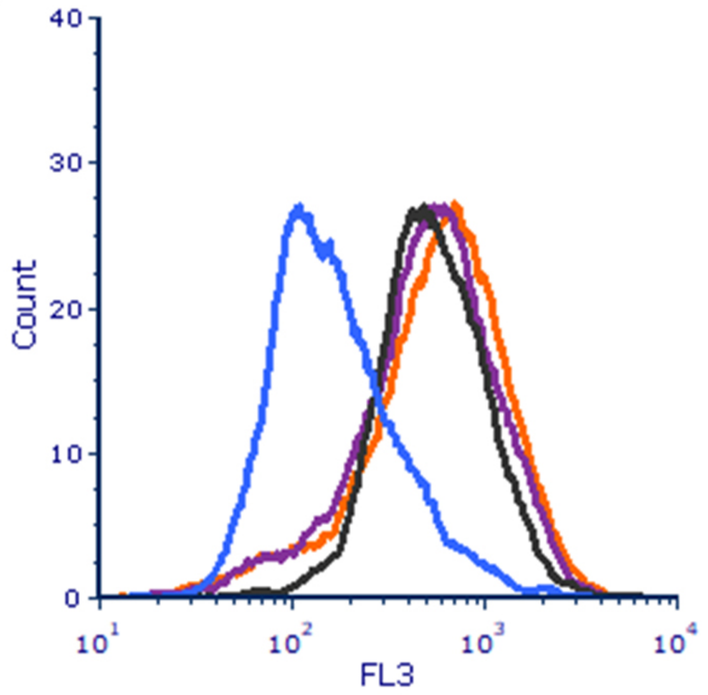

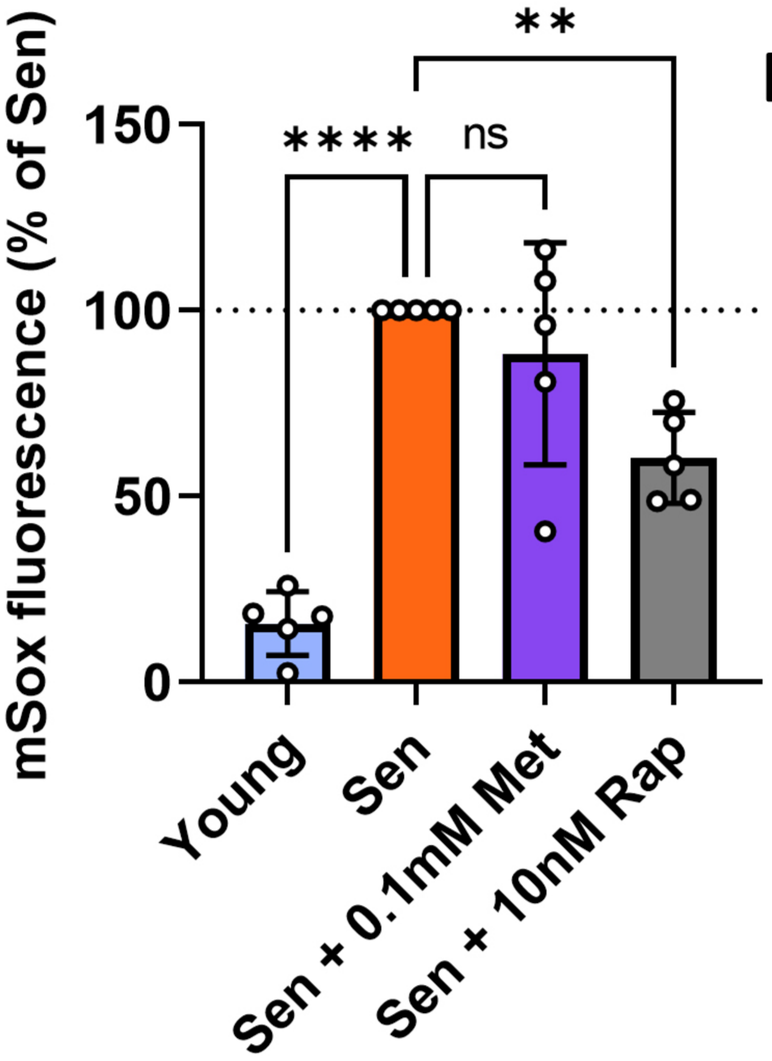

E)

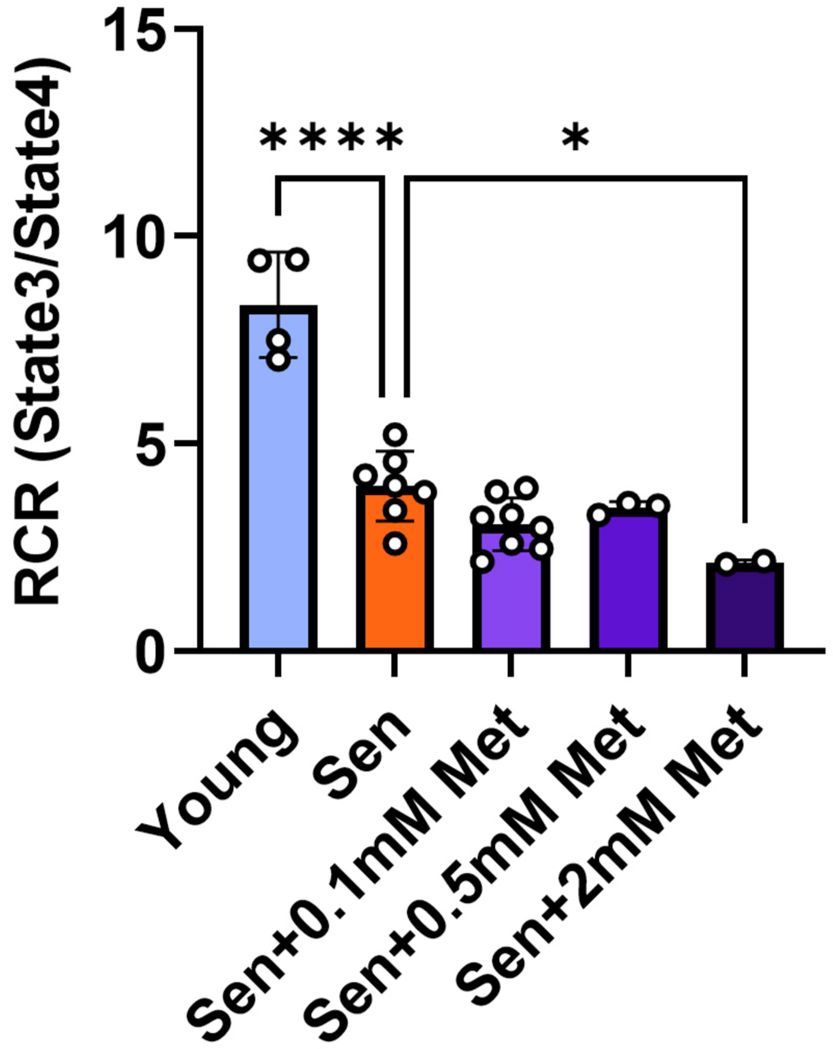

100nM Met

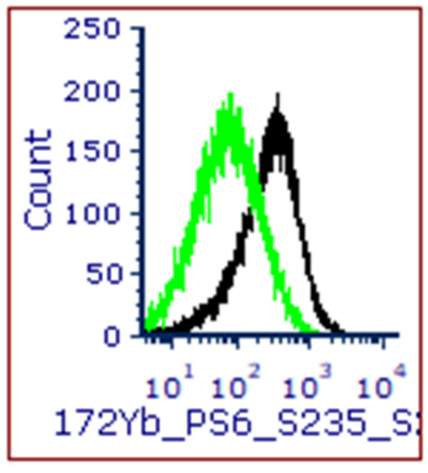

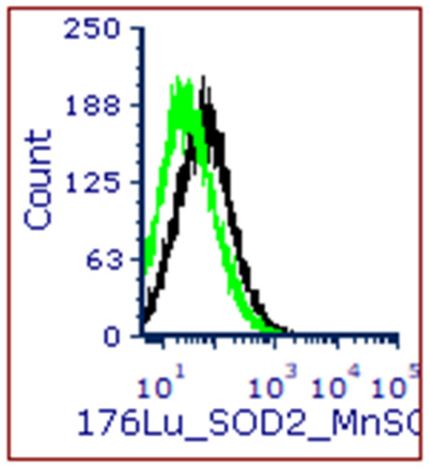

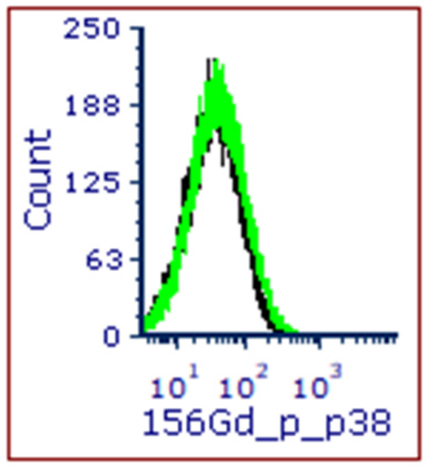

2mM Met

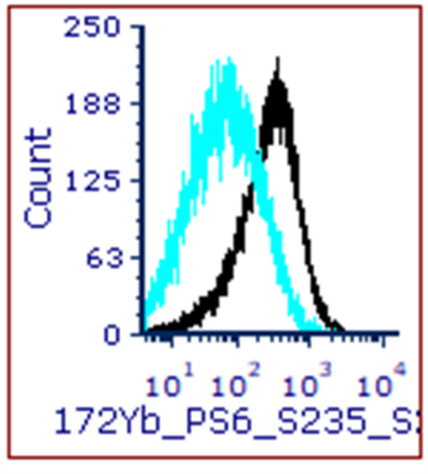

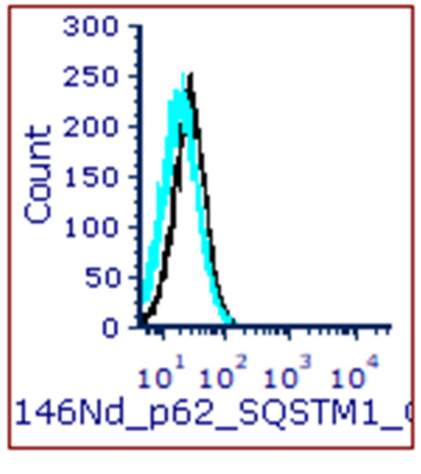

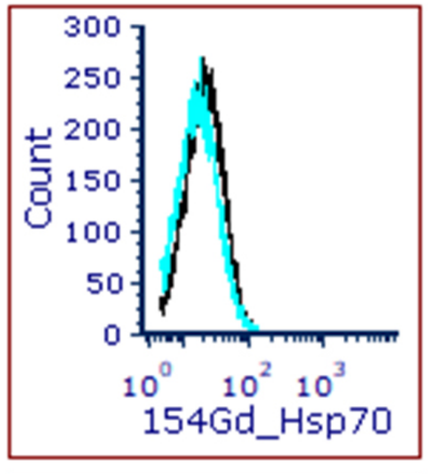

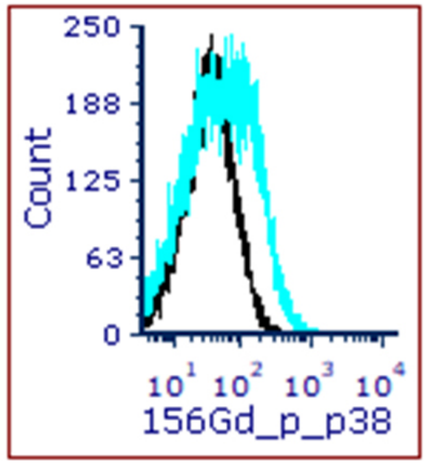

Starvation

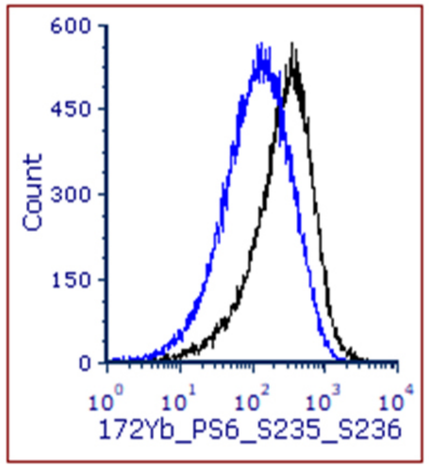

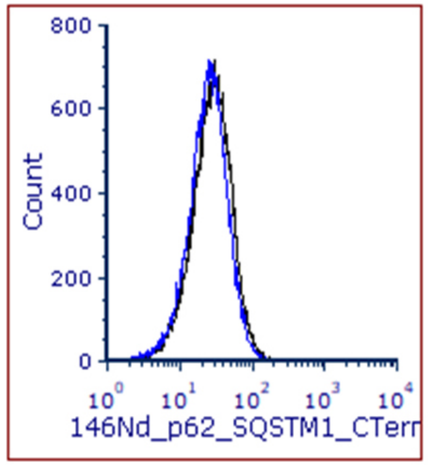

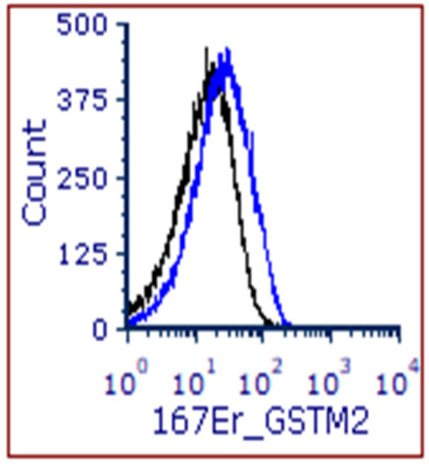

Heat Shock

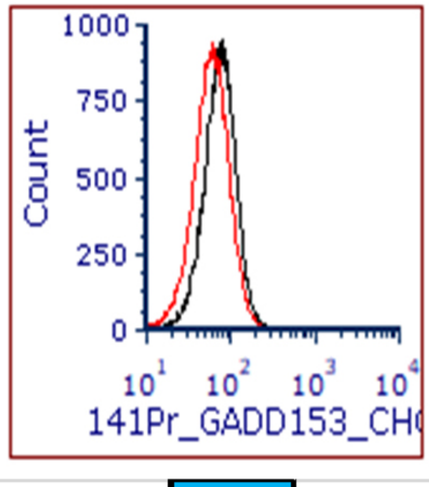

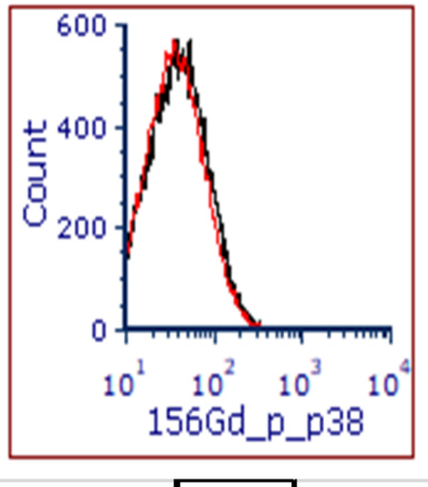

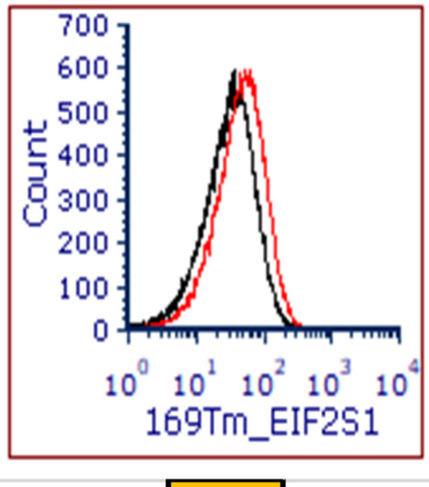

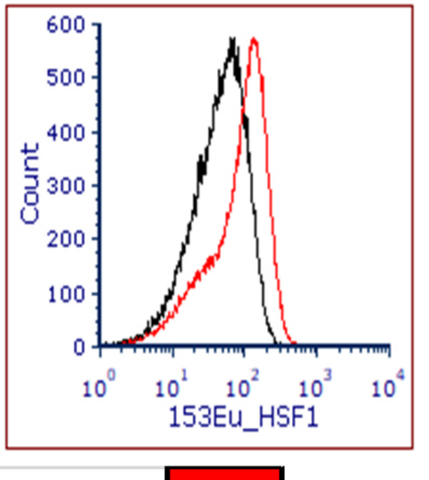

A)

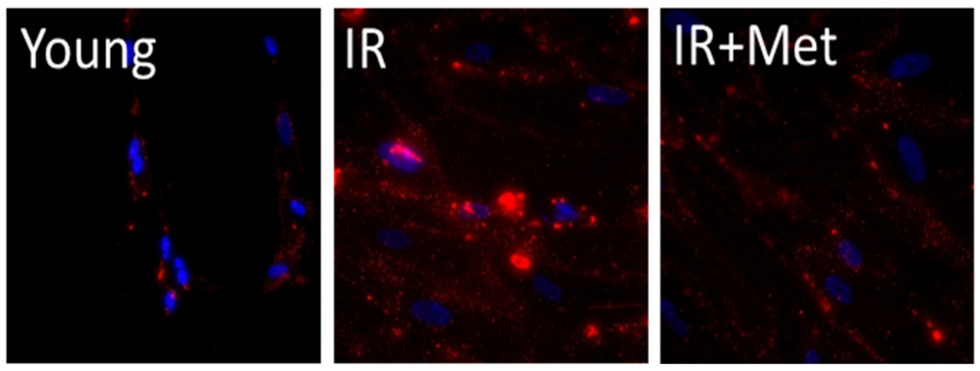
Young
IR
IR+Met

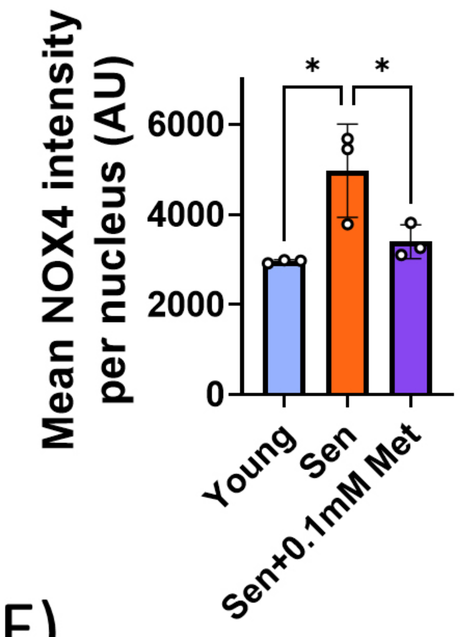
Mean NOX4 intensity per nucleus (AU)
6000
4000
2000
0
*
*
Young
Sen
Sen+0.1mM Met

B)

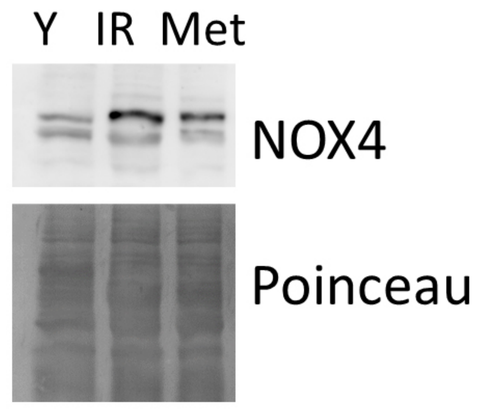
Y
IR
Met
NOX4
Poinceau

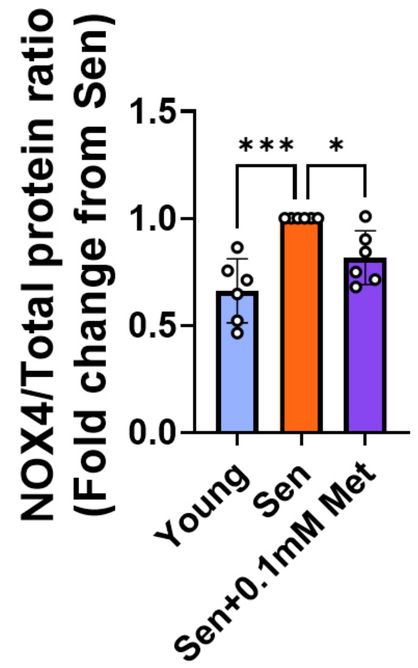
NOX4/Total protein ratio (Fold change from Sen)
1.5
1.0
0.5
0.0
***
*
Young
Sen
Sen+0.1mM Met

C)

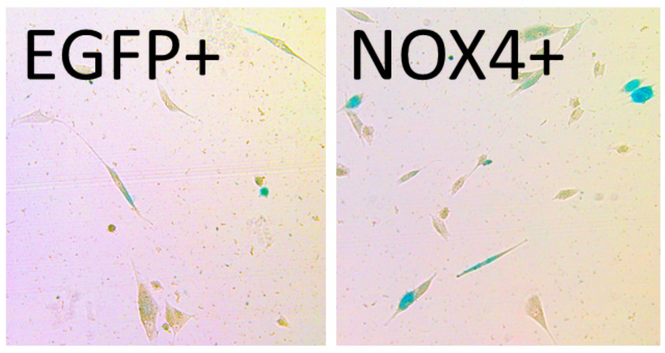
EGFP+
NOX4+

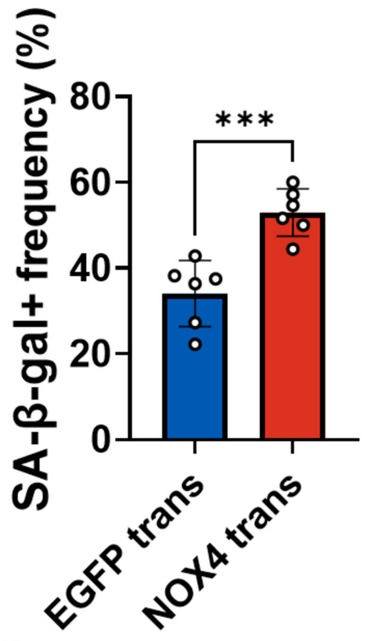
SA-β-gal+ frequency (%)
80
60
40
20
0
***
EGFP trans
NOX4 trans

D)

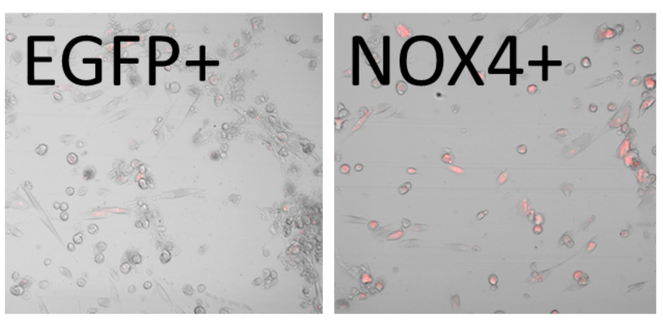
EGFP+
NOX4+

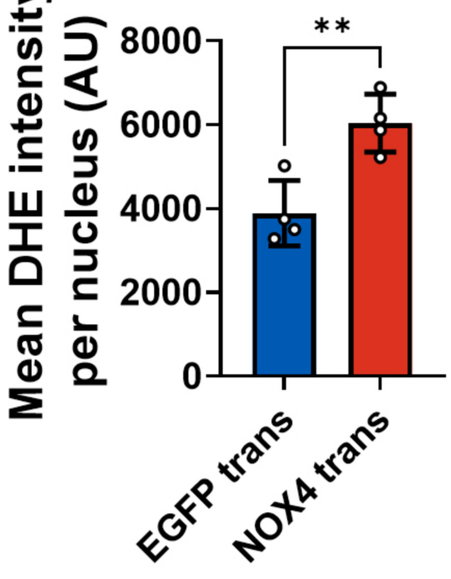
Mean DHE intensity per nucleus (AU)
8000
6000
4000
2000
0
**
EGFP trans
NOX4 trans

E)

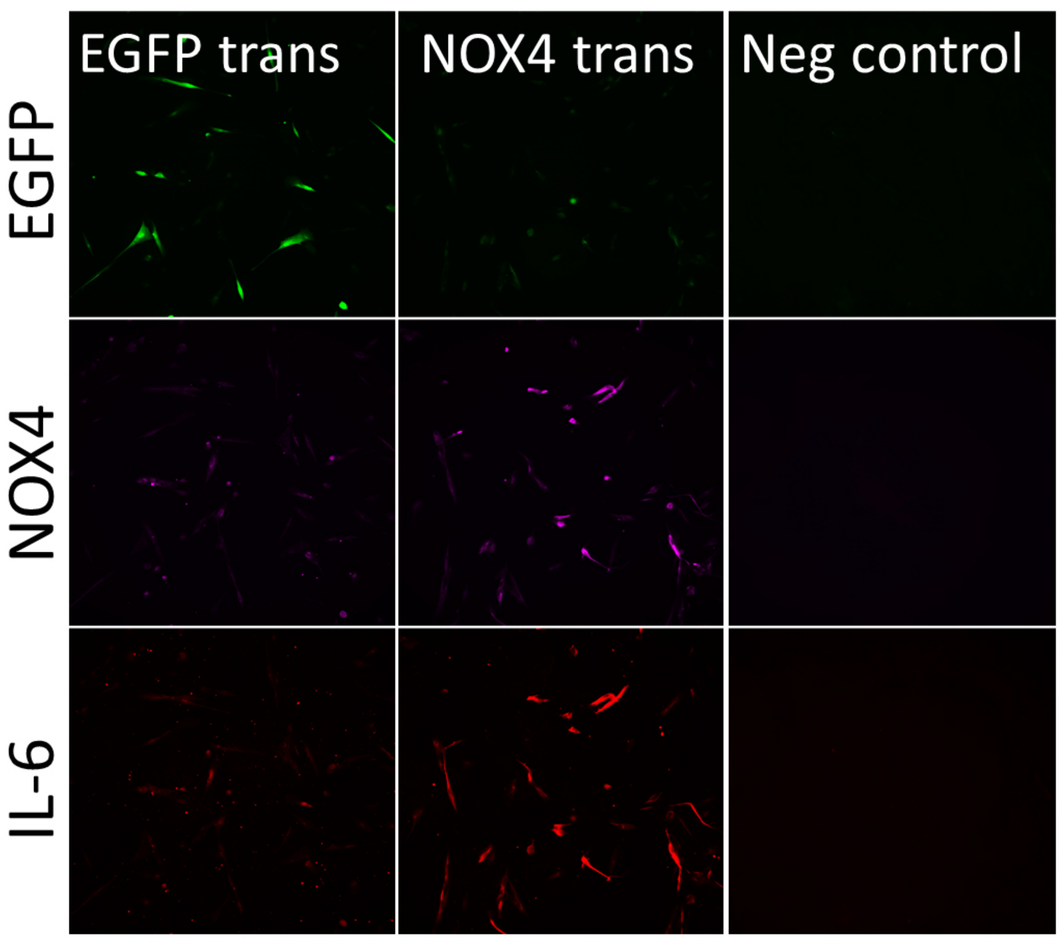
EGFP trans
NOX4 trans
Neg control
EGFP
NOX4
IL-6

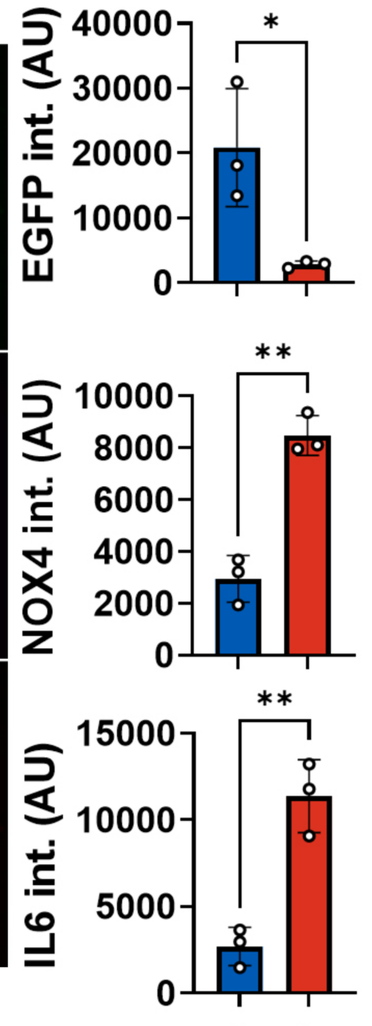
EGFP int. (AU)
40000
30000
20000
10000
0
*
NOX4 int. (AU)
10000
8000
6000
4000
2000
0
**
IL6 int. (AU)
15000
10000
5000
0
**
EGFP trans
NOX4 trans

F)

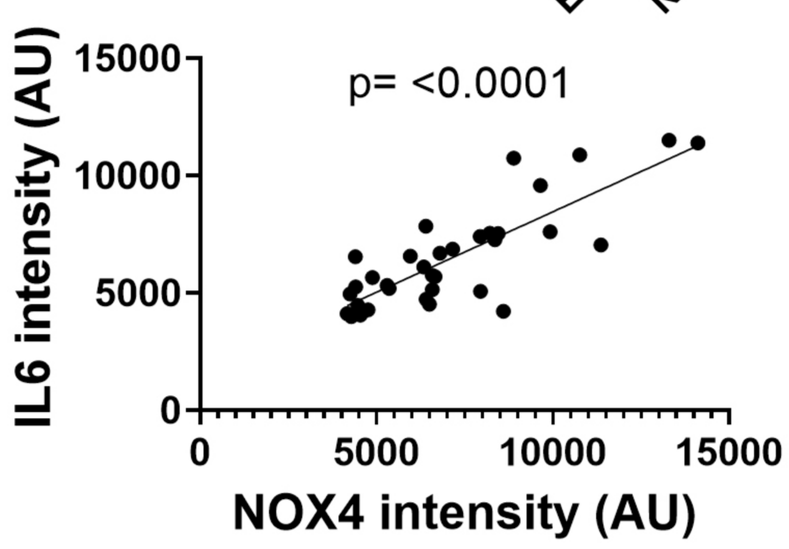
p= <0.0001
IL6 intensity (AU)
15000
10000
5000
0
0
5000
10000
15000
NOX4 intensity (AU)

G)

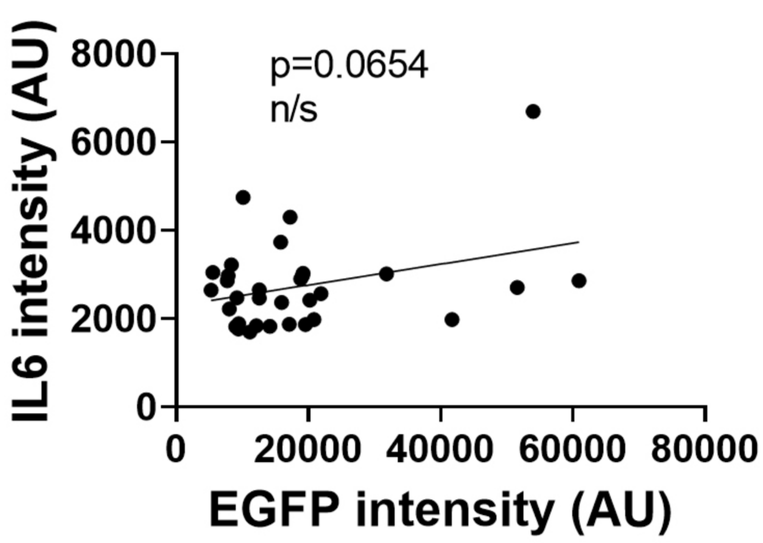
p=0.0654
n/s
IL6 intensity (AU)
8000
6000
4000
2000
0
0
20000
40000
60000
80000
EGFP intensity (AU)

H)

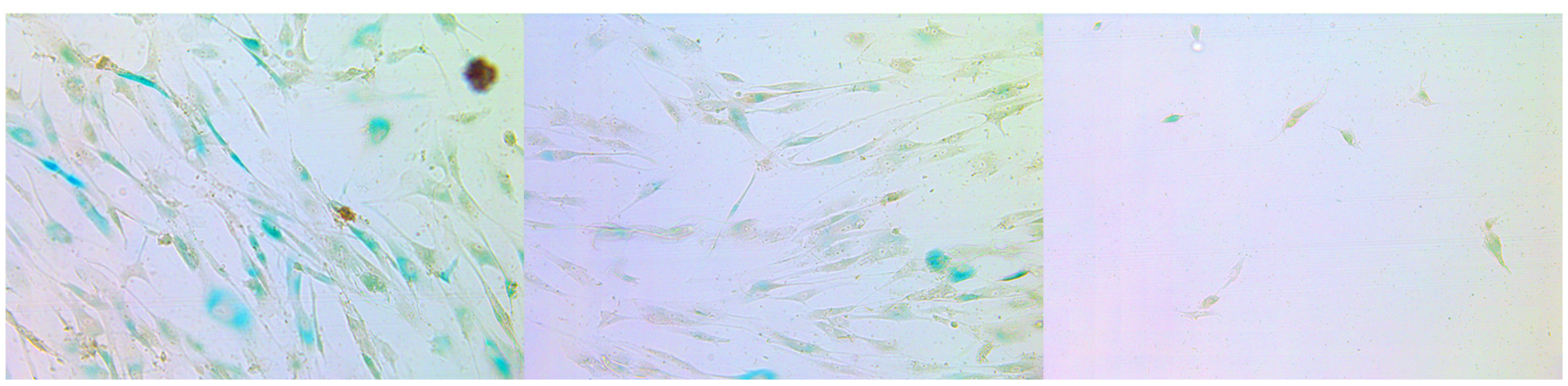
Control
10nM DPI
50nM DPI
Sen-β-Gal

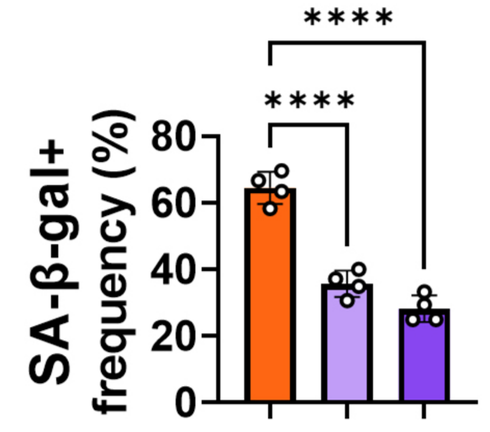
SA-β-gal+ frequency (%)
80
60
40
20
0
****
****

I)

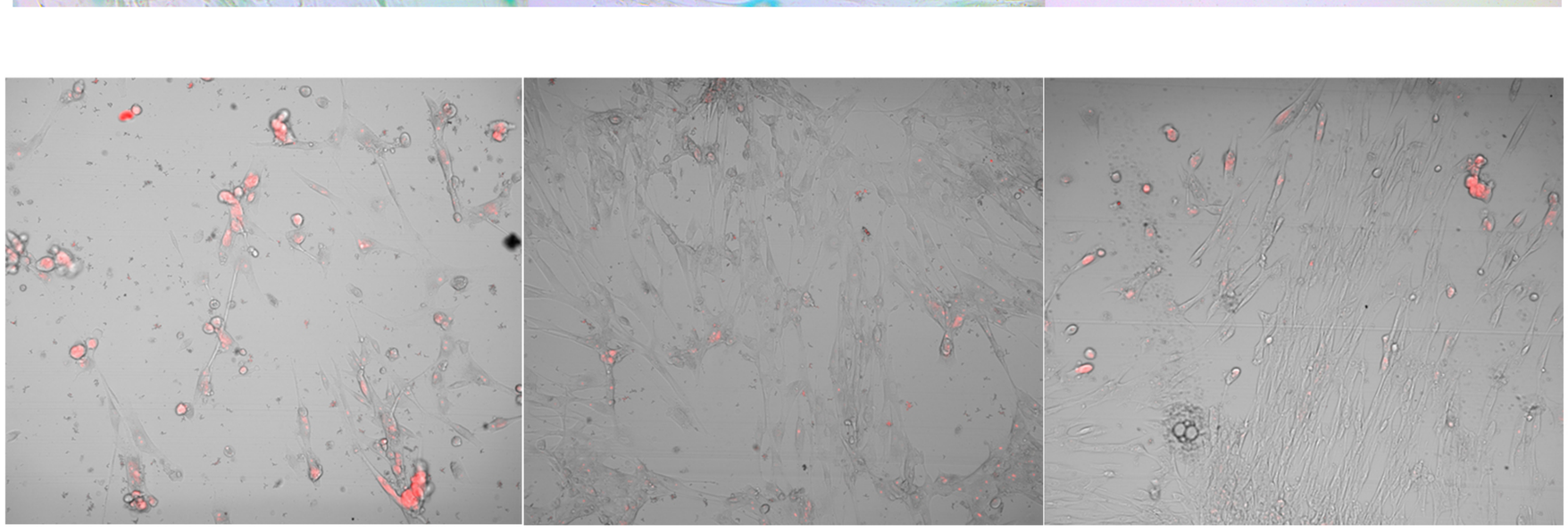
DHE

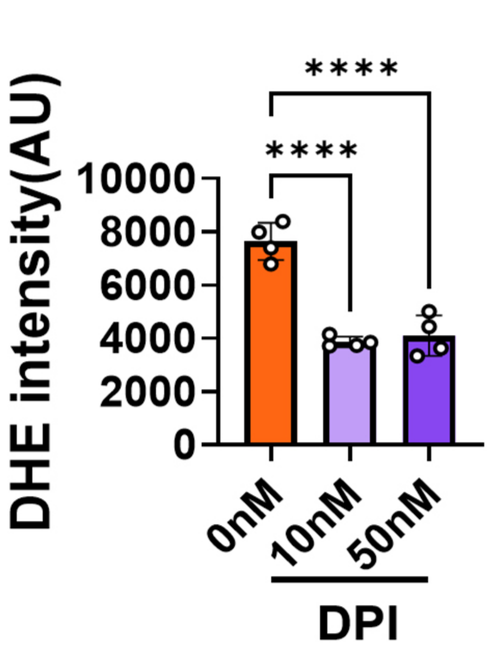
DHE intensity(AU)
10000
8000
6000
4000
2000
0
****
****
0nM
10nM
50nM
DPI

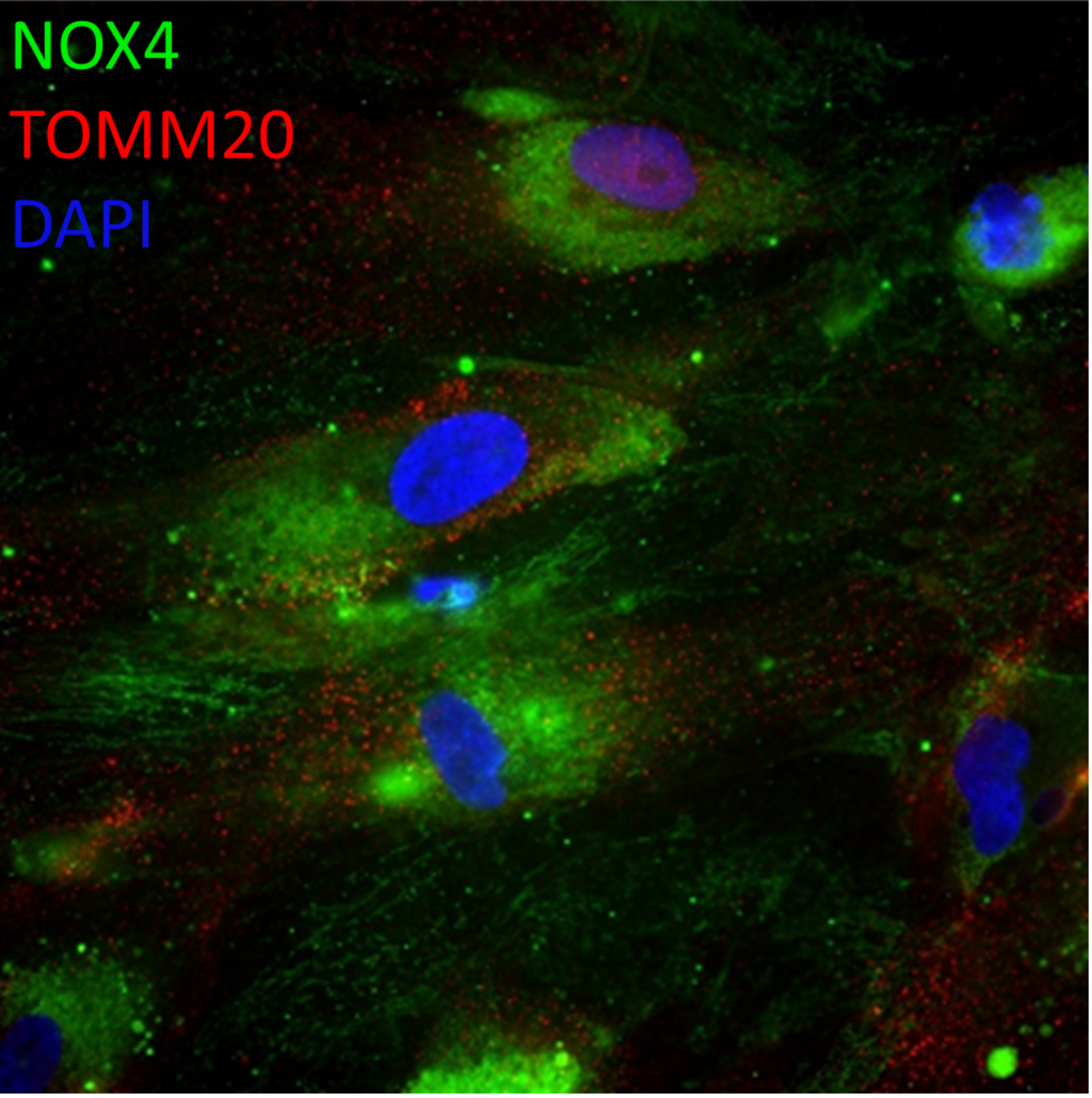
NOX4
TOMM20
DAPI